FEDERAL UNIVERSITY OF SÃO CARLOS
CENTER FOR EXACT SCIENCES AND TECHNOLOGY
GRADUATE PROGRAM IN MATERIALS SCIENCE AND ENGINEERING

UPCYCLING ORANGE WASTE INTO POROUS CARRIERS FOR ORGANIC PHASE-CHANGE MATERIALS

Laís Taguchi Possari

São Carlos-SP
2025

FEDERAL UNIVERSITY OF SÃO CARLOS
CENTER FOR EXACT SCIENCES AND TECHNOLOGY
GRADUATE PROGRAM IN MATERIALS SCIENCE AND ENGINEERING

UPCYCLING ORANGE WASTE INTO POROUS CARRIERS FOR ORGANIC PHASE-CHANGE MATERIALS

Laís Taguchi Possari

Doctoral thesis conducted under a cotutelle agreement presented to the Graduate Program in Materials Science and Engineering as a partial requirement to obtain the title of DOCTOR IN MATERIALS SCIENCE AND ENGINEERING conferred by the Federal University of São Carlos (UFSCar) and the title of DOCTOR IN NUMERICAL MECHANICS AND MATERIALS conferred by Paris Sciences et Lettres University (PSL)

Supervisors: Dr. Sílvia Helena Prado Bettini (UFSCar)
Dr. Tatiana Budtova (Cotutelle – Mines Paris-PSL)
Co-supervisor: Dr. Caio Gomide Otoni (Unicamp)
Funding agency: CAPES (grants no. 88887.671778/2022-00 and no. 88887.836065/2023-00)

São Carlos-SP
2025

DEDICATION

To the memory of Kyoko Yamamoto Taguchi, may your grace and wisdom forever guide my path.

To my parents, Akemi Taguchi Possari and Sidnei Antonio Possari, for the unfailing love and support.

VITAE

Master in Materials Science and Engineering by the Federal University of São Carlos (2021)

Bachelor in Materials and Manufacturing Engineering by the University of São Paulo (2017)

UNIVERSIDADE FEDERAL DE SÃO CARLOS

Centro de Ciências Exatas e de Tecnologia
Programa de Pós-Graduação em Ciência e Engenharia de Materiais

Folha de Aprovação

Defesa de Tese de Doutorado da candidata Laís Taguchi Possari, realizada em 07/10/2025.

Comissão Julgadora:

Profa. Dra. Sílvia Helena Prado Bettini (UFSCar)

Profa. Dra. Alessandra de Almeida Lucas (UFSCar)

Profa. Dra. Tatiana Budtova (Mines Paris)

Profa. Dra. Denise Freitas Siqueira Petri (USP)

Profa. Dra. Isabelle Capron (INRAE)

Prof. Dr. Julien Bras (Grenoble INP)

O Relatório de Defesa assinado pelos membros da Comissão Julgadora encontra-se arquivado junto ao Programa de Pós-Graduação em Ciência e Engenharia de Materiais.

ACKNOWLEDGEMENTS

The development of this work was made possible thanks to the invaluable support and assistance of several individuals and institutions. I would like to express my profound gratitude:

To my supervisors, Prof. Dr. Sílvia Helena Prado Bettini, Prof. Dr. Caio Gomide Otoni, and Prof. Dr. Tatiana Budtova, who have guided and supported me throughout this doctoral research. I am deeply grateful for all the opportunities you have given me, and for the trust you have put in my work and in this project. Prof. Sílvia and Prof. Caio, you gave me the chance to pursue a PhD and constantly inspired me to explore new research topics. Prof. Tatiana, with openness and generosity, you welcomed me to your laboratory and fully embraced the development of this work. Each of you has contributed in your own unique way to my professional and academic development, sharing with me not only your invaluable scientific knowledge, but also countless lessons on the many facets of the research work.

To the Graduate Program in Materials Sciences Engineering (PPGCEM) and Department of Materials Engineering (DEMa) of UFSCar, and to the Center for Materials Forming (Cemef) of Mines Paris-PSL, where most of the research work of this thesis was conducted.

To the jury members, Prof. Dr. Alessandra de A. Lucas, Prof. Dr. Denise F. S. Petri, Dr. Isabelle Capron, and Prof. Dr. Julien Bras, for kindly agreeing to dedicate your time and effort to the evaluation of this thesis. I am sincerely grateful for your willingness to contribute your expertise and valuable knowledge to this work.

To all those who kindly helped me with the experimental work: Julien Jaxel (PERSEE, Mines Paris) for the supercritical drying and thermal conductivity measurements; Frédéric Georgi (CEMEF, Mines Paris) for the guidance with SEM and optical microscopy; Rafaella F. Fernandes (FZEA-USP/DEMa-UFSCar) for the FT-Raman spectroscopy measurements; Guillaume Corvec (CEMEF, Mines Paris) for the assistance with the infrared camera; Lionel Freire for the guidance with DSC; Jéssica Pereira (PPGCEM/UFSCar) for the help with some SEM analyses; Marcos V. Basaglia

(PPGCEM/UFSCar) for some FTIR analyses; Giovanni Perotto and Camila Rinaldi (IIT) for the biodegradation measurements; Michel Brienzo and Patrícia F. Ávila (IPBEN-UNESP) for the cellulose, hemicellulose and lignin content analyses; Osvaldo Francisco de Souza Júnior, Lourival Varanda, Fernando Passareli, and Osvaldo José Correa (DEMa/UFSCar) for the continuous assistance with routine laboratory matters.

To JBT Company for donating the orange waste, CP Kelco for providing pectin, and Anton Paar and Ronan Behling for providing access to and technical support with the gas pycnometer.

To my esteemed friends and colleagues from the PhD program and research groups in Brazil: Bia, Marcos Nicolino, Marcos Basaglia, Iago, Lívia, Anderson, Rafael, and many others, for cultivating joyful and inclusive environments, as well as for the memorable moments we shared. A special thanks to Franklin, Erick, and Letícia for the enjoyable moments, shared experiences, and valuable advice.

To those who graciously welcomed me into the BIO group in France: Loris, Marion, Veronika, and Laurianne, for being so receptive and for the assistance with equipment and procedures I was not familiar with. A special thanks to Eleni, Hiba, and Sujie, who were particularly kind and extended their help to me on several occasions. Thank you all for the pleasant and welcoming atmosphere you created.

To all other friends and colleagues I had the pleasure of meeting in France: Bernardo, Camila, Juliana, Gustavo, Ricardo, Wanxiang, Lukas, and others, for the pleasant and supportive company during my time at Cemef.

This study was financed in part by the Coordenação de Aperfeiçoamento de Pessoal de Nível Superior - Brasil (CAPES) - Finance Code 001.

CAPES supported this research through the scholarships in Brazil (grant no. 88887.671778/2022-00) and during a one-year stay in France (grant no 88887.836065/2023-00), which provided us the honorable opportunity to establish a cotutelle agreement between UFSCar and Mines Paris-PSL. During this process, I could count not only on the support and efforts of my supervisors, but also on the invaluable help of Marcelo F. Pecenin (SRInter/UFSCar),

Marcelo C. Cavallaro (PPGCEM/UFSCar), and Florence Morcamp (Cemef/Mines Paris) with documentation and formal requirements, for which I am sincerely grateful.

This study was financed in part by the São Paulo Research Foundation (FAPESP, Brazil - processes no. 2021/12071-6 and no. 2020/07633-2).

Financial support was also provided by the National Council for Scientific and Technological Development (CNPq, Brazil) through the INCT Circularity in Polymer Materials (grant no. 406925/2022-4) and the grant no. 304753/2022-0.

Finally, I would like to express my profound gratitude to my cherished friends and family:

To my dear friends Polly, Hérisson, Eder, Gabriel (Tequis), Fabrício, Letícia, Thaís, Vivian, and Meyli, for the lasting friendships and the comforting knowledge that your love and support are always with me, no matter the distance;

To the precious friends I found in France, Mirna and Laëtitia, for the joyful and memorable moments we shared;

To my beloved partner, Chakib, for the unwavering support and for continuously inspiring me through your compassion, gentleness, and positive outlook on life;

To my brother Kevin for your constant support and care for our family;

To the most important people in my life, my parents Akemi and Sidnei, for being my greatest examples of respect, kindness, and resilience. Thank you for all your efforts in providing me with a quality education. I am deeply thankful for your unconditional support.

ABSTRACT

UPCYCLING ORANGE WASTE INTO POROUS CARRIERS FOR ORGANIC PHASE-CHANGE MATERIALS

This thesis investigates the upcycling of orange juice waste biomass into aerogels and cryogels, and their performance as organic carriers of phase-change materials (PCMs). PCMs can store and release thermal energy at nearly constant temperatures during phase transitions, typically solid–liquid, which makes them suitable for passive temperature regulation applications. Aqueous suspensions were prepared by subjecting the whole and fractionated biomass waste (namely peels, pulp, and bagasse) to a citric acid pre-treatment, which promoted the extraction and solubilization of pectin into the liquid phase, and the swelling and fibrillation of the insoluble fraction. The kinetic stability of suspensions was tuned by adjusting preparation parameters (e.g., washing or non-washing, biomass and citric acid contents), enabling the production of homogeneous 3D porous materials using different processing routes. Aerogels were prepared via non-solvent-induced phase separation (with ethanol or acetone) followed by drying with supercritical carbon dioxide, and cryogels via suspension freezing followed by lyophilization. Aerogel beads were also produced by dripping the biomass suspension in ethanol prior to supercritical drying. Porous materials with varied morphologies, textural and mechanical properties, thermal conductivities and biodegradation rates in seawater were obtained. Two organic PCMs, polyethylene glycol and coconut oil, were loaded into obtained porous materials via vacuum-assisted melt impregnation for dimensional stabilization. The resulting phase-change composites were characterized for their thermal behavior and leakage resistance above the PCMs melting temperature, showing that the porous materials' morphology and compatibility with the PCMs had a decisive impact on their performance as carriers for PCMs.

Keywords: aerogel; cryogel; porous materials; orange waste; biomass; pectin; PCM

RESUMO

VALORIZAÇÃO DE BIOMASSA REDISUAL DE LARANJA EM CARREADORES POROSOS PARA MATERIAIS DE MUDANÇA DE FASE

Esta tese investiga a valorização da biomassa residual oriunda da produção de suco de laranja em aerogéis e criogéis, e o desempenho destes como carreadores de materiais de mudança de fase (PCMs). PCMs são capazes de armazenar e liberar energia térmica a temperaturas quasi-constantes durante transições de fase, tipicamente sólido-líquido, lhes conferindo potencial de aplicação em sistemas de manutenção passiva de temperatura. Suspensões aquosas foram preparadas submetendo a biomassa integral e fracionada (casca, polpa e bagaço) a um pré-tratamento com ácido cítrico, que promoveu a extração e solubilização da pectina na fase líquida das suspensões, e o inchamento e fibrilação da fração insolúvel. A estabilidade cinética das suspensões foi otimizada por meio do ajuste de parâmetros de preparação (lavagem ou não da biomassa, teores de biomassa e ácido cítrico), possibilitando a produção de materiais porosos homogêneos por meio de diferentes rotas de processamento. Aerogéis foram obtidos via separação de fases induzida por não-solvente (etanol ou acetona), seguida de secagem com dióxido de carbono supercrítico; e criogéis pelo congelamento da suspensão seguido de liofilização. Adicionalmente, esferas de aerogel foram produzidas via gotejamento da suspensão em etanol e secagem supercrítica. Materiais porosos com diferentes morfologias, propriedades mecânicas, condutividades térmicas e cinéticas de biodegradação em água do mar foram obtidos. Dois PCMs orgânicos, polietilenoglicol e óleo de coco, foram incorporados aos materiais porosos via impregnação no fundido sob vácuo. Compósitos obtidos foram caracterizados termicamente e quanto à resistência a vazamentos acima da temperatura de fusão dos PCMs, que se mostrou dependente da morfologia dos materiais porosos e suas interações com os PCMs.

Palavras-chave: aerogel; criogel; materiais porosos; biomassa residual; resíduo de laranja; biopolímeros; PCM

RESUMÉ

VALORISATION DES DÉCHETS D'ORANGE EN SUPPORTS DE MATÉRIAUX À CHANGEMENT DE PHASE ORGANIQUES

Cette thèse étudie la valorisation de la biomasse résiduelle issue de la production de jus d'orange en aérogels et cryogels, ainsi que leurs performances en tant que supports de matériaux à changement de phase (PCMs). Les PCMs peuvent stocker et libérer de l'énergie thermique à des températures quasi constantes lors des transitions de phase, généralement solide-liquide, ce qui les rend adaptés aux applications de régulation thermique passive. Des suspensions aqueuses ont été préparées à partir de la biomasse entières et fractionnées (écorces, pulpe et bagasse), soumis à un prétraitement à l'acide citrique. Celui-ci a favorisé l'extraction et la solubilisation de la pectine à la phase liquide, ainsi que le gonflement et la fibrillation de la fraction insoluble. La stabilité cinétique des suspensions a été ajustée en modifiant les paramètres de préparation (lavage ou non-lavage de la biomasse, teneur en biomasse et en acide citrique), ce qui a permis de produire des matériaux poreux 3D homogènes par différentes voies de traitement. Les aérogels ont été obtenus par séparation de phases induite par non-solvant (éthanol ou acétone), suivie d'un séchage au dioxyde de carbone supercritique, tandis que les cryogels ont été préparés par congélation de la suspension puis lyophilisation. Des billes d'aérogel ont également été produites par gouttage de la suspension de biomasse dans l'éthanol avant séchage supercritique. Les matériaux poreux ont présenté des morphologies, propriétés mécaniques, conductivités thermiques et taux de biodégradation dans l'eau de mer variés. Deux PCM organiques, le polyéthylène glycol et l'huile de coco, ont été incorporés par imprégnation par fusion sous vide. Les composites obtenus ont été caractérisés quant à leur comportement thermique et leur résistance aux fuites au-dessus de la température de fusion des PCM, qui s'est avérée dépendante de la morphologie des matériaux poreux et de leurs interactions avec les PCM.

Mots-clés: aérogel; cryogel; matériaux poreux; biomasse; déchet d'orange; biopolymères; PCMs

PUBLICATIONS

Articles:

- POSSARI, L.T.; ÁVILA, P.F.; BRIENZO, M.; OTONI, C.G.; BUDTOVA, T.; BETTINI, S.H.P. Upcycling Orange Waste into Bio-Based Aerogels. ACS Sustainable Resource Management, v. 2, p. 944-952, 2025. doi: 10.1021/acssusresmgt.4c00511
- POSSARI, L.T.; PAULA, MARINA S. DE; NUNES, GEORGE F.; REIS, IAGO A.; BASAGLIA, MARCOS V.; OTONI, CAIO G.; BETTINI, SÍLVIA H.P. Bioplastics from orange processing waste and poly(lactic acid). Future Foods, v. 11, p. 100670, 2025. doi: 10.1016/j.fufo.2025.100670

Conference presentations:

- POSSARI, L.T.; OTONI, C.G.; BETTINI, S.H.P. Bioaerogels based on orange juice side-streams. Poster presentation. In: 8th EPNOE International Polysaccharides Conference, Graz, Austria. September, 2023.
- POSSARI, L.T.; OTONI, C.G.; BETTINI, S.H.P.; BUDTOVA, T. Upcycling citrus agro-industrial residues into bio-based porous materials. Oral presentation (online). In: ACS Spring, New Orleans, United States/Hybrid. March, 2024.
- POSSARI, L.T.; OTONI, C.G.; BETTINI, S.H.P.; BUDTOVA, T. Residual orange biomass derived porous materials. In: Nice Complex Days, Nice, France. February, 2024.

TABLE OF CONTENTS

LIST OF TABLES

LIST OF FIGURES

Page

SYMBOLS AND ABBREVIATIONS

AR Aspect ratio

ATR-FTIR Attenuated Total Reflectance – Fourier-Transform Infrared Spectroscopy

BET Brunauer-Emmett-Teller method

BOD Biochemical Oxygen Demand

$CaCl_2$ Calcium chloride

$CaCO_3$ Calcium carbonate

CNF Cellulose nanofibers

CO Coconut oil

CO_2 Carbon dioxide

DE Degree of esterification

D_{eq} Equivalent diameter

DTG Derivative thermogravimetric curve

E Elastic modulus

FT-Raman Fourier-Transform Raman Spectroscopy

HCl Hydrochloric acid

HG Homogalacturonan

HM High methoxyl (pectin)

HPLC High-Performance Liquid Chromatography

H_2SO_4 sulfuric acid

IR Infrared

LM Low methoxyl (pectin)

LR Loading ratio

LR_{th} Theoretical loading ratio

LR_{th}* Theoretical loading ratio corrected for volume shrinkage

MCC Microcrystalline cellulose

NaCl Sodium chloride

NaOH Sodium hydroxide

O_2 Oxygen

PCM Phase-change material

PEG Poly(ethylene glycol)

PVA	Poly(vinyl alcohol)
R_n	Roundness
RG-I	Rhamnogalacturonan-I
RG-II	Rhamnogalacturonan-II
SEM	Scanning electron microscopy
TG	Thermogravimetric curve
TGA	Thermogravimetric analysis
T_m	Melting temperature
WHC	Water holding capacity
XGA	Xylogalacturonan

ΔH_m	Melting enthalphy
ε	Latent heat efficiency
ε_r	Relative latent heat efficiency
ε_y	Yield strain
$[\eta]$	Intrinsic viscosity
λ	Thermal conductivity
ρ_{ap}	Apparent density
ρ_{sk}	Skeletal density
σ_y	Yield stress

CHAPTER 1 – GENERAL INTRODUCTION

1.1 Background

Orange (*Citrus sinensis*) is the most widely consumed citrus fruit in the world, with a global production of ca. 70 Mt in 2023 [1]. Approximately 30% of this output is destined for the orange juice industry [2], where 50-60% of *in natura* oranges are turned into by-products [3]. The (semi-)solid orange waste comprises mainly peels, seeds, membranes, and residual pulp [2]. Predominantly composed of organic matter (> 90%) and bearing high contents of moisture (ca. 75-85%) and soluble sugars (ca. 17%), these residues are highly susceptible to fermentation and microbial development [4–6]. Their mismanagement can lead to environmental and public health issues, such as groundwater contamination, methane emissions, soil microbiota disruption, and proliferation of disease vectors. Orange juice side streams are primarily landfilled, but are also commonly incinerated for energy recovery or reused in animal feed [4,7]. Hence, reutilizing these by-products for higher-added-value endings is advantageous from environmental, sanitary, and economic standpoints [2,3].

Converting orange waste biomass into new bio-based materials is a promising strategy within the emerging concept of a circular bioeconomy due to its composition rich in biopolymers, especially pectin (up to 40%, dry basis), as well as active substances like polyphenols and limonoids [2,8,9]. Most studies have focused on the extraction of these components and their further use in polymer-based materials: either as the main component (i.e., as the matrix; e.g., pectin, (hemi)cellulose), or as functional additives (e.g., phenolic extracts, essential oils) [5,9,10].

An alternative and promising approach is to utilize orange waste biomass in its entirety, i.e., without fractionation or purification. Recent studies [11–18] have demonstrated the production of cast films based on such “bulk” orange waste. Acid (partial) hydrolysis has shown promising results, with weak and non-toxic acids favoring milder and more environmentally friendly procedures, especially citric acid [11–15]. In addition, filaments from orange residual pulp

were produced by twin-screw extrusion with glycerol as a plasticizer [19]. In both cases, authors stated that the high pectin content in the orange waste enabled the formation of a cohesive pectin matrix, in which insoluble lignocellulosic fibers were dispersed [13,15,19].

Pectin is a branched, anionic, and water-soluble heteropolysaccharide, with typical gelling ability, film-forming properties, and biodegradability [20,21]. Since 2013, pectin has been successfully used to produce porous materials, like cryogels and aerogels [22–28]. In this context, upcycling pectin-rich orange waste biomass into aerogels and cryogels is a promising, yet largely unexplored, strategy for their valorization. While literature has focused on films and filaments from orange juice residues, the production of 3D porous materials from this abundant waste could expand possibilities of morphology, properties, and applications.

Aerogels constitute a class of porous materials characterized by high specific surface areas (> 100 m^2/g), high porosities (> 90%), and low densities (< 0.2 g/cm^3). They present morphologies predominantly composed of micropores and/or mesopores (< 50 nm in diameter) and, occasionally, small macropores (50 to a few hundred nanometers) [29–31]. They are usually derived from gels, solutions, or suspensions, from which the solvent or dispersant is removed in supercritical conditions, usually with carbon dioxide (CO_2) [25,31,32]. Supercritical conditions avoid the development of capillary pressure, which is usually the reason for pore collapse in evaporative drying. It should be noted that aerogels are usually defined according to their properties, and not by the processing route, although a consensus is yet to be achieved [31]. For example, silica aerogels can be obtained via ambient pressure drying (after functionalization of silica gels) [33], as well as some bio-based aerogels [34,35]. Freeze-drying from tert-butanol may also result in aerogels [36,37].

So far, bio-based aerogels (also referred to as “bio-aerogels”) have been produced mainly from neat polysaccharides (e.g., starch, pectin, chitosan, and cellulose and its derivatives) and, sometimes, proteins [20,38]. Generally, biopolymers are dissolved, sometimes gelled, and the solvent is exchanged to one miscible with supercritical CO_2, which is then used to perform the

supercritical drying [25,39]. Ethanol and acetone are commonly used, which are also non-solvents for most polysaccharides. Consequently, solutions can be directly shaped via non-solvent-induced phase separation, and the gelling step is omitted [28,30]. An illustration of these procedures is presented in Figure 1.1.

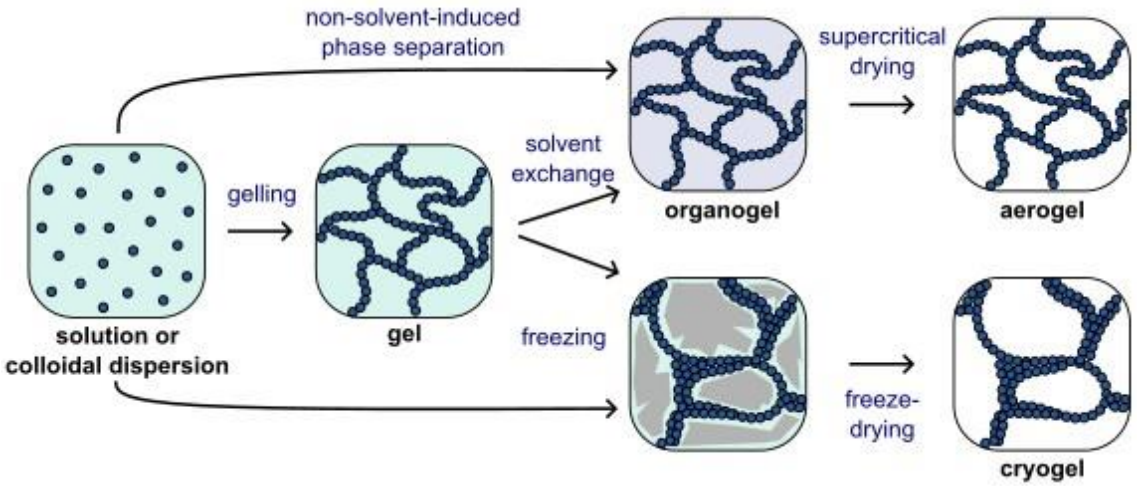

Figure 1.1: Schematic illustration of the typical procedures for preparing bio-based aerogels and cryogels.

Only a few studies dealt with aerogels from agri-food wastes, including stale bread [40], apple pomace [41], and spent coffee grounds [41]. Gibowsky et al. [42] produced aerogel powders based on several plant tissues, including orange peels and pulp, by shredding those tissues in a blender prior to solvent exchange, milling, and supercritical drying. Aerogel powders bearing 285-322 m^2/g of surface area and 0.02-0.08 g/cm^3 of density were produced in this study.

Cryogels constitute another type of porous materials, produced by freezing gels, solutions or suspensions; and sublimating the solvent, usually water, via freeze-drying (or lyophilization) (see Figure 1.1) [39]. Strictly speaking, cryogels are based on solutions that are gelled upon freezing [43], but this term is usually expanded to all types of ice-templated and freeze-dried materials. This terminology is commonly employed in the field of bio-based porous materials [30,31], and also adopted throughout this thesis. Bio-based cryogels have been developed mostly from neat biopolymers like pectin [23,44],

starch [45,46], and cellulose [47,48]; but also from some biomass wastes, including those from citrus fruits (e.g., orange [49,50], pomelo [51,52], and grapefruit peels [53]).

Supercritical drying and freeze-drying are used to avoid the development of capillary pressure during liquid evacuation under evaporative drying, yet the resulting morphologies and properties are remarkably different. Both drying methods give rise to open-pore structures. While the former preserves the wet network to a higher extent, originating nanostructured networks; the latter significantly alters the pore structure due to ice crystals growth (Figure 1.1), typically leading to large pores, at the micrometer scale, and thus low specific surface areas [25,32].

The literature has focused mainly on aerogels and cryogels derived from neat pectin and other biopolymers extracted from biomasses [23,25,44–48,54]. However, pectin isolation conventionally requires the use of strong mineral acids (e.g., hydrochloric acid, sulfuric acid), posing risks to human health and increasing the environmental footprint, in addition to involving waste generation and numerous operational steps [20,55]. Repurposing bulk biomass waste into porous materials like aerogels and cryogels, preferably through mild and non-hazardous treatments, is a strategy to mitigate those issues. Moreover, the dispersed cellulosic fibers may act as mechanical reinforcement for the pectic matrix [56,57].

Porous materials have been increasingly investigated as carriers for phase-change materials (PCMs) [58,59]. PCMs are materials with high phase-change latent heat and relatively narrow transition temperature ranges. As a consequence, they are capable of storing and releasing large amounts of thermal energy as they undergo phase transitions and thus at approximately constant temperatures. Accordingly, PCMs have been applied in passive temperature management systems, such as in the storage and transportation of thermosensitive products (e.g., food, vaccines, drugs), thermal protection of electronic devices, smart textiles and construction materials designed for improved thermal comfort [60,61].

PCMs are classified according to their chemical composition: inorganic, organic, or a mixture of both (eutectic or hybrid). Inorganic PCMs include mainly hydrated salts, but also neat salts and metals for high temperature applications [61,62]. Despite boasting high latent heat (130-400 J/g), these PCMs have high supercooling degrees due to low nucleation rates and high chemical reactivity [63]. Organic PCMs, in contrast, are widely employed due to their high availability and latent heat (up to ca. 250 J/g), low cost, broad range of phase-change temperatures (-5 to 80 °C), lower supercooling degrees, and chemical stability. Examples include paraffin waxes, poly(ethylene glycol) (PEG), and fatty acids [64–66].

Most PCMs operate via solid-liquid transitions. As a consequence, dimensional instability and leakage are critical issues that hinder their practical application. One strategy to mitigate these drawbacks is the incorporation of PCMs into porous materials, such as aerogels and cryogels, that act as physical supports by retaining the PCMs through capillary forces [67,68]. Both supercritical drying and freeze-drying give rise to open-pore structures, allowing high PCM loading ratios, but remarkably different morphologies. The performance of porous materials as shape-stable and leakage-proof carriers for PCMs depends directly on their textural properties (e.g., porosity, pore structure, and specific surface area) and interactions with the impregnated PCM [69,70]. The latter results from the porous carrier-PCM combination, while the former can be tailored through the choice of drying procedure and other processing parameters (e.g., biomass/biopolymer concentration, pH, gelation or not, etc.) during the preparation of the porous materials [27,32].

Different bio-based porous structures have been used to carry organic PCMs, including those derived from neat biopolymers (e.g., chitosan [70,71], alginate [70,72], pectin [67,73,74]), and from bulk biomasses (e.g., wood [75,76], wheat bran [77,78], and fruit peels [79,80]). Citrus waste-based porous materials explored as PCM carriers predominantly exhibit large macroporous structures (dozens to hundreds of micrometers) stemming from directly freeze-drying [49,50,81,82] (i.e., without any pre-treatment besides washing, cutting, etc.) or evaporative drying [68,83].

Despite significant advances in the development of bio-based carriers for PCMs in recent years, this emerging topic faces several challenges, including enhancing thermal performance and leakage resistance, exploring diverse biomass sources, and developing more eco-friendly procedures for producing porous carriers [63,84].

In summary, aerogels and cryogels derived from orange biomass waste are scarce in the literature, especially aerogels, which are limited to aerogel powders [42]. In turn, those obtained from neat pectin have shown promising results for a wide range of applications (e.g., packaging, controlled drug release, and thermal and acoustic insulation) [25,39,44]. Thus, upcycling bulk pectin-rich orange waste into porous materials is a potential alternative to help mitigate the safety, efficiency, and waste drawbacks related to pectin isolation [20,55]. This approach could also expand the possibilities of different shapes, morphologies, properties, and applications of orange waste-based materials, currently focused on cast films [11–18]. Moreover, the influence of distinct pore morphologies on the performance of biomass waste-based PCM-carriers remains underexplored, and nanoporous structures derived from citrus waste have not been investigated as potential carriers for PCMs yet.

1.2 Objectives and hypotheses

Given the overview provided above, the objectives of this thesis were:

(i) To investigate the feasibility of converting orange waste biomass into aerogels and cryogels using a citric acid pre-treatment; and

(ii) To evaluate the performance of these materials as carriers for organic PCMs.

Furthermore, the specific hypotheses that guided the execution of this research work were as follows:

- The citric acid hydrolysis pre-treatment is expected to partially deconstruct the orange waste biomass, promoting substantial pectin extraction to the liquid phase (along with other water-soluble compounds, such as sugar

and some phenolic compounds) and facilitating the loosening and swelling of the insoluble fraction.

- The kinetic stability and physicochemical properties of the resulting suspensions can be modulated by varying the preparation parameters (e.g., biomass washing or non-washing, biomass and citric acid concentrations), which introduces changes in the liquid phase composition, inter-particle friction, and acidity of the system. Exploring these parameters may enable the production of kinetically stable suspensions suitable for fabricating homogeneous 3D porous materials.
- The different orange biomass fractions obtained as juice processing waste (namely, peels, bagasse, and pulp) likely differ in biochemical composition and morphology, which may also influence the kinetic stability and physicochemical properties of their suspensions, due to varying recalcitrance to the citric acid pre-treatment.
- Orange waste-based suspensions with adequate kinetic stability can be processed into aerogels and cryogesl using traditional routes employed for neat biopolymers.
- The non-solvents used for aerogel preparation (e.g., ethanol and acetone) interact differently with biomass and CO_2, potentially leading to varied properties depending on non-solvent choice.
- The presence of well-dispersed insoluble fractions may provide a mechanical reinforcement effect to the resulting materials.
- Properties and morphological features of aerogels and cryogels may be influenced by the use of different orange biomass fractions as starting matter as well, due to their possibly distinct responses to the citric acid pre-treatment (e.g., varying insoluble content, and disruption and swelling degrees of the insoluble fractions).
- Aerogel beads from orange waste biomass, bearing similar morphology and properties as their monolithic counterparts, can be designed to shorten the solvent exchange process, which is a diffusion-driven and time-consuming stage of aerogel production.

- Owing to their nanostructured networks, aerogels are expected to outperform cryogels as leakage-proof carriers for organic PCMs, since smaller pores provide enhanced capillary forces that prevent PCM leaching in their molten state. Varying levels of physical interactions between the porous carriers and PCMs likely influence their leakage resistance as well.

1.3 Thesis overview

Given the aforementioned objectives, this thesis is organized in five Chapters, described as follows:

The present Chapter, **Chapter 1**, introduces the background and motivation of this work, defines the research objectives and hypotheses, and provides an overview of the content of the following Chapters.

Chapter 2 is dedicated to the biochemical characterization of the three orange waste biomass fractions (peels, bagasse, and pulp) and a "mixed" biomass (fractions mixed at their corresponding percentages in the bulk orange waste). Extractives, pectin, cellulose, hemicellulose, lignin and ash contents are presented, discussed, and compared to the literature. Thermogravimetry and water-soluble content analyses complement these results. This Chapter further discusses how preparation parameters (biomass washing or non-washing with water, biomass concentration, and citric acid concentration) and biomass fractions (peels, bagasse, and pulp) influenced the resulting suspensions' kinetic stability, rheological behavior and physicochemical properties (e.g., insoluble content, and insoluble fractions' swelling capacity). Key factors and underlying mechanisms governing the stability of orange waste-based suspensions are investigated and correlated with the preparation parameters and the orange biomass composition. Conditions leading to the best kinetic stability are selected to proceed with the production of porous materials.

Chapter 3 considers the feasibility of preparing porous materials from orange waste biomass after the citric acid treatment (best conditions selected from Chapter 2). The morphological and textural properties (volumetric shrinkage, density, porosity and specific surface area) of porous monoliths are

assessed and correlated with the different processing routes utilized. Ethanol and acetone are evaluated as non-solvents for the production of aerogels, and aerogels' properties are compared to those of cryogels. The effect of the different biomass fractions is examined for both aerogels and cryogels. Drying conditions and resulting morphologies are correlated with the materials' thermal conductivity, mechanical behavior, and biodegradability. Lastly, aerogel beads were produced, characterized in terms of size and shape, and compared to their monolithic counterparts (regarding shrinkage, density, morphology, and specific surface area).

Chapter 4 explores the potential of porous materials with distinct shapes, specific surface areas, and pore structures as carriers of organic PCMs. Two PCMs bearing different physicochemical characteristics and phase-change properties are explored: PEG and coconut oil. The thermal behavior of the obtained phase-change composites and of the neat PCMs are presented and discussed. Impregnation efficiency, shrinkage upon PCM impregnation, and leakage resistance of the phase-change composites are also examined.

Chapter 5 summarizes the key findings of this thesis, while a **Perspectives and Future Works** section addresses the potential pathways to complement and continue this research.

A summary of the organization of this thesis and the content of each Chapter is presented in Figure 1.2.

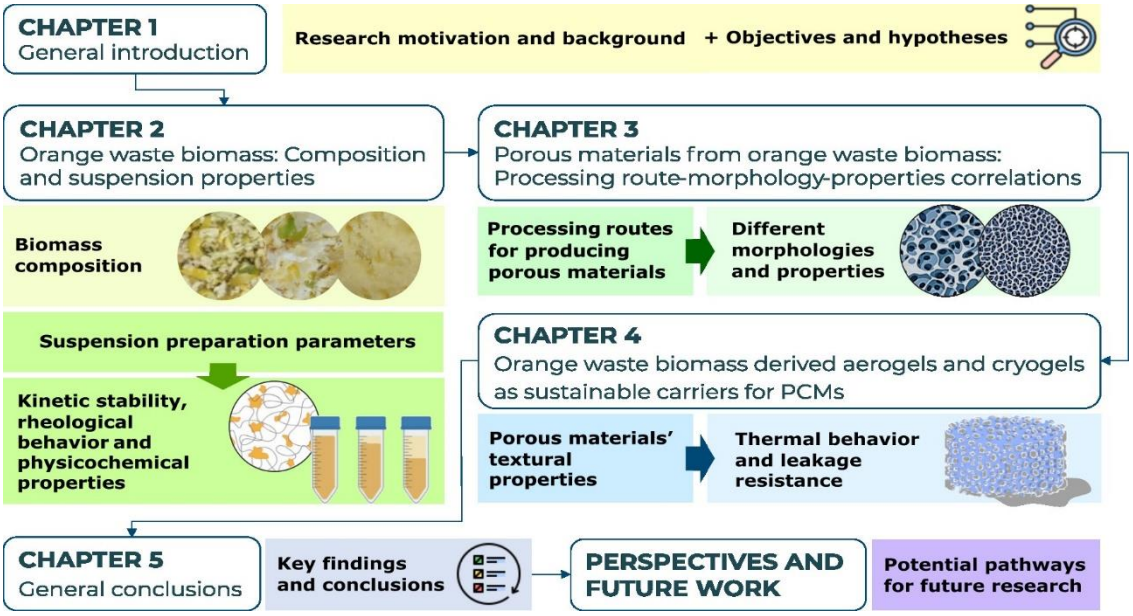

Figure 1.2: Schematic overview of this thesis. Created, in part, with BioRender.com

CHAPTER 2 – ORANGE WASTE BIOMASS: COMPOSITION AND SUSPENSIONS PROPERTIES

2.1 Introduction

As discussed in the General Introduction, the orange juice industry generates substantial amounts of biomass waste (ca. 9 Mt per year) [1–3]. Improper management of this waste can lead to numerous adverse impacts on the environment and public health. When not landfilled, the orange biomass waste is mainly destined for low-added-value endings, such as incineration and cattle feed production [3,85].

Different valorization pathways have been investigated, as discussed later (see Section 2.2.3), yet, a more holistic approach to converting bulk orange biomass waste into novel materials has garnered growing academic interest in recent years [5,9]. Nevertheless, the inherent complexity and variability of the biochemical composition of biomass feedstocks pose significant challenges to achieving materials with controlled and reproducible properties [8]. Therefore, a deeper understanding of biomass structure and composition is essential for advancing strategies to upcycle biomass waste into novel materials, and to elucidate processing-structure-properties correlations of the resulting products.

The difficulty to achieve complete biomass solubilization is also an obstacle to this approach [8]. To produce cast films, the orange biomass waste is typically dispersed in water and subjected to different pre-treatments (e.g., (thermo)chemical, (thermo)mechanical) [11–15,17,18,86], giving rise to heterogeneous systems (i.e., suspensions), inherently susceptible to macroscopic phase separation. A hydrolysis pre-treatment using citric acid, a weak and non-toxic acid, was employed in this work. Although this type of pre-treatment exploits the high pectin content of orange biomass, it is unable to completely dissolve all biomass components (e.g., cellulose, lignin) [11,13,87]. Hence, the kinetic stability of the resulting suspensions was a critical aspect in this study, as it pursued the development of macroscopically homogeneous 3D porous materials from bulk orange waste.

In this context, this Chapter evaluates how the composition and morphology of orange biomass waste, as well as the preparation conditions (washing the biomass with water or not, biomass concentration, and citric acid concentration) affect the physicochemical properties, rheological behavior, and kinetic stability of the resulting suspensions.

2.2 Theoretical Background and Literature Review

2.2.1 Orange fruit structure and processing

This work focused on biomass fractions derived from various parts of processed orange fruits. The orange fruit is produced by the species *Citrus sinensis,* belonging to the family Rutaceae, and its macroscopic structure is presented in Figure 2.1.

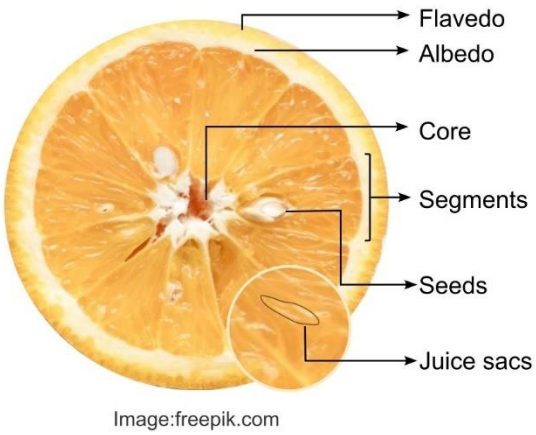

Figure 2.1: Anatomy of the orange fruit in cross-section.

The orange peels consist of two distinct regions: the epicarp (or flavedo) and the mesocarp (albedo) (Figure 2.1). The flavedo is the thin and colored outer layer, carrying pigments and glands, filled with essential oils (primarily D-limonene, ca. 90%), packed between cells. While the albedo is the thicker inner region (2–5 mm) composed of a spongy white tissue, rich in pectic substances and flavonoids [88]. The internal part of the fruit, the endocarp (or pulp), contains numerous small spindle-shaped juice vesicles packed into segments

(10–14 per fruit) (Figure 2.1). Segments, in turn, are delimited by membranes, may contain seeds, and are arranged around a central region with the same composition and structure as the albedo, known as the core [88,89].

Several processes and machines have been developed for orange juice extraction. One typical process employed in the industry consists of four stages (Figure 2.2a and b). First, the fruits are placed between two moving cups with intermeshing teeth (1). Then, the cups secure the fruit, and a small peel disk (or "plug") is cut from the bottom of the orange (2), through which the endocarp is extracted by applying pressure with the cups (3). The essential oil is removed as the fruit is pressed and collected with a water spray flow. At this point, most of the peels are discharged and the endocarp (the orange "flesh") enters a tube located below the cups (called the "pre-finisher" tube), where it is squeezed to extract the juice. The juice containing suspended solids is collected, while the previously cut peel disks, segment membranes, core, and seeds are discarded. Finally, the extracted juice is transferred to the finishing step (step 5, Figure 2.2a), where the suspended solids (mainly floating juice sacs, the "residual pulp") are separated from the juice (via sieving, centrifuging, etc.) [90,91].

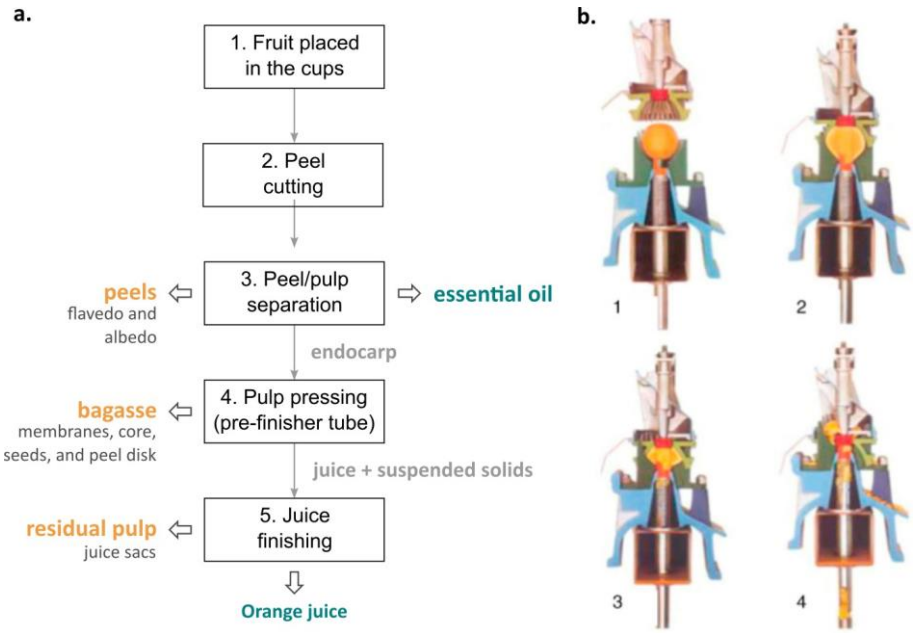

Figure 2.2: (a) Orange juice processing diagram, including the juice extraction (1-4) and finishing (5) stages. (b) Schematic illustration of the juice extraction steps, reproduced from [91] with permission from Springer.

2.2.2 Orange waste composition

Orange waste biomasses obtained after the juice extraction and finishing processes are known to contain high contents of pectin (up to 40%) as well as other biomacromolecules like cellulose, hemicelluloses, and lignin [4,9,92]. These biopolymers constitute the plant cell walls and middle lamella of plant tissues, often being referred to as “structural components”. Their contents in different orange biomasses may vary depending on the fruit variety, climate, soil quality, nutrient availability, harvest time, and other factors [2,3,93].

In addition to the cell wall structural components, non-structural molecules are also present in the orange waste biomass, such as soluble sugars (fructose, glucose, xylose, sucrose, and rhamnose), essential oils, waxes, pigments, polyphenols, and organic acids. These components, generally of low molecular weight, are typically classified as extractives [8,88,94]. Sometimes, non-structural intracellular biopolymers, such as starch and proteins, are also present [93].

Extractives are found in high concentrations in orange biomass (30-60%, dry basis) and may influence their conversion into valuable compounds and materials [9,95]. Structural biopolymers, in turn, play a decisive role in the context of materials development [10]. Therefore, they are discussed in more detail the following sections.

2.2.2.1 Structural biopolymers

Figure 2.3a presents an illustration of the plant cell wall and the middle lamella. Cellulose is the primary structural component of plant tissues (Figure 2.3b), consisting of D-glucose units linearly linked by β(1→4) glycosidic bonds. Cellulose chains self-assemble into hierarchical nano- and microfibrillar structures, which are bound together by an amorphous matrix composed of other biomacromolecules, namely, pectin, hemicellulose, and lignin. The cellulose microfibrils consist of amorphous regions alternated with crystalline parts (55–75%), that present high mechanical and chemical resistance [93,96,97].

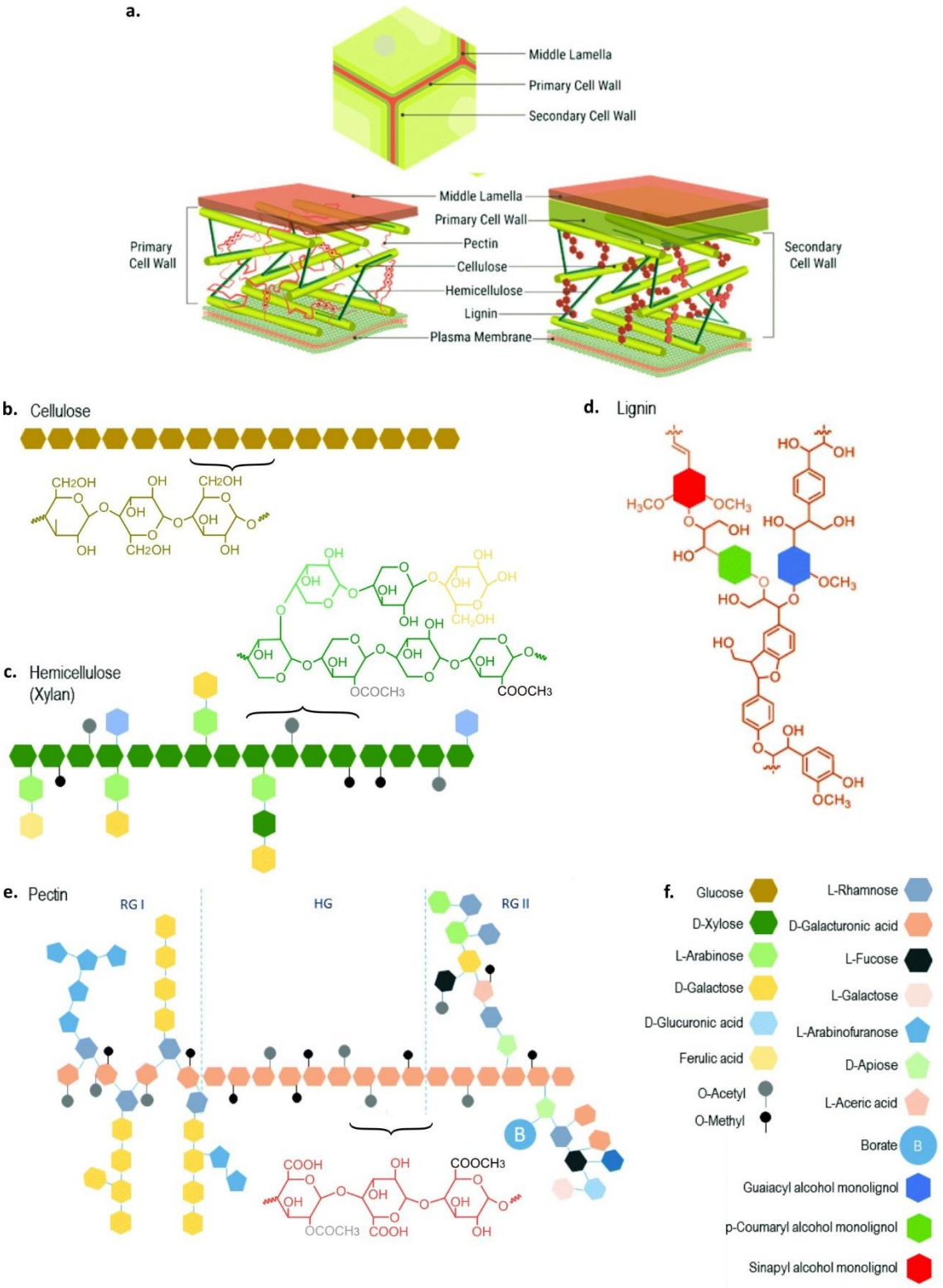

Figure 2.3: (a) Schematic model of the plant cell wall structures and main components: (b) cellulose, (c) hemicellulose, (d) lignin, and (e) pectin. (f) Main components constituting units. Adapted from [93], licensed under CC BY 3.0.

Hemicelluloses (Figure 2.3c) constitute a group of complex branched macromolecules with a lower molecular weight (300–5,000 repeating units) compared to cellulose. Monosaccharides present in hemicelluloses include pentoses (xylose, arabinose), hexoses (glucose, mannose, galactose), and uronic acids (Figure 2.3f). They may also exhibit some degree of acetylation [93,96,97].

Lignin is an aromatic biomacromolecule, organized in cross-linked networks that result from polymerizing propyl-phenolic repeating units (Figure 2.3d), also called monolignols (Figure 2.3f). These units are randomly linked via ether (C-O-C) or carbon-carbon (C-C) bonds. Lignin provides mechanical strength to plant tissues, protects cellulose from microbial degradation, and increases cell wall hydrophobicity, thereby facilitating the transport of water and nutrients [93,98].

Cellulose and hemicellulose are present in both primary and secondary cell walls. The latter is formed when cell growth and division have ceased, and lignin is also present to provide stiffness and structural stability. The former is typical of growing cells, making them thinner and more flexible. In this case, lignin is absent, and pectin is present. Pectin is also the main component of the middle lamella, providing adhesion and flexibility [93,97].

Orange waste biomass is particularly rich in pectin, and this feature is widely explored for valorization routes (traditionally, pectin isolation and, recently, orange waste-based films) [9,99]. Pectin is a branched, anionic, and water-soluble polysaccharide, predominantly composed of homogalacturonan (HG) (at least 65%), in which D-galacturonic acid units are linked by α(1→4) glycosidic bonds, and its carboxyl groups are partially methyl-esterified or acetylated (Figure 2.3e) [20,21,25]. It can be classified as either high methoxyl (HM) or low methoxyl (LM) depending on the degree of esterification (DE): 50–75% in the former and below 50% in the latter [21,99].

In addition to HG, the main structural components of pectin include xylogalacturonan (XGA), rhamnogalacturonan-I (RG-I), and rhamnogalacturonan-II (RG-II), which are branched segments composed of

other neutral sugars besides D-galacturonic acid (Figure 2.3e and f) [21]. The DE, monosaccharide composition, molecular weight, and branching degree of pectin may vary depending on its origin and extraction method [20].

Pectin exhibits a typical ability to gel in aqueous solutions. At pH levels below 3.0–3.5 (pKa of pectin's carboxylic acid groups), gelation occurs due to molecular entanglements stabilized by hydrogen bonds and hydrophobic interactions (acid gelation) [25,27]. At pH above 3.0–3.5, its non-esterified groups become deprotonated, forming carboxylates ($RCOO^-$). The addition of cations, such as Ca^{2+}, promotes ionic crosslinking between molecules (ionic gelation).

2.2.3 Orange waste valorization

When not landfilled, the orange biomass waste from juice production is typically destined for low-added-value uses, frequently incineration for energy recovery and cattle feed production [3,85]. Currently, industries can extract and purify the essential oil from orange peels, while a small share of the latter is used to extract pectin for commercial/industrial purposes [7]. Nevertheless, most of the biomass is still discarded or underutilized in these scenarios.

Research on orange waste valorization includes the production of biochar [100,101] and biofuels [102], but focuses heavily on extraction methods of components of interest; including biopolymers like pectin, (nano)cellulose, and hemicellulose, and active compounds like essential oils and phenolic extracts [9,10]. These components find applications in the food, cosmetics, and pharmaceutical sectors, while also presenting great potential for developing bioplastics (i.e., biodegradable and/or bio-based polymer-based materials). Biopolymers usually exhibit film-forming properties and have been extensively studied as bio-based and biodegradable alternatives to fossil-based and non-biodegradable plastics, especially concerning single-use applications. In addition, essential oils and phenolic extracts have been incorporated into biodegradable/compostable polymers (either synthetic or natural) to provide functional properties (e.g., antioxidant, antimicrobial) [9,10].

Recently, upcycling agri-food side-streams in their integrity (or “bulk” waste, i.e., without chemical extraction and/or purification processes) into new bio-based materials has emerged as a promising strategy [8]. In addition to valorizing waste produced at an industrial scale, this approach offers a wide range of advantages: i) reducing the use of harsh chemicals involved in extraction processes; ii) utilizing the biomass as a whole, thus mitigating “new” waste generation; and iii) saving processing operations and time [8,16].

One widely explored direction in this context is the use of orange waste as fillers in polymeric matrices for tailored properties and reduced cost, using either natural (e.g., gelatin [103], sodium alginate [104] , and starch [105,106]) or synthetic polymers (e.g., poly(butylene succinate-*co*-adipate) [107], poly(lactic acid) [108–111], and poly(vinyl alcohol) [112]). A different approach was recently reported, where the juice residual pulp was plasticized with glycerol via extrusion and further melt-blended with poly(butylene adipate-*co*-terephthalate) [113] and poly(butylene succinate) [19].

Over the past few years (2017-2025), studies have demonstrated that all-orange waste cast films can be produced [11–15,17,18,86]. Generally, the residue is dispersed in acid solutions (acid hydrolysis pre-treatment) to disrupt the plant tissue and partially extract biopolymers into the liquid phase, mainly pectin, enabling the formation of a cohesive matrix upon drying. Citric acid has been frequently used, in most cases coupled with heat treatments (35-70 °C) [11–15,86] (see example in Figure 2.4a), and sometimes with physical treatments like sonication [86], high-speed homogenization [14], or ultrafine grinding [13]. Acetic acid [17] and hydrochloric acid (HCl) [18] were also investigated for the same purpose. Lastly, homogeneous films from orange biomass waste were obtained without acid via hydrothermal processing in an autoclave (Figure 2.4b) [16]. Glycerol was employed as a plasticizer in these studies, with only a few exceptions [15,17]. Other additives have been used to modify mechanical and barrier properties, such as cross-linking agents [12,15], other natural polymers (e.g., gum arabic [114] and plasticized chitosan [115]), and nanoparticles [86,114].

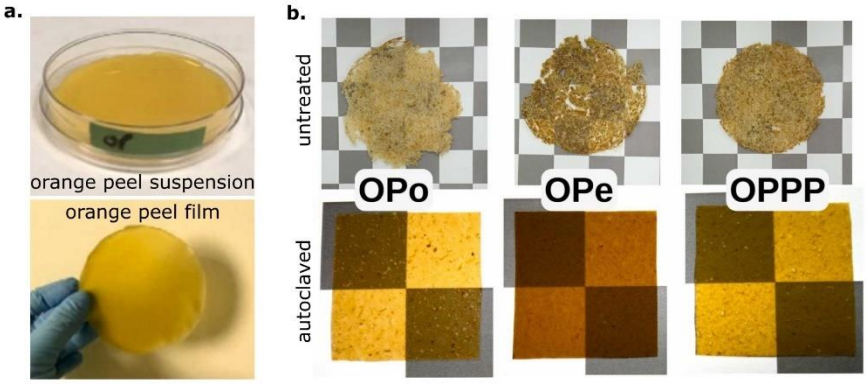

Figure 2.4: (a) Orange peel-based suspension (5%) prepared in 0.1 M citric acid at 35 °C, and film obtained after drying. Reproduced from [15] with permission from Elsevier. (b) Films were obtained from untreated and autoclaved orange waste, namely orange pomace (OPo), orange peel (OPe), and mixed pomace, peel, and finisher pulp (OPPP). Reproduced from [16] with permission from Elsevier.

The first orange waste-based cast films were reported by Bátori and co-authors [11], who produced films from orange peels (2%) hydrolyzed in 1% citric acid solutions at 70 °C, and plasticized with 7% glycerol. Peels were first washed with water to remove soluble sugars, as unwashed biomass was reported to give rise to brittle and heterogeneous films. Macroscopic holes and stratified morphologies were observed in the oven-dried films due to phase separation issues. An incubator shaker was used to perform drying under continuous rotation, resulting in a smoother texture with only microscopic voids. In a subsequent study [12], the preparation conditions previously described were modified to circumvent heterogeneity issues. Authors investigated the effects of acid gelling of the endogenous pectin (i.e., pectin extracted from orange waste into the liquid phase) in the presence of D-(+)-glucose, and of incorporating maleic anhydride as a cross-linking agent. Only the latter led to a more homogenous and compact morphology, although results did not suggest chemical cross-linking. A more recent study from the same research group [13] demonstrated the particle size effects on the mechanical properties of orange (and ginger) waste-based films: multiple cycles of ultrafine wet grinding reduced

the size of insoluble particles, thereby enhancing their reinforcing effect on the pectic matrix.

The effect of particle sizes, resulting from dry grinding, on the properties of cast films from orange (and pomegranate) peels was evaluated by Karakus and co-authors [14]. Different citric acid (3 and 5%) and glycerol concentrations (7 and 10%) were investigated as well, while the orange peel content was kept at 2%. Overall, increased levels of citric acid and glycerol reduced the films' tensile strength, but the particle size did not show a clear influence. The ionic gelling of the endogenous pectin in orange peel-based cast films was also evaluated [15]. Dried and ground peels were hydrolyzed in 0.1 M citric acid at a 5% concentration. Then, the pH of the resulting suspension was adjusted to 4.5, and gelling was promoted by adding 0.6 mmol calcium chloride ($CaCl_2$) or calcium carbonate ($CaCO_3$). Gelling with $CaCl_2$ enhanced the films' stiffness, whereas $CaCO_3$ improved their moisture resistance.

The valorization of orange waste into all-biomass waste materials is a recent research topic and has advanced significantly for cast film production, yet remains largely underexplored for developing porous materials. Few studies reported producing porous materials based on orange waste via freeze-drying [49,50] or supercritical drying [42]. In all cases, they are either directly dried (i.e., without pre-treatment) [49] or coupled with polymeric matrices/binders (e.g., starch [50]) or cross-linkers, such as aminated MXene [116]). Other citrus wastes (e.g., pomelo and grapefruit peels) have been explored as precursors for porous materials using similar strategies [52,68,117,118] and hydrothermal pre-treatments [51,53]. A comprehensive literature review on porous materials based on neat biopolymers and agri-food wastes is provided in Chapter 3.

Research on bulk orange waste-derived films has shown that acid hydrolysis is a suitable pre-treatment for harnessing the high pectin content of orange biomass waste [13,15]. In this context, heterogeneous systems are employed as precursors (i.e., suspensions), and phase segregation emerges as a critical factor in the production of homogeneous 3D porous materials, as targeted in this work. Hence, a brief review of biomass-based suspensions and their properties, focusing on kinetic stability, is presented in the next Section.

2.2.4 Biomass-based suspensions

Suspensions derived from plant biomasses, generally aqueous, have been used to obtain films [11–15,17,18,86], coatings [15,93], emulsions [119–121], and porous materials [51,77,118,122]. One challenge of this approach is that the insoluble phase, dispersed in a continuous liquid medium, sediments with time, leading to macroscopic phase separation [11]. Dispersed systems are, in general, thermodynamically unstable and susceptible to aggregation, sedimentation, coalescence, and other destabilization mechanisms. When these processes occur at sufficiently low rates, remaining negligible within a timeframe appropriate for the intended application, the system can be considered kinetically stable. Hence, the term stability may, in some cases, refer specifically to the kinetic stability, as also adopted throughout the present study [123]. The kinetic stability is influenced by the viscosity and density of the continuous phase, interparticle interactions (including steric hindrance, van der Waals interactions, and hydrogen bonding), particle-solvent interactions (e.g., solvation/hydration), and the shape, density, and size distribution of the dispersed phase [123].

Enhancing the stability of agri-food biomass-based suspensions typically requires some degree of modification of the plant tissue to adjust the suspensions' physicochemical and rheological properties, seeking to achieve appropriate stability levels for the envisioned applications [121]. Studies on beetroot residual pulp- [120] and soybean waste-based suspensions [121] showed that the combination of different pre-treatments (sonication combined with either heating or microwaving; and ball-milling combined with high-pressure treatments, respectively), enhanced suspension stability and increased the size of insoluble particles. For soybean waste suspensions, increased viscosities were also achieved after the pre-treatments [121]. Results suggested that the disruption and the structural loosening of the plant tissue led to more open structures with higher surface areas, which favored the exposure of hydrophilic groups and the hydration of insoluble particles, as well as the extraction of biopolymers into the aqueous phase. The authors concluded that the stability of

the suspensions was closely related to the morphology and hydration capacity of the insoluble fractions, along with the composition of the liquid phase [120,121].

Depending on size, morphology, and concentration, swollen insoluble particles can form interconnected networks through physical bonds and entrap the liquid phase [124]. Such structures can increase the viscosity and storage modulus of suspensions, as observed in orange biomass-based suspensions [125,126]. The presence of soluble pectin can further amplify this effect. It has been suggested that pectin may act as a binding agent, similarly to its role in the middle lamella of plant tissues, facilitating the formation of three-dimensional networks of swollen insoluble fibers [124,127].

Bruno et al. [128] compared untreated citrus biomass (species not informed) suspensions with those treated with high-shear rates or high-pressure treatments. Both treatments increased suspension stability compared to the untreated biomass, although the latter was more efficient. The high-pressure treatment decreased particle size, whereas high-shear rates led to the opposite effect. Suspensions' complex modulus was improved by increasing the citrus biomass fraction and the speed of the high-shear pre-treatment, whereas the high-pressure intensity did not alter the rheological properties significantly. Authors argued that the high-pressure pre-treatment is more efficient in breaking down aggregates, enhancing particles' ability to interact with water and form more compact networks, thereby reducing mobility in the systems and phase separation kinetics. However, increasing the pressure did not lead to additional improvements. Optical micrographs showing said networks of disrupted citrus particles are shown in Figure 2.5.

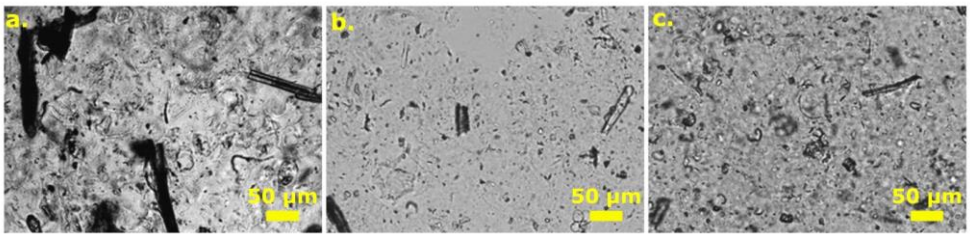

Figure 2.5: Optical micrographs of 1% citrus biomass suspensions subjected to the (a) high-shear treatment with a speed of 8,000 rpm, and high-pressure

treatments with (b) 1020 atm, and (c) 1700 atm of pressure. Reproduced from [128] with permission from Elsevier.

Other studies investigated the effects of various pre-treatments on citrus biomasses [126,129] and their suspensions' physicochemical properties [125,130], but with no correlations with their stabilities. Different methods have been explored (i.e., alkali treatments [126,129], high-shear [126,129,130], and high-pressure homogenization [125]) to obtain suspensions with potential applications in the food sector as rheology- and texture-modifying agents, and as natural emulsion stabilizers [126,131,132].

The acid hydrolysis with citric acid has emerged as an efficient and non-hazardous method to produce cast films from orange waste biomass, and studies have focused on the properties of the resulting films [11–15,86]. The stability of biomass suspensions becomes critical when used as precursors for 3D materials, and phase separation issues have been reported even when producing films [11]. Nevertheless, the effects of acid hydrolysis, as a pre-treatment for citrus biomass, on the resulting suspensions and aiming at the production of novel materials has not been investigated to date.

2.2.5 Concluding remarks

Overall, existing literature on biomass-based suspensions suggests that their stability is heavily influenced by the biomass composition, the insoluble content, and the insoluble fraction's morphology and hydration/swelling capacity. In this context, the present Chapter examines the biochemical composition of the orange biomass waste and its fractions (peels, bagasse, and pulp), and their conversion into aqueous suspensions with optimized kinetic stability, to enable the preparation of 3D porous materials (as explored in Chapter 3). A mild hydrolysis with citric acid pre-treatment is employed. Various processing parameters (biomass washing or non-washing, biomass and citric acid concentrations, biomass fraction type) influencing the orange waste-based suspensions' stability are investigated and correlated with preparation

parameters and suspension properties (e.g., rheological behavior, insoluble fractions' content, swelling capacity).

2.3 Materials and Methods

2.3.1 Materials

Orange (*Citrus sinensis*, variety Pera Rio) waste biomass from juice production was donated by JBT Company (Araraquara, Brazil). The waste was obtained using the JBT FoodTech system [91], which follows the process described in Section 2.2.1 and presented in Figure 2.2.

The orange waste was received in three fractions, namely: peels (flavedo and albedo), bagasse (core, segment walls, and small amounts of seeds and peels), and residual pulp (juice sacs) (Figure 2.6a). As informed by the provider, the bulk orange waste biomass consisted of 56% peels, 28% bagasse, and 16% residual pulp (hereafter referred to as "pulp"). A mixture of such fractions at their respective percentages was also used and referred to as "mixed".

Absolute ethanol (99%; Fisher), anhydrous citric acid (Synth), hydrochloric acid (HCl) (37%; Synth), sulfuric acid (H_2SO_4) (Merck).

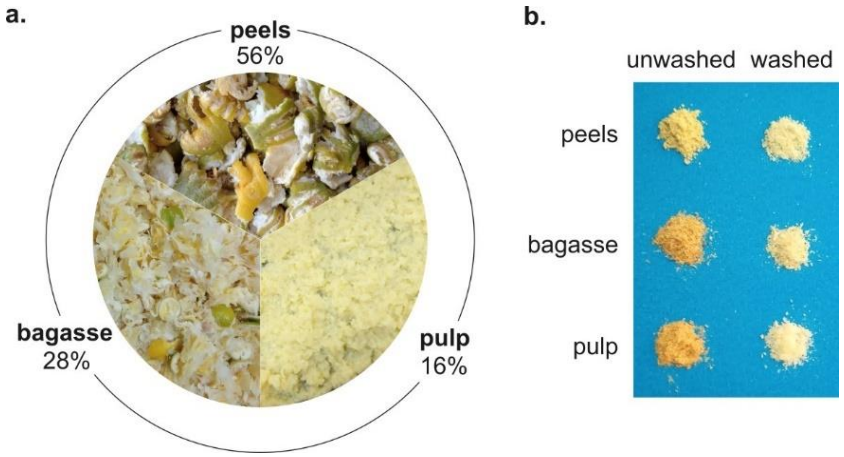

Figure 2.6: (a) Biomass fractions used in this work and their respective mass percentages in the bulk orange waste. (b) Unwashed and washed biomass fractions after drying and grinding.

2.3.2 Orange waste biomass preparation

Each biomass fraction was soaked overnight and rinsed with tap water to remove impurities and soluble sugars [11]. This procedure was repeated, and the biomass fractions were dried (48 h, 45 °C, air-circulating oven), ground in liquid nitrogen, and sieved (mesh 35, 500 µm). Lastly, the biomass was dried at 45 °C under vacuum for 5 h to remove condensed water and labeled “washed”. The same drying procedures were applied to the neither soaked nor rinsed biomass, named “unwashed”. Figure 2.6b presents images of the dried and ground biomass fractions.

2.3.3 Orange waste biomass characterization

2.3.3.1 Dry matter content

The dry matter content of each biomass fraction (washed and unwashed) was determined, in triplicate, using a Marte ID-50 moisture analyzer. Samples were heated to 105 °C, and the dry mass was recorded once the mass variability was within 0.5% for 30 s.

2.3.3.2 Water-soluble content

To assess the efficiency of the washing procedure in removing soluble sugars, washed or unwashed mixed biomass (1 g) was added to 150 mL of distilled water and stirred for 24 h at 23 °C. Solids were collected by vacuum filtration, dried (105 °C, 15 h), and weighed. The water-soluble content was calculated, in triplicate, with Eq. 2.1:

$$water - soluble\ content\ (\%) = 1 - \frac{m_{RT}}{m_i} \times 100 \qquad (2.1)$$

where m_{RT} was the mass of the dried solids collected after extraction, and m_i the initial orange waste mass, dry basis.

The biochemical composition of the washed biomass fractions was evaluated as their suspensions boasted higher stability (see Section 2.4.1).

2.3.3.3 Extractives content

The content of extractives in each washed biomass fraction was determined by Soxhlet solvent extraction. First, the filter paper was dried (air-circulating oven, 105 °C, 15 h) and weighed. Each fraction (2 g) was then placed inside the filters, and subjected to 6 h-Soxhlet extractions using ethanol followed by distilled water (4-5 cycles per hour). Extractions were performed in triplicate, and Eq. 2.2 was used to calculate the content of extractives:

$$extractives\ (\%) = \frac{m_{ext} - m_{fil}}{m_i} \times 100 \qquad (2.2)$$

where m_{ext} was the mass of the filter with the extracted sample after drying, and m_{fil} was the dry filter mass.

2.3.3.4 Pectin content

Pectin content in each washed fraction was determined by acid hydrolysis extraction [16] in a 0.032 M HCl (pH=1.5) solution, at a liquid/solid ratio of 50, 95 °C, and under vigorous stirring, for 1 h. Vacuum filtration was applied to the biomass dispersed in HCl, and the liquid phase was stored in a separate vessel, while the solids were collected. Solids were then subjected to another hydrolysis cycle with the abovementioned conditions. Vacuum filtration was applied again for phase separation. Pectin was precipitated from the liquid phase from both hydrolysis cycles with cold acidified ethanol (1 mL of 37% HCl to 374 mL of ethanol, resulting in 0.032 M HCl), filtered under vacuum using filter paper, rinsed twice with pure ethanol, dried in Petri dishes (air-circulating oven, 105 °C, 15 h), and weighed. The pectin content in each biomass fraction was calculated in triplicate with Eq. 2.3:

$$pectin\ (\%) = \frac{m_{pec} - m_{dish}}{m_i} \times 100 \qquad (2.3)$$

where m_{pec} was the mass of the dried Petri dish with the extracted pectin, and m_{dish} was the mass of the Petri dish.

2.3.3.5 Cellulose, hemicellulose, and lignin contents

Extractive- and pectin-free washed biomass fractions were used to determine the content of cellulose, hemicellulose, and lignin according to the NREL/TP-510-42618 procedure [133]. All analyses were performed in triplicate. Briefly, each biomass fraction (0.3 g) was hydrolyzed in 72% H_2SO_4 (3 mL), at 30 °C, for 1 h. Samples were then diluted with 84 mL of distilled water and autoclaved at 121 °C and 1.2 kgf/cm² for 1 h. Once the samples were cooled down, vacuum filtration was applied. The retained solids were dried and weighed to determine the acid-insoluble lignin content with Eq. 2.4.

$$acid\ insoluble\ lignin\ (\%) = \frac{m_{lig} - m_{ash}}{m_{epf}} \times 100 \qquad (2.4)$$

where m_{lig} was the mass of dried acid-insoluble lignin, m_{ash} the content of ash (see Section 2.3.3.6), and m_{epf} was the mass of extractive- and pectin-free biomass on a dry basis.

The liquid fraction was used to determine the acid-soluble lignin, cellulose, and hemicellulose contents. The acid-soluble lignin content was calculated via UV-visible spectroscopy (BEL, UV-M51) at 280 nm, using Eq. 2.5.

$$acid\ soluble\ lignin\ (\%) = \frac{A_{280} \times DC \times V}{m_{epf} \times \varepsilon_{lig}} \times 100 \qquad (2.5)$$

where A_{280} was the absorbance at 280 nm, DC the dilution coefficient, V the hydrolysate volume (86.73 mL), and ε_{lig} the absorptivity coefficient (25 L/g.cm) [133]. Acid-soluble and acid-insoluble lignin contents were summed and reported as the total lignin content.

Cellulose and hemicellulose were depolymerized into their constituting sugars (monomers) during the hydrolysis with H_2SO_4, of which concentrations in the hydrolysate were determined with High-Performance Liquid

Chromatography (HPLC), using a Waters chromatograph equipped with a refraction index detector (Waters 2414) and a Biorad Aminex HPX-87P column. The analysis was conducted at 85 °C, using ultrapure water as mobile phase, with a flow rate of 0.6 mL/min, and an injection volume of 20 µL. Calibration curves were built using the following standards: glucose (cellulose monomer), xylose, mannose, arabinose, and galactose (hemicellulose monomers). Eq. 2.6 was used to calculate their concentrations.

$$cellulose/hemicellulose\ (\%) = \frac{C_{DC} \times F_{AC} \times V \times 10^{-3}}{m_{epf}} \times 100 \qquad (2.6)$$

where C_{DC} was the corresponding sugar(s) concentration obtained via HPLC in mg/mL, already corrected for the dilution coefficient, F_{AC} was the anhydro correction factor used to convert the monomeric sugar concentration to polymeric sugar concentration (0.88 for pentoses, and 0.90 for hexoses), V the filtrate volume (86.73 mL), and m_{epf} the mass of the extractive- and pectin-free sample [133].

2.3.3.6 Thermogravimetry and ash content

The thermal decomposition behavior of washed and unwashed biomass fractions was evaluated via thermogravimetric analyses (TGA), carried out using a TA Instruments Q50 device. Samples (15-17 mg) were heated from 30 to 600 °C at 5 °C/min under nitrogen flow (60 mL/min), followed by a 10-min isotherm under oxygen flow (60 mL/min). To complete the compositional analyses, the average ash content of washed biomass fractions was calculated in triplicate using Eq. 2.7.

$$ash\ (\%) = \frac{m_{600}}{m_i} \times 100 \qquad (2.7)$$

where m_{600} was the sample mass after the isotherm at 600 °C, under an oxidative atmosphere.

2.3.4 Suspension preparation

Orange biomass waste (washed or not) was added to citric acid aqueous solutions (the concentration of biomass varied from 1 to 4 wt%, and of citric acid from 0 to 5 wt%) and hydrolyzed at 90 °C, under vigorous stirring, for 2 h (Figure 2.7). Suspensions containing individual biomass fractions were labeled “peels”, “bagasse”, and “pulp”. Suspensions were also prepared by mixing the three different fractions in their respective percentages in the bulk biomass (Figure 2.6a) in citric acid; these were referred to as “mixed”.

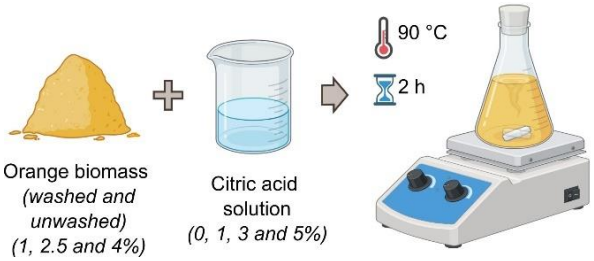

Figure 2.7: Schematic illustration of biomass suspension preparation via acid hydrolysis. Created with BioRender.com.

2.3.5 Suspension characterization

2.3.5.1 Kinetic stability

Suspensions consisted of an aqueous phase with a dispersed insoluble fraction, comprising fibers and particles that sedimented over time. To make homogeneous aerogels, this phase separation should be avoided. Bench stability tests were performed with 35 mL of suspensions prepared under various conditions (washed and unwashed biomass, and different biomass and citric acid concentrations) for 3 d at 23 °C. Three days were selected as it is the average duration of solvent exchange needed to prepare aerogels (see Chapter 3, Section 3.3.2.1).

Kinetic stability was calculated in triplicate using Eq. 2.8:

$$kinetic\ stability\ (\%) = \frac{V_s}{V_i} \times 100 \qquad (2.8)$$

where V_s was the volume of the sedimented insoluble fraction, and V_i was the total volume (35 mL). Graduated tubes were used to measure the volumes.

2.3.5.2 Rheological behavior

Steady-state rheological analyses of the obtained suspensions were conducted with Couette geometry (2-mm gap) using a TA Instruments ARES rheometer at 23 °C. Shear rate sweeps ranged from 0.1 to 500 s^{-1}.

2.3.5.3 Insoluble content

The insoluble content of suspensions was determined as reported in [134]: the samples were centrifuged to separate the insoluble fraction from the liquid phase (7698 *g*, 10-15 min), followed by washing with citric acid solutions twice (at the same concentrations as used for suspension preparation), and then with distilled water until the supernatant reached pH 6. The samples were centrifuged at 7698 *g* between washings for 10-15 min. The insoluble fraction was dried under vacuum at 105 °C for 15 h and weighed (m_{ins}). The insoluble fraction content was calculated in triplicate with Eq. 2.9.

$$insoluble\ content\ (\%) = \frac{m_{ins}}{m_i} \times 100 \quad (2.9)$$

2.3.5.4 Water holding capacity (WHC)

The WHC of the insoluble fractions was calculated, in triplicate, using Eq. 2.10 [119] and by measuring the mass of the hydrated (m_h) and dried (m_d) insoluble fractions: m_h was obtained by separating the insoluble fraction from the suspension via centrifugation at 7698 *g* for 15 min, draining excess liquid by inclining the centrifuge tubes at ca. 60 °C for 10 min, and weighing; m_d was obtained by drying the insoluble fractions at 50 °C under vacuum until constant weight.

$$WHC\ (g\ /g\ ) = \frac{m_h - m_d}{m_d} \quad (2.10)$$

2.3.5.5 Insoluble fraction morphology

The morphology of insoluble fractions was assessed by optical microscopy using a Keyence VHX 7000 digital microscope (100 and 150x magnifications). The insoluble fractions were washed and dispersed in 45 mL of water. Dispersions were then diluted with water (dilution factor = 5) and sandwiched between glass slides before observation.

2.3.5.6 Attenuated Total Reflectance – Fourier-Transform Infrared Spectroscopy (ATR-FTIR)

The liquid and insoluble fractions of the suspensions were separated by centrifugation, and the polysaccharides present in the liquid phase were precipitated with ethanol. After drying, these polysaccharides and the insoluble fraction were analyzed by ATR-FTIR, using a Thermo Nicolet Avatar 370 spectrometer. Spectra were collected in the wavenumber range from 4000 to 525 cm^{-1}, with 50 scans, and a 2-cm^{-1} resolution.

2.3.5.7 Fourier-Transform Raman Spectroscopy (FT-Raman)

The polysaccharides precipitated from the liquid phase and insoluble fractions (see previous Section) were also analyzed by FT-Raman. Spectra were collected on a Bruker MultiRAM spectrometer with a Nd:YAG laser (1064 nm) (1024 scans, from 3500 to 33 cm^{-1}, 4 cm^{-1} resolution).

2.4 Results and Discussions

2.4.1 Orange waste biomass composition

Thermogravimetric (TG) and derivative thermogravimetric curves (DTG) of washed and unwashed biomass fractions are presented in Figure 2.8. Until 100 °C only sample dehydration occurred, which was followed by biomass decomposition at different stages, as shown by the DTG curves (Figure 2.8b and d): I – decomposition of volatile and low-molecular-weight components,

observed at ca. 150°C; II – decomposition of pectin at ca. 210-230 °C, overlapped with that of hemicellulose moieties; III – hemicellulose complete decomposition (ca. 250°C); IV – cellulose decomposition (320-330 °C); and V – lignin's broad decomposition peak (250-550 °C) with contributions from that of cellulose as well [17,135].

The shoulder assigned to stage I was observed only for the unwashed samples, and the decomposition peaks of the structural components (stages II-V) were more distinct in the curves of washed biomass fractions. Washing removed low-molecular-weight substances that are soluble in water at room temperature, such as soluble sugars, organic acids, and certain flavonoids [136,137].

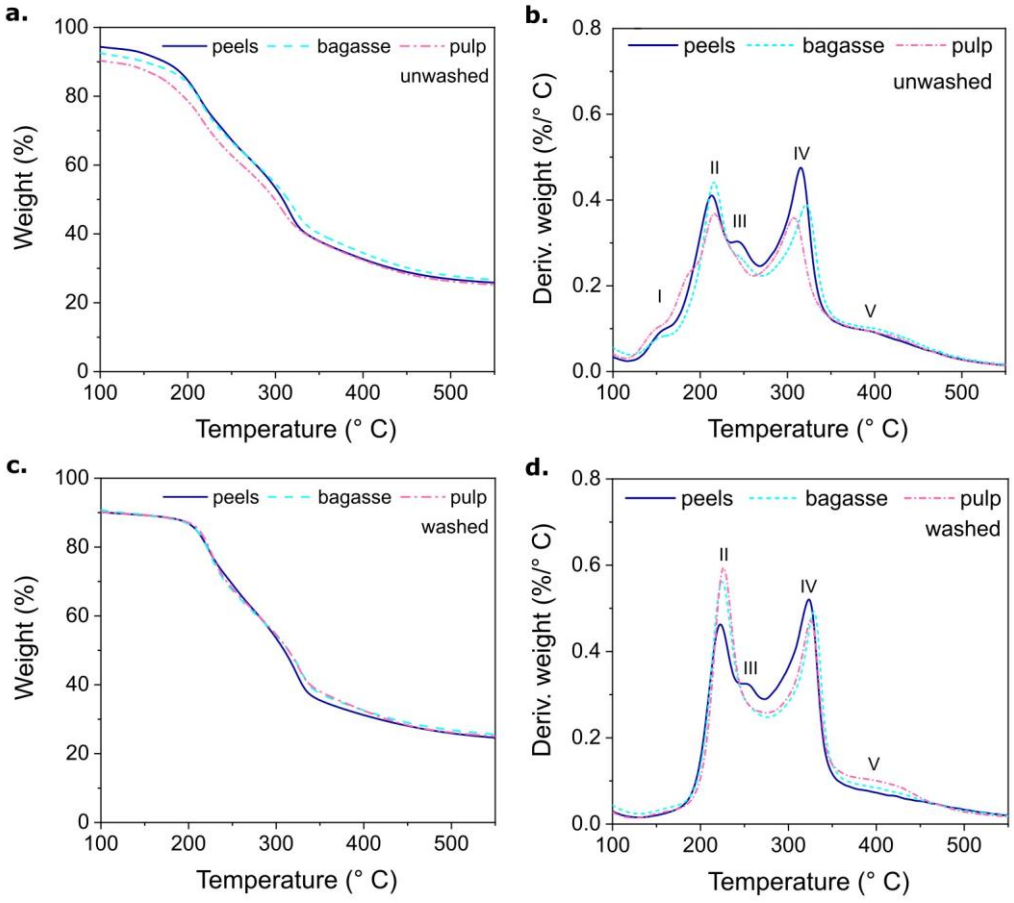

Figure 2.8: TG (left) and DTG (right) curves for each biomass fraction (a, b) unwashed and (c,d) washed.

The presence of low-molecular-weight molecules was detrimental to the stability of biomass suspensions (see Section 2.4.2.1), therefore, washed biomass fractions were chosen to further investigate the orange biomass waste composition. Results are shown in Table 2.1.

Orange biomass extractives were primarily polar and soluble in water and ethanol [95], including pigments (mainly carotenoids, but also chlorophyll and xanthophylls), terpenes and terpenoids from the essential oil, phenolic acids (e.g., caffeic, ferulic, coumaric, and sinapinic acids) and flavonoids (mainly hesperidin, naringin, narirutin, and eriocitrin) [2,88]. Orange waste biomass is a conventional source for pectin extraction and has been recently investigated for cellulose isolation as well due to their high contents, although values reported vary due to biomass variability (variety, ripeness, etc.) [5,10]. Previous studies have reported pectin dry mass fractions ranging from 15 to 40% [6,138,139]. At the same time, the cellulose content ranged from 8 to 37% [138,139].

Table 2.1: Composition of the washed orange biomass fractions.

Components	**Biomass (wt%)**			
	Mixed	**Peels**	**Bagasse**	**Pulp**
Ethanol extractives	7.1 ± 0.8	7 ± 1	8.4 ± 0.2	5.7 ± 0.4
Water extractives	30.7 ± 0.9	29 ± 1	34 ± 1	30.8 ± 0.8
Pectin	36 ± 1	35 ± 3	40.5 ± 0.6	32 ± 2
Cellulose	12.8 ± 0.4	14.9 ± 0.7	8.5 ± 0.1	13.2 ± 0.4
Hemicellulose	4.2 ± 0.2	4.8 ± 0.3	3.0 ± 0.3	4.3 ± 0.1
Lignin	5.3 ± 0.7	5 ± 1	2.8 ± 0.4	10 ± 1
Ashes	2.9 ± 0.7	3 ± 1	2.1 ± 0.3	3 ± 1
Total	99	99	99	99

A study from Santos et al. [16] investigated the same biomass fractions (obtained from the same variety and company, Pera Rio and JBT Company, respectively), from which cast films were obtained. Results revealed similar

compositions for each biomass fraction, albeit the content of extractives was higher, as no washing step was conducted.

Hemicellulose and ash contents were low and nearly the same for all biomass fractions. The lignin content varied between the biomass fractions, yet remained overall lower than that of pectin, cellulose, and extractives.

The high pectin content of the orange biomass fractions was confirmed (32-40%) and in accordance with the literature [6,16,95]. When targeting materials development, this feature has been exploited to produce cast films, frequently using acid hydrolysis as biomass treatment [11,14,17,18]. Pectin is easily removed from the biomass into the aqueous phase in acidic media and under high temperatures (75-100 °C), while cellulose, hemicellulose, and lignin remain predominantly insoluble under such conditions [11,16,92]. As a consequence, phase separation was an issue observed in the literature [11], and also faced in preliminary tests during this work.

2.4.2 Orange waste biomass suspensions' properties

A preliminary visual screening of 2.5% biomass suspensions (mixed, peels, bagasse, and pulp) in 3% citric acid (conditions initially determined based on the literature [11,15,17,114]) revealed insoluble fraction sedimentation. Therefore, the production of homogeneous aerogels, one of the main objectives of this work, was unfeasible. To find the conditions leading to non-separated suspensions for up to 3 d (time needed to complete solvent exchange, see Chapter 3, Section 3.3.2.1), the stability and properties of mixed biomass suspensions were investigated by varying the washing/non-washing of the biomass, and biomass and citric acid concentrations. After the optimal conditions in terms of stability of mixed biomass suspension were found, the stability and properties of suspensions made from each biomass fraction were investigated using the selected conditions.

2.4.2.1 Influence of biomass washing and concentration on suspension properties

First, the citric acid concentration was maintained at 3%, and the stability of the mixed biomass suspension was investigated as a function of biomass concentration and the washing/non-washing step. As shown in Figures 2.9a and b (values are also shown in Table A.1 of the Appendix A), suspension stability was favored by the washing step and increased biomass concentrations. For example, the stability (Eq. 2.8) of samples containing 4% washed mixed biomass was within 93-98% after three days, compared to only 40% for 1% unwashed suspensions.

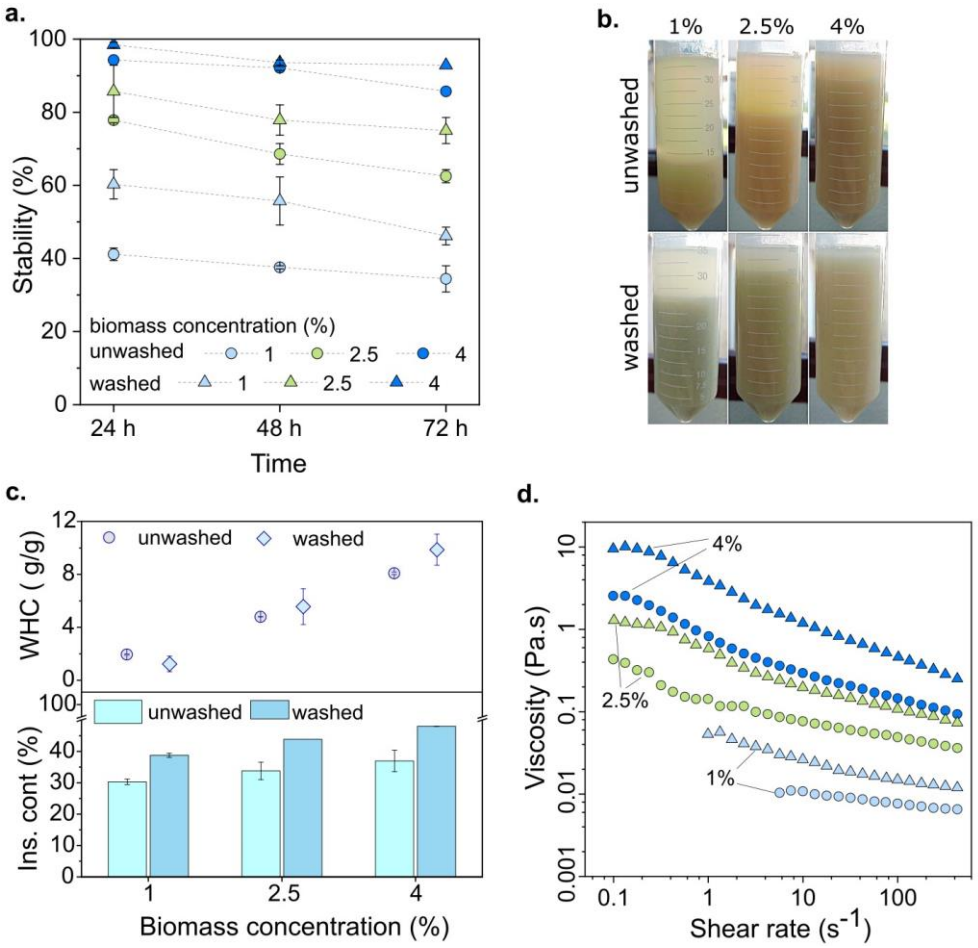

Figure 2.9: (a) Stability of mixed biomass suspensions over time, (b) digital images of suspensions after 72 h, (c) WHC and insoluble content as a function of biomass concentration for washed and unwashed samples, and (d) viscosity

vs. shear rate of suspensions of mixed washed (triangles) and unwashed (circles) biomass at different concentrations. Acid concentration was 3%.

The insoluble content (Eq. 2.9) increased with biomass concentration, and was lower for unwashed biomass suspensions (30-37%) when compared with their washed counterparts (39-48%) (Figure 2.9c and Table A.1). Washing removed low-molecular-weight substances (e.g., soluble sugars, organic acids, and some flavonoids) [136,137]: the room-temperature water-soluble content of the non-hydrolyzed orange biomass decreased from 47.4±0.3% for unwashed to 17±1% for washed samples. For the same biomass concentration, the proportion of biopolymers solubilized in the liquid phase was higher in the washed biomass-based suspensions than in those from their unwashed counterparts.

The insoluble fractions' swelling capacity, expressed in WHC (Eq. 2.10), increased with biomass concentration (Figure 2.9c and Table A.1). Higher biomass concentration may have favored inter-particle collisions, which are hypothesized to induce inter-particle friction and breakage. As a result, the surface area of particles potentially increased, improving water accessibility, followed by swelling and an increase in WHC. The WHC was not significantly affected by the washing step (Figure 2.9 c and Table A.1).

The flow curves of washed and unwashed mixed biomass suspensions at different biomass concentrations are presented in Figure 2.9d. Suspensions' exhibited shear-thinning behavior and viscosities increased with biomass concentrations owing to the greater inter-particle friction. Higher viscosities were also observed for washed biomass suspensions compared to their unwashed counterparts, due to the removal of water-soluble, low-molecular-weight compounds during washing, thereby increasing the concentration of biopolymers in the liquid phase. Increased viscosities slowed down sedimentation and enhanced suspension stability.

Previous studies [120,121] have reported that swollen plant fibers can form three-dimensional networks by interacting with each other and immobilizing the aqueous phase within these networks. This contributes not

only to the different rheological behavior, but also to the entrapment of the liquid phase, thereby limiting phase separation. A more pronounced shear thinning behavior at higher biomass concentrations (Figure 2.9d) may also reflect the presence of such networks and their disruption under shear stresses, in addition to the orientation of solubilized biopolymer molecules under flow.

2.4.2.2 Influence of citric acid concentration on suspension properties

Samples containing 4% washed mixed biomass boasted the best kinetic stability among those analyzed. However, some phase separation was still observed within the first day (98%), and suspension stability decreased to 93% after three days (Figure 2.9a and b). It was previously demonstrated that increasing acid concentration enhanced pectin extraction to the aqueous phase [92], which may increase the liquid phase viscosity and improve the suspensions' stability. Thus, the influence of citric acid concentration on suspension stability, WHC, and insoluble content was investigated. The mixed biomass concentration was maintained at 4%.

Increased acidity improved the stability of washed mixed biomass suspensions (Figure 2.10a and b, and Table A.2), which could be attributed to the enhanced extraction of pectin into the liquid phase. The viscosity was increased with higher acid concentration (Figure 2.10d), although the insoluble content decreased from 74% in the absence of citric acid to about 45% at 5% acid (Figure 2.10c and Table A.2), also suggesting higher pectin content in the continuous phase. Literature proposes that pectin may play an important role in improving the kinetic stability of biomass suspensions by acting as a "binder" and structuring the network of insoluble swollen fibers [124]. WHC of the insoluble fraction varied from 10 to 13 g/g, and did not depend on acid concentration within the experimental errors (Figure 2.10c and Table A.2).

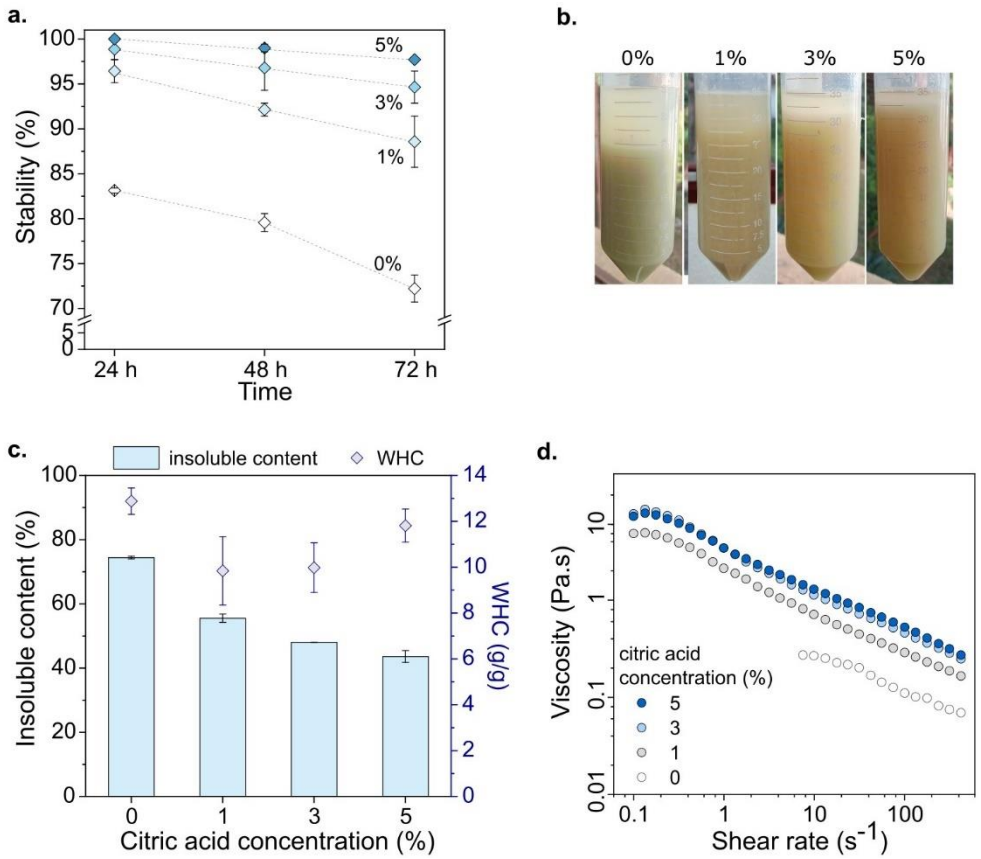

Figure 2.10: (a) Suspension stability over time, (b) Digital images of suspensions after 72 h, (c) WHC and insoluble content, and (d) viscosity vs. shear rate for the suspensions of 4% washed mixed biomass at different citric acid concentrations.

2.4.2.3 Influence of the biomass fraction type on suspension properties

Since the suspensions with 4% washed mixed biomass and 5% citric acid remained stable during the first 24 h and with 98% stability after 72 h (Figure 2.10a), these conditions were used to analyze the properties of suspensions made from each biomass fraction (namely, peels, bagasse, and pulp). The bagasse- and pulp-based suspensions showed higher stability (Figure 2.11a and b, and Table A.3) and slightly higher WHC than the peel-based suspension (Figure 2.11c), which exhibited the lowest viscosity (Figure 2.11d). The insoluble content was the same for all biomass suspensions within experimental errors (Figure 2.11c and Table A.3).

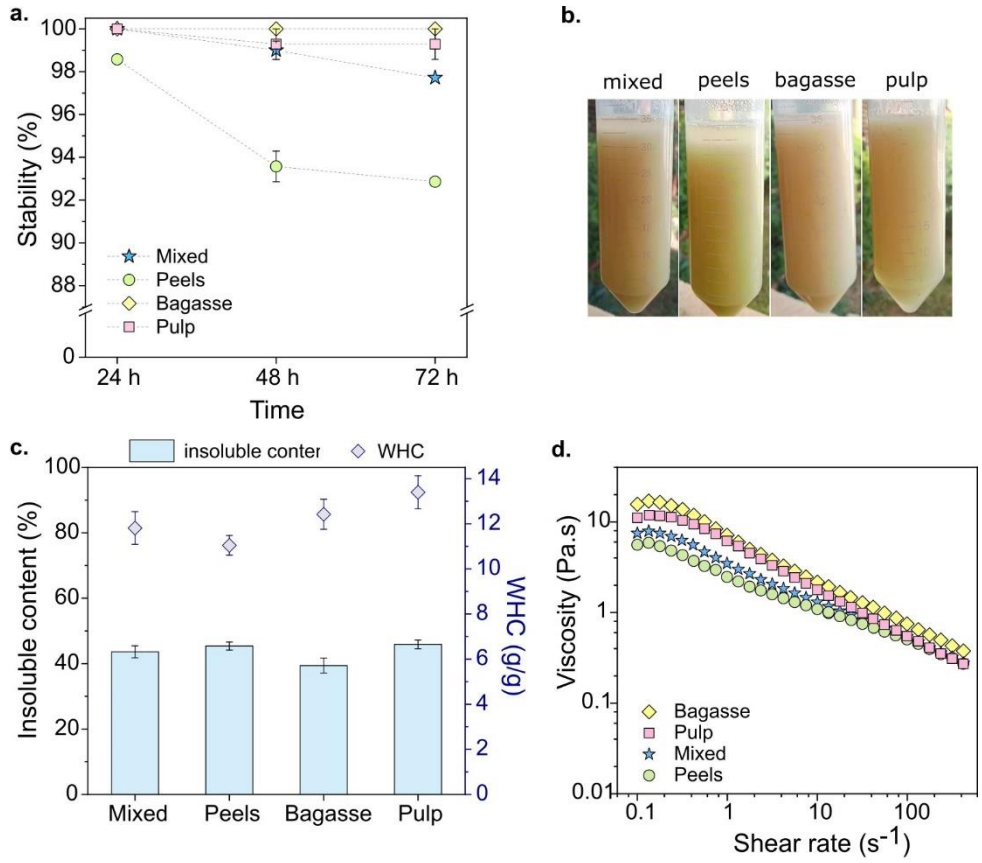

Figure 2.11: (a) Stability over time, (b) digital images of suspensions after 72 h, (c) WHC and insoluble content, and (d) viscosity *vs* shear rate for the suspensions containing different biomass fractions. Biomass and acid concentrations were 4% and 5%, respectively.

Optical microscopy images (Figure 2.12a) indicated that all suspensions had swollen particles of varying dimensions. The suspension from bagasse exhibited a high fibrillation extent, whereas the pulp-based one contained both particles and fibers (Figure 2.12b). Peels' insoluble fraction was denser and fragmented into smaller particles (Figure 2.12a).

Bagasse had the highest content of extractives and pectin, and the lowest cellulose content compared to the other biomass fractions (Table 2.1). Cellulose is more recalcitrant to the pre-treatment used compared to extractives and pectin [97]; and removing middle lamellae biopolymers, like pectin, was previously linked to fibrillated morphologies of flax fibers [87]. The high degree of fibrillation of the bagasse insoluble fibers was possibly influenced by their composition (Table 2.1), and contributed to the higher stability and viscosity of

bagasse suspensions. Although the pulp and peels had similar contents of cellulose, pectin, and extractives; the pulp tissue is thinner and softer than the peels, in addition to being previously disruption during juice extraction [7,42]. These aspects may have facilitated its fibrillation and pectin extraction into the aqueous phase, thus contributing to the higher stability, viscosity and WHC of pulp-based suspensions.

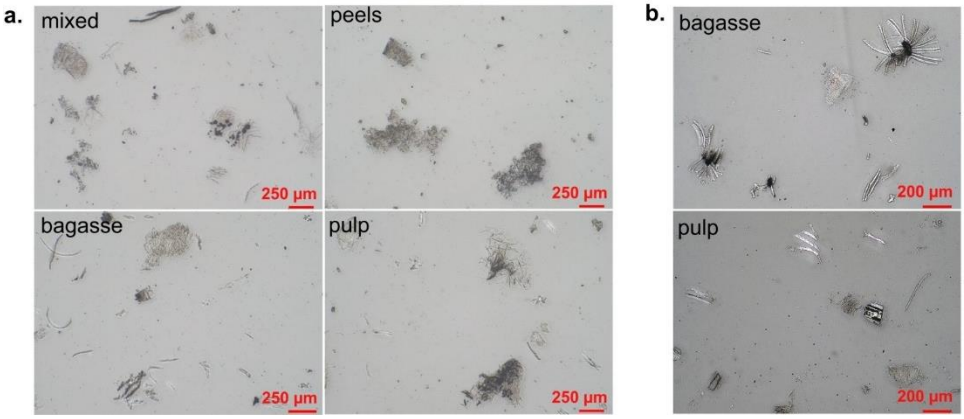

Figure 2.12: (a) Optical micrographs of the insoluble fractions, and (b) zoomed in on bagasse and pulp fibrillated fibers from diluted suspensions prepared with 3% biomass and 5% citric acid (see Section 2.3.5.5).

FTIR and FT-Raman spectroscopies (Figure 2.13) further evidenced pectin extraction to the liquid phase as a result of the citric acid pre-treatment, while cellulose, hemicellulose, and lignin remained in the insoluble fraction.

FTIR spectra (Figure 2.13a) showed that, when compared with the insoluble fraction, the polysaccharides precipitated from the liquid phase presented higher intensities in bands attributed to the pectin structure: 1700-1750 cm^{-1} and 1630 cm^{-1}, assigned to the C=O stretching vibrations of ester bonds and carboxylate ions; as well as typical signals from pectin units' ring vibration at 833, 873, 1230, 1320, 1390, and 1100 cm^{-1} (mostly galacturonic acid but also mannose, glucose, and/or galactose) [140–142].

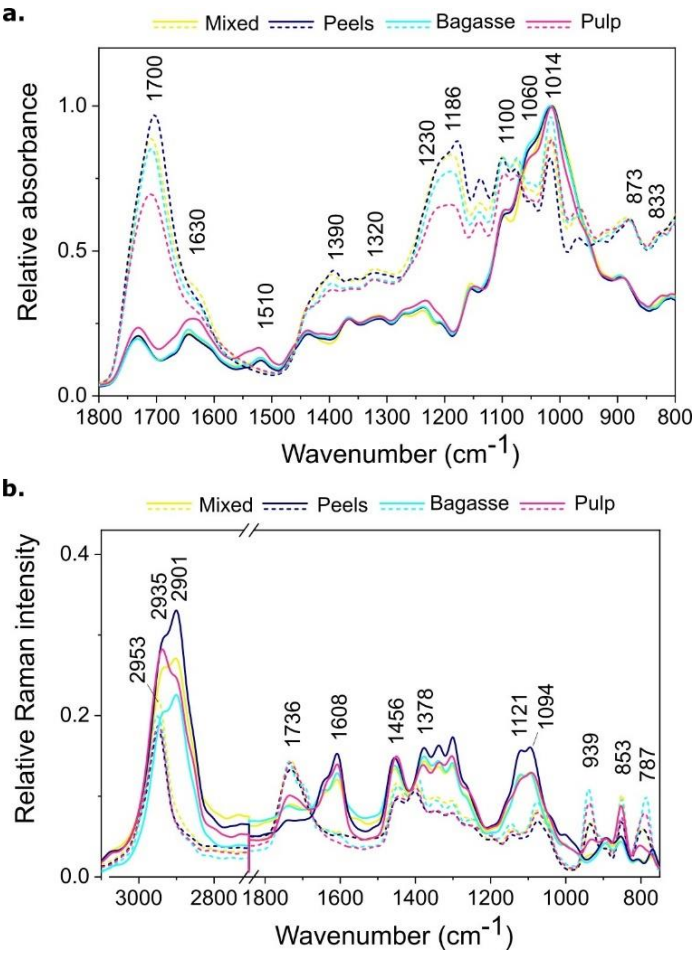

Figure 2.13: (a) FTIR and (b) FT-Raman spectra of the insoluble fraction of the suspensions (solid) and the polysaccharides precipitated from the liquid phase (dashed) for the different biomass fractions.

The band around 1000-1014 cm^{-1} is attributed to stretching vibrations of C-C and C-O groups present in cellulose, hemicellulose, and pectin backbones, as well as to cellulose CH_2OH groups, which would explain its strong intensity in all spectra [140,142]. Bands that were more prominent in the insoluble fractions' spectra are associated with cellulose and lignin, which likely remained insoluble after the acid hydrolysis procedure (C–OR stretching vibrations at 1060 cm^{-1} and lignin aromatic rings' C=C vibrations at 1510 cm^{-1}, respectively [95,143]).

FTIR results were corroborated and complemented by FT-Raman spectroscopy (Figure 2.13b). High-intensity bands in the 3100-2800 cm^{-1} region, typically assigned to C-H stretching vibrations of pectin, hemicellulose, and cellulose (2953, 2935, and 2091 cm^{-1}, respectively) were observed. The first

was exhibited by the spectra of polysaccharides precipitated from the suspensions' liquid phase, whereas the other two were present in the insoluble fractions [141,144]. Other bands assigned to pectin moieties had higher intensities in the spectra of the precipitated polysaccharides. The typical band centered at 853 cm^{-1} is attributed to the skeletal vibration of pectin's α-glycosidic bonds [144], and those at 939 and 787 cm^{-1} were previously associated with galactan and arabinogalactan, respectively [141].

In addition, bands typically assigned to cellulose (1378 cm^{-1}, bending vibrations of HCC, HCO and HOC groups; and 1121 and 1094 cm^{-1}, glycosidic bonds stretching) and hemicellulose (1456 cm^{-1}) had higher intensities for the insoluble fraction samples. The C=O stretching vibration band centered at 1736 cm^{-1} is assigned to both pectin and hemicelluloses [144]. Surprisingly, the insoluble fractions showed higher intensity at 1608 cm^{-1}, which can be associated with calcium pectate [145]. This suggests that pectin was not fully extracted to the liquid phase, as molecules bound to the middle lamella by ionic interactions might have been more resistant to the citric acid pre-treatment.

2.5 Conclusions

Given that one of the main objectives of this thesis was the fabrication of homogeneous 3D aerogels, the kinetic stability of the suspensions used as their precursors emerged as a critical aspect. Accordingly, the kinetic stability of the suspensions was investigated to select the optimal preparation conditions. Correlations between suspensions' preparation parameters, physicochemical properties, and stability were explored by varying biomass preparation (washing or non-washing), and biomass and acid concentrations. In addition, the influence of biomass fraction type on suspensions' properties was also evaluated.

The biochemical composition of each orange biomass fraction was examined. Only washed fractions were investigated for their composition, as it was observed that their suspensions presented superior stability than those from unwashed biomass. All fractions were predominantly composed of

extractives, pectin, and cellulose, bearing lower contents of hemicellulose, lignin, and ashes. Their high pectin content (32-40%) provides great potential for their conversion into materials with pectin as a continuous phase, and acid hydrolysis proved to be a suitable pre-treatment to overcome biomass recalcitrance. Citric acid was chosen for a safe and “green” process.

The stability of the resulting suspensions was greater for washed biomass and higher concentrations of biomass and citric acid. Washing removed low-molecular-weight substances, while higher biomass concentrations increased the viscosity and the water-holding capacity of the insoluble fractions. Higher acidity enhanced pectin extraction and decreased the insoluble content. The influence of the biomass fraction (peels, bagasse, and pulp) on suspension stability was also evaluated. Pulp and bagasse suspensions had higher stability and viscosity, which were associated to fibrillated insoluble fractions and higher WHC.

Finally, the preparation conditions yielding suspensions stable enough to enable the production of macroscopically homogeneous aerogel monoliths were achieved: washing biomass with water, 4% biomass, and 5% citric acid. These conditions were then adopted for the production of orange waste-based porous materials, aerogels and cryogels. The impact of different processing routes on their morphological features and properties are presented in the next Chapter.

CHAPTER 3 – POROUS MATERIALS FROM ORANGE WASTE BIOMASS: PROCESSING ROUTE-MORPHOLOGY-PROPERTIES CORRELATIONS

3.1 Introduction

Bio-based aerogels and cryogels (see definitions in Chapter 1) are open-pore, lightweight (< 0.2 g/cm³) solid materials derived from renewable sources. These materials have been investigated for a wide range of applications, including thermal and acoustic insulation, adsorption of water pollutants, controlled drug delivery, and sustainable packaging [20,29].

Bio-based aerogels and cryogels are mostly produced from neat polysaccharides [30,146]. As previously mentioned, isolating these biopolymers from bulk biomass entails some drawbacks (e.g., discarding valuable parts of the biomass, the use of harsh chemicals, and multiple operational steps). These issues can be mitigated by using bulk biomass (i.e., without fractionation or purification) as starting matter instead [8,16].

Orange waste has been successfully repurposed into cast films [11–15,17,18,86] owing to its high pectin content [13,15,19]. Only a few studies explored its conversion into porous materials [42,49,50,116], yet the influence of the processing conditions and the use of acid hydrolysis pre-treatments to leverage its high pectin content on the porous materials' properties remains unexamined. The pore structure and properties of bio-based aerogels and cryogels are strongly correlated with the drying technique and other processing parameters, such as the type of biomass, pre-treatment, non-solvent for aerogels, freezing temperature and ice growth direction for cryogels, and others [27,42,44,147].

The previous Chapter (Chapter 2) explored the preparation and properties of kinetically stable suspensions from different orange biomass fractions (mixed, peels, bagasse, and pulp – see Section 2.3.1) using a citric acid pre-treatment to create a pectin-rich continuous phase, which can act as matrix for self-standing materials upon drying. Turning biomass waste into suspensions prior to producing porous materials may thus facilitate the

production of differently shaped 3D materials, which is another aspect that has not been explored in the literature [42,49,50,116].

Given this context, this Chapter explores how different processing routes influence the properties and morphological features of porous materials, aerogels and cryogels, produced from orange waste suspensions.

3.2 Theoretical Background and Literature Review

3.2.1 Aerogels and cryogels

The term “aerogel” was coined by S.S. Kistler in the early 1930s, when he synthesized the first aerogels, including the most widely known silica aerogel, but also those derived from other precursors, such as inorganic materials (e.g., alumina, nickel tartrate, and ferric, tungstic, or stannic oxides) or organic (e.g., cellulose, agar, gelatin, and egg albumin) [148,149]. In his studies, Kistler explains aerogels simply as dry gels, i.e., gels containing air instead of a liquid within their porous networks [148,150].

Currently, aerogels are defined by the IUPAC (International Union of Pure and Applied Chemistry) as microporous solids (pore diameter below 2 nm) derived from wet gels [151]. However, this is a rather restrictive approach and generally not adopted in modern literature. Instead, the term aerogel typically refers to materials bearing very low density (< 0.2 g/cm³), high porosity (> 90%), and high specific surface area (> 100 m²/g), although there is still no formal consensus. In this context, aerogels encompass a wider range of nanostructured mesoporous (2–50 nm in diameter) and macroporous (> 50 nm in diameter) materials [31,150]. The latter definition is herein adopted.

Aerogels are traditionally obtained via sol-gel processes followed by supercritical drying using CO_2. When other drying methods are employed, such as evaporative and freeze-drying, the resulting materials are commonly referred to as xerogels and cryogels, respectively [25,30], terms also adopted in this thesis. It should be noted that it is possible to achieve high-surface-area

aerogels via freeze-drying [37] or evaporative drying [34,35,152], although such cases remain exceptions.

Evaporative drying typically leads to the collapse of the wet network due to increasing capillary forces during solvent evaporation. Such forces arise from strong intermolecular interactions between the solvent and the pore walls, exceeding cohesive forces within the solvent itself, and are manifested by the presence of a concave meniscus [30,153]. Quantitatively, the capillary pressure is expressed by the Young–Laplace equation (Eq. 3.1):

$$P_c = \frac{2\gamma \cos\theta}{R} \quad (3.1)$$

where P_c is the capillary pressure, γ is the interfacial tension between the liquid and gas phases, θ is the contact angle between the solid and liquid phases, and R is the pore radius [30,153]. Figure 3.1 illustrates capillary forces acting inside an individual pore and the variables involved in Eq. 3.1.

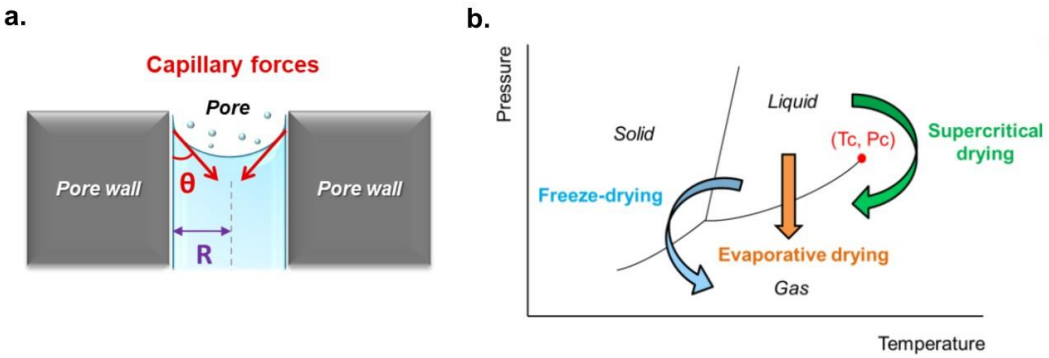

Figure 3.1: (a) Schematic illustration of capillary forces acting on a pore filled with liquid. (b) Schematic illustration of different drying procedures. Reproduced from [153].

Supercritical drying and freeze-drying are the preferred methods for producing porous materials, as they prevent capillary pressure that stems from liquid evaporation. The former is characterized by a transition of a liquid into its supercritical state, in which there is no liquid-gas interface (see Figure 3.1b). This allows for the evacuation of the solvent without drastic changes in the wet

gel structure, giving rise to the typical open-pore, nanostructured, and interconnected morphology of aerogels [25,30,31]. Usually, CO_2 is used for drying in supercritical conditions owing to the mild temperatures and pressures required (35-50 °C and 8-20 MPa, respectively), which is particularly important for making aerogels from polysaccharides [146,154].

One critical aspect of the supercritical drying is that the solvent within the wet gel network must be miscible with supercritical CO_2. For biopolymers, the initial solvent/dispersant is usually water; hence, a solvent exchange step is required prior to supercritical drying. Ethanol and acetone are commonly used, which are also non-solvents for most biopolymers. As a consequence, they can trigger a non-solvent-induced phase separation (sometimes also referred to as “coagulation”), enabling the formation of a stabilized network without a prior gelation step. In some cases, gelation is still carried out to strengthen the wet gel structure, and control the resulting dried gel properties [25,30,31].

Freeze-drying, in turn, consists of freezing the wet material (solutions, dispersions, or gels) followed by solvent sublimation (solid-gas transition, see Figure 3.1b). During freezing, polymer chains are segregated by the ice crystals’ growth front and ultimately compacted at their boundaries once impingement occurs, thereby templating the porous structure. As a consequence, cryogels typically exhibit sheet-like pore walls and large pores (up to dozens and/or hundreds of microns), yielding lower specific surface areas and densities compared to aerogels [25,30,31].

Figure 3.2 illustrates the common routes to prepare aerogels and cryogels, and the typical resulting morphologies.

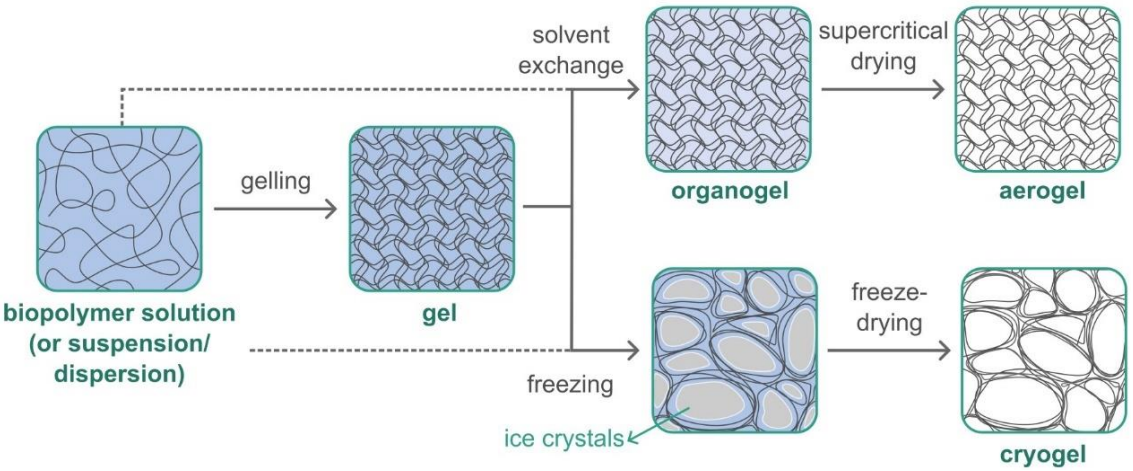

Figure 3.2: Illustrative flowchart of common preparation processes, drying routes, and resulting morphologies of aerogels and cryogels.

Bio-based aerogels, also called “bio-aerogels”, represent a new generation of organic aerogels derived from renewable resources, like biomass and/or neat biopolymers, extracted from biomass. These materials have been systematically investigated over the past two decades [22]. Similar to the more traditional types of aerogels (e.g., silica, resorcinol-formaldehyde, and synthetic polymer-based aerogels), bio-based aerogels are nanoporous solid materials with high porosities (> 90%), low densities (0.02–0.3 g/cm^3), and high specific surface areas (100–600 m^2/g) [20,22,155].

Freeze-drying has also been employed for producing bio-based cryogels. These materials are suitable for applications involving acoustic and electrical insulation, water remediation, tissue engineering, drug delivery, packaging, among others [20,29] Mainly polysaccharides have been used as starting matter for bio-based aerogels and cryogels, with cellulose, chitosan, and alginate being at the forefront of the scientific output in recent years [30,146], but proteins and lignin have also been explored [20,55] (Figure 3.3a).

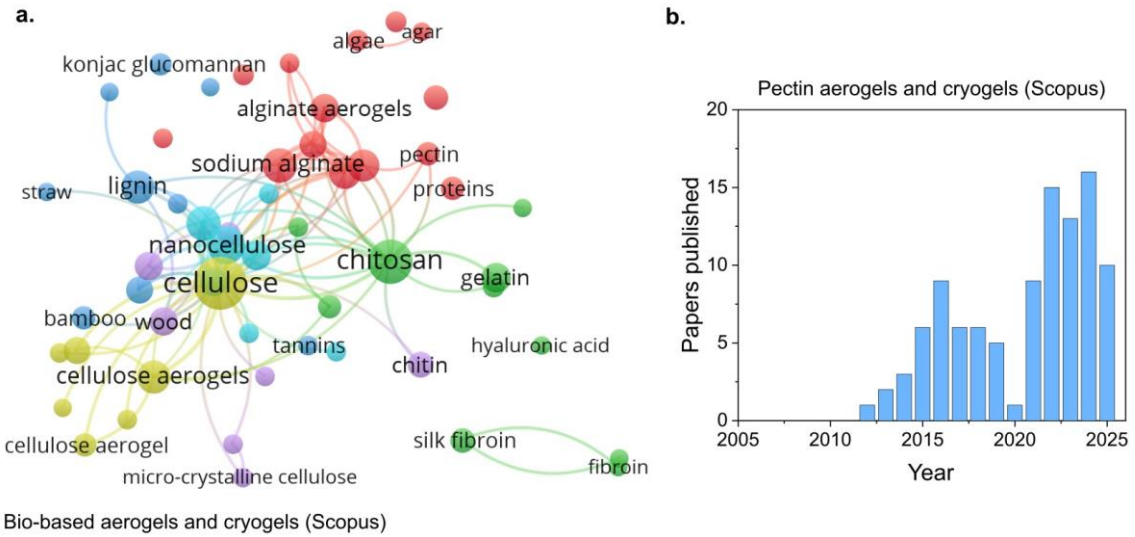

Figure 3.3: (a) A key-word occurrence map of bio-based aerogels and cryogels' starting matter[1], and (b) Publication volume on pectin aerogels and cryogels per year[2]. Data was taken from Scopus-indexed publications in the last 20 years (see footnotes).

Pectin-based aerogels and cryogels represent an emerging research topic, with a rapid growth in literature starting from 2012 in Scopus-indexed journals (Figure 3.3b). Their remarkable and tunable properties make them sustainable materials with promising technological potential [25,27,44], as discussed in the next Section.

3.2.1.1 Aerogels and cryogels from neat pectin

As previously detailed in Chapter 2 (Section 2.2.2.1), pectin consists of a class of branched, anionic, and water-soluble heteropolysaccharides found in the cell walls and middle lamella of plant tissues. Pectins bear a typical gelling

[1] A key-word occurrence map was built with the VOSviewer software using results from the Scopus query: (TITLE-ABS-KEY (aerogel OR cryogel) AND TITLE-ABS-KEY (bio-based OR biomass OR biopolymer)) OR (TITLE-ABS-KEY (bioaerogel OR bio-aerogel)) AND PUBYEAR > 2004 AND PUBYEAR < 2026 AND (LIMIT-TO (DOCTYPE, "ar")). A 10-fold occurrence threshold
was set, and bio-based starting matter-related key-words were filtered (fillers or synthetic polymers sometimes used as reinforcement were excluded).

[2] Scopus query: (TITLE-ABS-KEY (aerogel OR cryogel OR bioaerogel OR bio-aerogel) AND TITLE-ABS-KEY (pectin)) PUBYEAR > 2004 AND PUBYEAR < 2026 AND (LIMIT-TO (DOCTYPE, "ar"))

ability (either in acid conditions or in the presence of cations) and great potential for the production of aerogels and cryogels [20,21].

Supercritically dried pectin aerogels typically exhibit fibrillar open-pore structure, with nanometric pores and pore walls (Figure 3.4a). Pectin cryogels, in contrast, display sheet-like interconnected macropores due to the compaction of pectin chains induced by ice-templating (Figure 3.4b) [21,26]. As a consequence, the specific surface area of pectin aerogels ranges from ca. 200 to 600 m^2/g, while reaching only a few dozens for pectin cryogels (up to ca. 20 m^2/g) [23,25,27,156]. Density, in turn, remains within a similar range for pectin aerogels and cryogels (0.05-0.2 g/cm^3) [23,27,57].

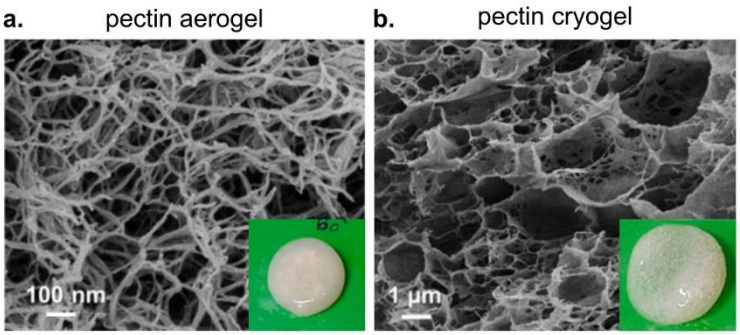

Figure 3.4: Scanning electron micrographs of a pectin (a) aerogel, and (b) cryogel and their respective digital images at the bottom. Samples were prepared from a 6% pectin solution at pH 2.0, and a molar ratio of Ca^{2+} to pectin carboxyl groups of 0.2. Reproduced from [25] with permission of Elsevier.

Only a few studies have dealt with alternative drying methods to produce pectin-based materials with increased surface area. These include freeze-drying after replacing water with tert-butanol solutions (surface area up to 300 m^2/g) [37] and evaporative drying using water/isopropyl alcohol or n-propyl alcohol mixtures (surface area up to 90 m^2/g) [157].

Even when employing supercritical drying alone, several processing parameters can be varied to tailor the morphology and textural properties of pectin-based aerogels. For example, tunable processing parameters include pectin concentration, solution pH (acid gelation or non-gelation), the presence of cations and their concentration (ionic gelation), or templating the pectic

network via non-solvent-induced phase separation of non-gelled solutions [22,27,155,158]. These factors dictate the state of the matter, network stability, and rheological properties prior to solvent exchange, thereby influencing the extent of shrinkage upon solvent exchange and drying, as well as the resulting aerogel properties (e.g., apparent density, pore size, and specific surface area) [27,158].

Groult and Budtova [27] evaluated the influence of pectin concentration, pH, type, and concentration of cations (Ca^{2+} and Na^{+}) on the ultimate textural properties of pectin aerogels. The authors demonstrated that, overall, low-viscosity pectin solutions undergo greater contraction than more viscous solutions and gels in the presence of the non-solvent and upon supercritical drying. Higher shrinkage leads to denser structures with smaller pores, thus providing higher specific surface areas. Similar correlations were also identified when comparing weaker and stronger gels (Figure 3.5).

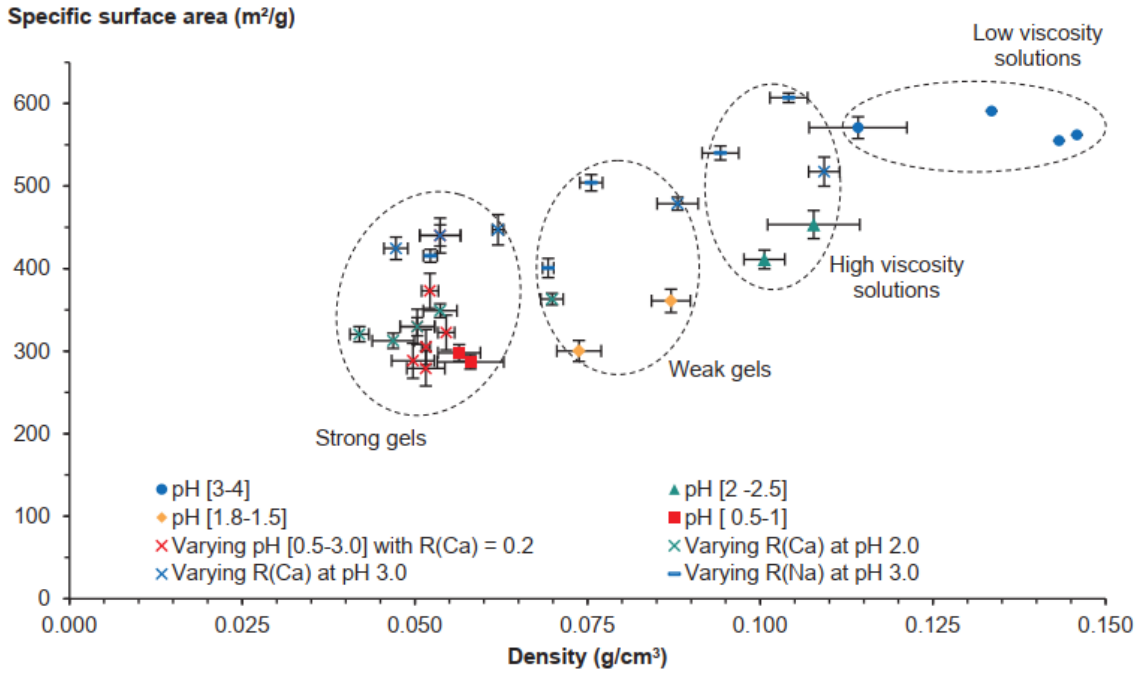

Figure 3.5: Specific surface area vs. apparent (or bulk) density of low-methoxyl pectin aerogels prepared at different conditions. Pectin concentration was 3% and the non-solvent was ethanol. Reproduced from [27] with permission from Elsevier.

Moreover, Figure 3.5 shows that pectin networks formed by ionic gelation with Ca^{2+} shrink less than those gelled in the presence of Na^{+} due to weaker ionic bonding in the latter, giving rise to aerogels with larger pores and reduced specific surface area (ca. 400-520 m²/g vs. 550-600 m²/g, respectively). The ratio R of Ca^{2+} to COO^{-} ranged from 0.1 to 0.6, and the non-solvent was ethanol [27]. In another study [158], lower molar ratios of Ca^{2+} and Sr^{2+} (R = 0.01-0.1) did not influence the aerogels' surface area (230-290 m²/g), albeit the overall linear shrinkage and density exhibited significant variations (ca. 30-50% and 0.08-0.14 g/cm³, respectively). In this case, the non-solvent was acetone.

The non-solvent used can also influence the properties of neat pectin aerogels. Groult and Budtova [27] observed that aerogels obtained using acetone as non-solvent had higher specific surface areas than those using ethanol (approximately 600-630 m²/g vs. 520-600 m²/g, respectively). Pectin concentrations ranged from 3 to 6% and the solution pH was 3.

Different molecular configurations of pectin, like the average molecular weight, branching degree, and degree of esterification, can also impact the volumetric shrinkage during the aerogel preparation steps (solvent exchange and drying) and the ultimate aerogel properties. Higher specific surface area was observed for non-gelled low-methoxyl (LM) pectin aerogels (510 m²/g) when compared to high-methoxyl (HM)-based ones (384 m²/g), while the apparent densities were similar (0.077 and 0.086 g/cm³, respectively). In both cases, the pectic network was formed via non-solvent-induced phase separation using ethanol [28]. Rudaz at el. [22] showed otherwise for aerogels produced via acid gelation: specific surface areas and densities were similar regardless of pectin's degree of esterification (230-270 m²/g and 0.09-0.13 g/cm³). The non-solvent was also ethanol. In addition to the degree of esterification, the influence of pectin's branching degree and molecular weight on Ca^{2+}-gelled pectin aerogel beads was also evaluated. Shrinkage levels were altered, but no significant influence on the aerogels' surface area was observed [155]. It should also be noted that comparison of data from literature is not obvious as, in addition to numerous processing parameters (e.g., polymer concentration, solution pH, gelation or not, type of non-solvent), solvent

exchange routes (placing the sample directly in a non-solvent or stepwise solvent to non-solvent replacement) and supercritical drying conditions (temperature, pressure, depressurization rate) also influence aerogel properties.

Potential applications of aerogels strongly depend on their textural properties. Pectin aerogels have been explored mainly as drug delivery systems [24,155,156,159], but also in the food sector [146] and as functional packaging [39]. Mechanical properties of pectin aerogels have not been widely evaluated in the literature, despite their importance for several practical applications. Reported elastic moduli range from 0.5 to 18 MPa (13 to 107 MPa.cm³/g, when normalized by the apparent density) [22,153], which can be enhanced by incorporating nanoparticles [39].

One promising aspect of pectin aerogels is their potential as superinsulating materials (i.e., materials with thermal conductivity below that of the air in ambient conditions, 0.025 W/m·K). Pectin aerogels with thermal conductivity values ranging from 0.015 to 0.025 W/m·K have been reported [22,26,39,54]. This has been ascribed to the presence of mesopores smaller than 70 nm, which corresponds to the mean free path of air gas molecules (at 25 °C and 1 atm), thereby reducing the gas-phase conductivity within the aerogel to values below that of the air. This phenomenon is known as the Knudsen effect [26,30].

Pectin cryogels do not reach the superinsulation threshold, but still exhibit relatively low thermal conductivities (0.032–0.049 W/m·K) [44], that are comparable to those of conventional expanded polystyrene (EPS) (0.032-0.037 W/m·K) and polyurethane foams (0.021-0.024 W/m.K) [31]. These materials rely on fossil-based feedstocks and pose serious environmental issues when mismanaged [160]. In addition, pectin cryogels have been investigated for food applications [161,162], acoustic insulators [44], water pollutants adsorbents [163,164], and active packaging materials when combined with other components, like cellulose nanofibers [165] and egg albumin [166].

As mentioned above, intrinsic aspects of pectin can influence the cryogel structure. It has been reported that higher molecular weights tend to impair ice crystal growth by immobilizing neighboring water molecules through hydrogen

bonds, thus giving rise to coarser morphologies [167]. Most research focuses on modifying the morphological features and properties of pectin cryogels by applying different preparation conditions [23,44,164,168]. For instance, the ice crystal growth kinetics directly influence cryogel morphologies. Anisotropic pectin porous monoliths with tuned morphological features were produced by directional freezing in the presence of sodium chloride (NaCl), at different concentrations, and using different freezing media [44]. Smaller pores and lower densities were achieved by imposing larger temperature gradients and decreasing salt concentration. Densities ranged from 0.032 to 0.056 g/cm³, and the compressive modulus from 0.9 to 3.7 MPa (or 37-109 MPa.cm³/g). Similar conclusions were drawn by Ma and co-authors [168] for Ca^{2+}-gelled pectin-sucrose hydrogels subjected to isotropic freezing under different temperatures prior to freeze-drying.

Altering the pectin network formation mechanism also brings significant changes to the structure and properties of the resulting cryogels. For example, Nešić et al. [39] evaluated the influence of ionic cross-linking with Ca^{2+}, non-solvent-induced phase separation using a tert-butanol/water solution, and a combination of both mechanisms, in which Ca^{2+} was incorporated into the tert-butanol/water mixture, on pectin cryogels' characteristics. The pore size decreased from 150–400 μm in the first scenario to 10–50 μm in the two latter cases, where tert-butanol triggered phase separation. In contrast, the water solubility of the resulting cryogels was affected solely by ionic cross-linking: after 24 hours, solubility was 100% when gelation was induced exclusively by tert-butanol, but dropped to 5% when Ca^{2+} cross-linking was applied, regardless of the presence of tert-butanol. Chemical cross-linking of pectin using polyethyleneimine and ethylene glycol diglycidylether also led to smaller pores with thicker walls [163]. The compressive elastic modulus was increased at the expense of the ultimate deformation, which was reduced from 50% for non-cross-linked pectin to 20% at a degree of modification of 7.67%, approximately. Chen and co-authors [57], in turn, increased pectin content (2.5-15%) and incorporated clay (0-5%) prior to freeze-drying. As expected, both variables enhanced the cryogels' stiffness (0.04 to 114 MPa, corresponding to 1.3-603

MPa.cm³/g when normalized by density) and increased densities (from 0.03 to 0.18 g/cm³).

The vast majority of studies found in the literature employ neat pectin and other biopolymers (either in molecular form or as colloidal particles) isolated from biomass for the production of bio-based aerogels and cryogels. As previously mentioned, extraction procedures generally entail the use of harsh chemicals, waste generation (including a valuable portion of the biomass), and numerous operational steps [20,55]. The direct conversion of biomass into aerogels and cryogels emerges as a promising alternative to mitigate these drawbacks.

3.2.1.2 Aerogels and cryogels from bulk biomass waste

Studies using bulk agro-industrial biomass waste to produce porous materials are predominantly focused on cellulose-rich biomass waste, like sugarcane bagasse, pineapple leaves, coconut shells, and others [147,169]. Different strategies have been used in this context, mainly alkali and/or bleaching pre-treatments (either prior or *in situ*) [170–172] to separate lignin and hemicelluloses from cellulose. Other biomass processing methods include the mechanical fibrillation of cellulose [173] and its dissolution in ionic liquids [174,175] or lithium chloride/dimethyl sulfoxide solutions [174,176]. Freeze-drying is the most widely explored drying technique, sometimes followed by carbonization [147,169].

Orange peels, specifically, have been directly upcycled into biochar via chemical activation using phosphoric acid or potassium hydroxide, followed by carbonization [100,101], and also freeze-dried to obtain porous materials [49,50,116]. Orange peels, cut and washed with ethanol, were directly freeze-dried before carbonization, creating large macropores of approximately 100-300 µm (Figure 3.6a) [49]. In this case, ice templating is possible due to the inherent high water content of “fresh” orange peels (about 75%), i.e., before any drying [4]. Orange waste collected from cafes (specific parts not reported) was subjected to a similar procedure: peels were washed with water and ethanol, shredded into small particles, oven-dried, and finally freeze-dried prior to

carbonization [50]. In this case, rather dense materials were obtained (a porosity of ca. 20% was estimated by the authors from SEM images, see Figure 3.6b, left) due to the previous oven-drying, hence, starch (2.5-20%) was incorporated as binder to achieve higher porosities (Figure 3.6b, right). Orange peel powders were also cross-linked with aminated MXene prior to freeze-drying, resulting in materials with a surface area of up to 14 m²/g [116]. Other types of citrus waste have been used to produce porous materials via freeze-drying, for example, fresh and cut pomelo peels (albedo only) (Figure 3.6c) [52], hydrothermally treated pomelo peel powders (Figure 3.6d) [51], and autoclaved grapefruit peels [53].

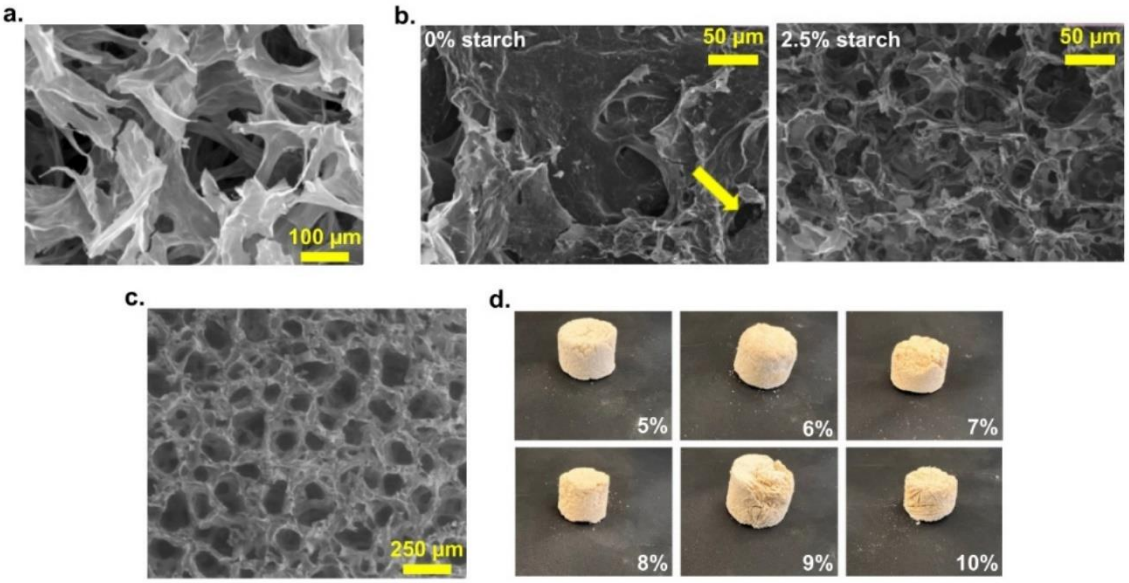

Figure 3.6: (a) Freeze-dried and carbonized fresh orange peels' morphology. Reproduced from [49] with permission from Elsevier. (b) Morphologies of orange peel-based carbon cryogels with 0% and 2.5% starch (left and right, respectively). Reproduced from [50], licensed under CC BY 4.0. (c) Morphology of freeze-dried pomelo albedo. Reproduced from [52], Copyright 2024 American Chemical Society. (d) Digital images of cryogels from pomelo peel powders (particle size of 125 µm) dispersed in water at different concentrations (shown at bottom right). Reproduced from [51], licensed under CC BY 4.0.

A few innovative studies have developed high-surface-area aerogel particles from plant biomass after minimal pre-treatments. Fresh apple pomace and hot-water-washed spent coffee grounds were directly subjected to solvent exchange with ethanol, grinding, and supercritical drying [41]. Resulting in aerogel powders with ca. 200 m^2/g of surface area, and distinct densities (0.016 and 0.19 g/cm^3, respectively). Recently, a similar procedure was applied, except that the plant tissues were thoroughly washed with water and shredded in an aqueous medium using a domestic blender, to a wide range of plant materials, including mostly edible parts (pulps) but also peels [42]. Only powders were produced. Twenty different types of tissues were studied, including pomelo, orange, orange peels, banana peels, nectarine, radish, onion, mushrooms, and others [42]. Specific surface areas ranged from 100 to 350 m^2/g, which the authors attributed to the intrinsic porous structures of plant tissues, albeit acknowledging that such interpretations are limited by the biomass diversity encompassed in this study. Cytoplasmic bridges (for mass transport of nutrients, water, and other substances) and the biopolymer networks, present in the primary and secondary cell wall structures, are cited as examples of such inherent nanoporous structures. Varied morphologies were observed, and those from soft water-rich biomasses resembled the network structure from neat pectin or cellulose aerogels. The visual aspect and internal structure of aerogel powders produced from orange biomasses are shown in Figure 3.7.

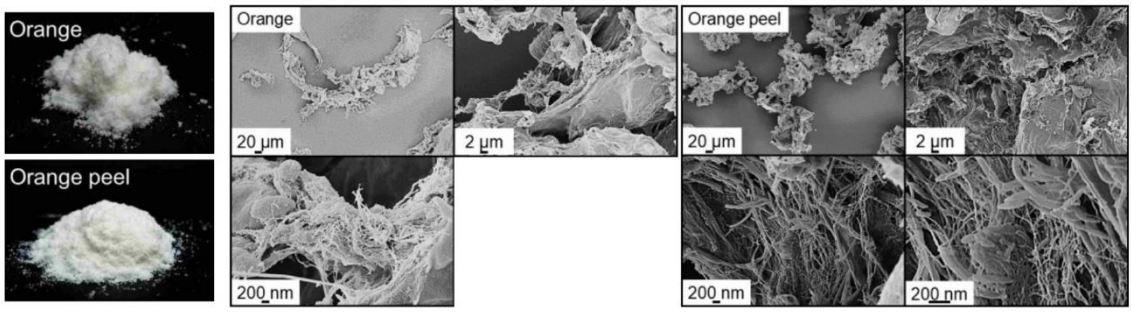

Figure 3.7: Digital images (left) and scanning electron micrographs (right) of aerogel powders from orange pulp (top) and peels (bottom). Reproduced from [42], licensed under CC BY-NC 3.0.

3.2.2 Concluding remarks

In summary, most studies have focused on cellulose-rich bulk biomass wastes to produce mainly cryogels, with aerogels being produced to a lesser extent, while employing pre-treatments that leverage their high-cellulose content. Similar approaches to pectin-rich residual biomasses, like orange juice waste, remain unexamined despite promising results using mild acid hydrolysis to obtain orange peel-based cast films [11–15]. Moreover, the research on nanostructured aerogels from orange waste is very limited, and the effects of using different parts of biomass waste and processing routes are also yet to be explored. Hence, this Chapter discusses the influence of orange biomass fractions (peels, bagasse, pulp, and mixed) on the internal morphologies and properties of cryogel and aerogel monoliths, the latter produced using different non-solvents (ethanol and acetone). Finally, the preparation and properties of aerogel beads made from orange waste were also investigated.

3.3 Materials and Methods

3.3.1 Materials

Orange (*Citrus sinensis*, variety Pera Rio) waste biomass fractions were provided by JBT Company (Araraquara, Brazil): peels, bagasse, and pulp (see details in Section 2.3.1). Each fraction was washed twice with tap water, dried, ground, and sieved (mesh 35, 500 µm) as described in Section 2.3.2.

Commercial low-methoxyl (LM) pectin (GENU pectin type LM-102 AS) was donated by CP Kelco (Limeira, Brazil) and used as received. The degree of esterification was 30%, as informed by the manufacturer, and the molecular weight was estimated as described in Section 3.3.3.6. Absolute ethanol (99%; Fisher) and anhydrous citric acid (Synth) were used.

3.3.2 Porous materials preparation

Porous materials were produced from orange waste biomass suspensions, which were prepared under the optimal conditions selected in

Chapter 2: 4% of washed biomass was mixed into 5% of citric acid solutions and heated at 90 °C, for 2 h, under vigorous stirring (Figure 3.8a). The four orange biomass fraction types were used as starting matter (mixed, peels, bagasse, and pulp – see section 2.3.1). Neat LM pectin was processed using the same procedures to produce reference materials.

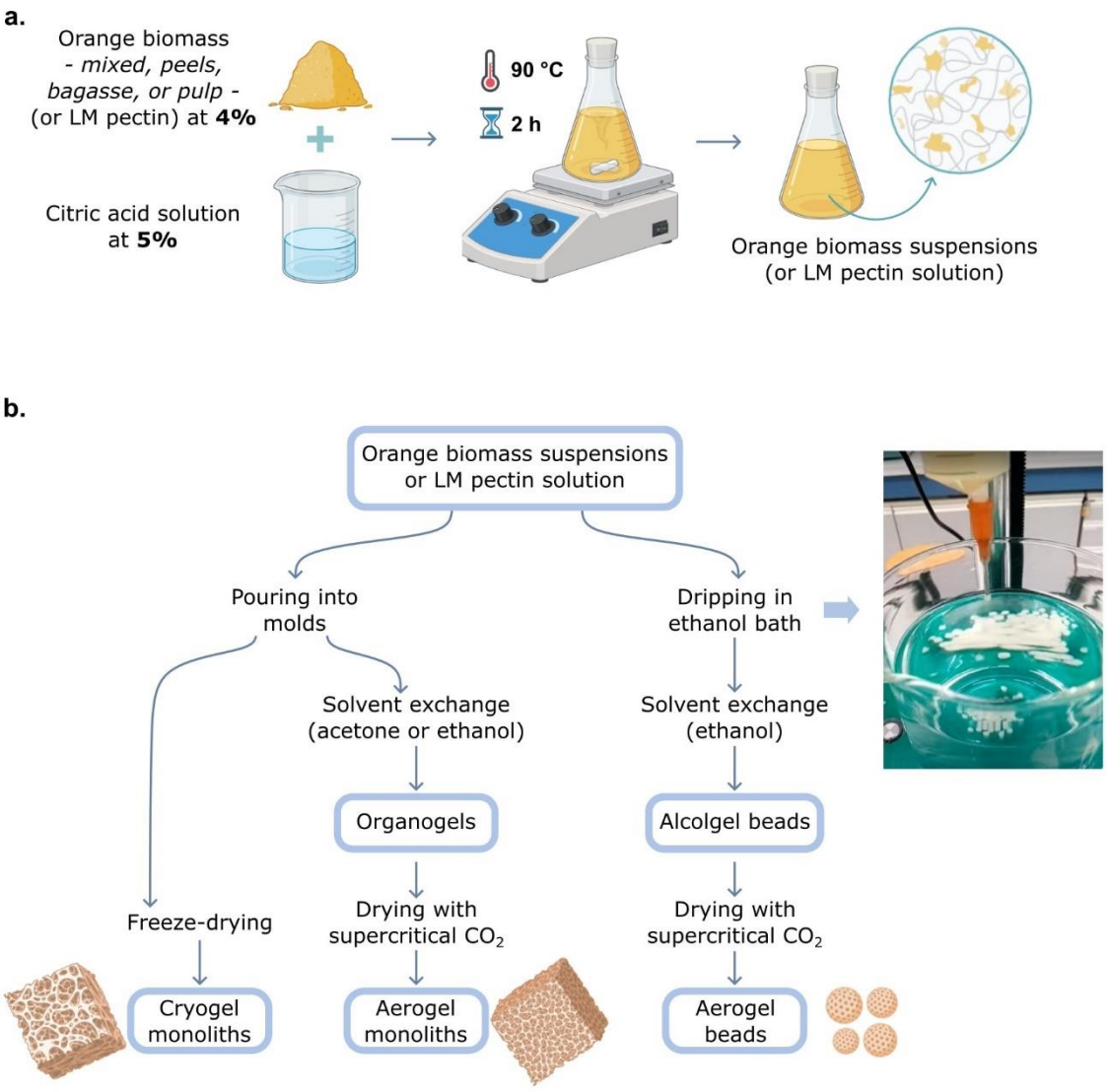

Figure 3.8: (a) Schematic illustration of the suspension preparation conditions. (b) Flowchart illustrating the different processing routes herein employed to obtain orange waste-based porous materials, and a digital image of the beads production (right). Created with BioRender.com.

Different processing routes were carried out with the obtained suspensions: (i) freeze-drying to produce cryogel monoliths, (ii) supercritical drying with CO_2 after solvent exchange with ethanol or acetone, producing monolithic aerogels; and lastly, (iii) mixed biomass was used to investigate the production of aerogel beads as well. Procedures are detailed below and summarized in Figure 3.8b.

3.3.2.1 Preparation of aerogel monoliths and beads

For monoliths, biomass suspensions or LM pectin solutions (see Figure 3.8a) were poured into polypropylene molds, and bubbles were removed after mild centrifugation (24 *g*, 1-4 min). A non-solvent-induced phase separation (or "coagulation") was triggered by carefully covering the suspensions with 50% non-solvent/distilled water solutions, using either ethanol or acetone. Coagulated samples were then subjected to a progressive solvent exchange: the ethanol/acetone ratio was increased to 75% in the following exchange step and then kept at 100% for the remaining washing steps until the water content was below 0.05%. The same procedure was followed to produce LM pectin samples as a reference material.

Organogel beads were produced by the dripping method (Figure 3.8b, image at the right) using mixed biomass suspensions, which were prepared as described above (Figure 3.8a), but diluted with distilled water to avoid clogging during bead production. A dilution factor of 4/3 was used, thus decreasing the biomass concentration to 3%. After bubble removal (24 *g*, 2-3 min), suspensions were carefully poured in a 20 mL syringe coupled with a 15-gauge blunt-tip needle (1.37 mm internal diameter) at about 1 cm from an 8-cm-high ethanol bath. Droplets were produced using a home-made setup, with a Razel R99 syringe pump vertically assembled over a planarly rotating platform, controlled by a frequency inverter Rexroth EFC 5610. The flow rate was 70 mL/min. Solvent exchange was then carried out with absolute ethanol. For comparison, aerogel monoliths were also produced from suspensions of the same concentration, 3%, following the same procedure described above for monoliths.

Organogels (monoliths and beads) were dried using supercritical CO_2 at the Center for Processes, Renewable Energy and Energy Systems (PERSEE)/Mines Paris-PSL. Samples were placed inside the autoclave vessel and covered with the corresponding non-solvent. After closing the vessel, the system was heated to 37 °C, filled with CO_2 until about 40 bar, and the excess non-solvent was purged. The pressure was then increased to 80 bar, and a dynamic wash was carried out for 4 h. Samples for testing mechanical properties were larger, therefore, the dynamic washing pressure and duration had to be increased to 90 bar and 5 h, respectively. Samples were collected after overnight depressurization (4 bar/h).

3.3.2.2 Preparation of cryogel monoliths

After bubble removal (24 *g*, 2-3 min), biomass suspensions and LM pectin solutions were placed inside polypropylene molds, frozen at -5 °C, and freeze-dried with a Cryotec Cosmos 80 machine at -80 °C for 72 h.

3.3.3 Characterization of the porous materials

3.3.3.1 Shrinkage

Volumetric shrinkage was calculated using Eq. 3.2:

$$shrinkage\ (\%) = \frac{V_i - V_f}{V_i} \times 100 \qquad (3.2)$$

where V_i and V_f correspond to sample volume before and after the corresponding processing step, respectively.

Shrinkage during two steps were considered for aerogel samples, namely, during solvent exchange (from suspensions to organogels) and during supercritical drying (from organogels to aerogels). The total shrinkage (from suspension to aerogel) was also estimated. Only one step was used for cryogels, the freeze-drying procedure (from suspension to dried material). For monoliths, the volume was calculated from height and diameter measurements

with a 0.001-mm precision caliper. At least 8 monolithic specimens were measured for each sample type. Beads' volume was calculated from their average equivalent diameter, which was obtained via digital image processing (see details in Section 3.3.3.10). The dimensions of beads were measured 20 min after coagulation (to ensure enough dimensional stability for manipulation), after the solvent exchange was completed, and after the supercritical drying (aerogel beads). At least 100 beads were measured for each processing step.

3.3.3.2 Apparent density and porosity

The apparent (or bulk) density (ρ_{ap}) was calculated from the samples' mass per volume ratio. Monoliths' dimensions were measured with a digital caliper, with a precision of 0.001 mm. At least 8 specimens of aerogel and cryogel monoliths were evaluated. Beads' volume was measured with a Micromeritics GeoPyc 1360 (19.1 mm chamber, 25 N consolidating force). At least 20 beads were used for each replicate, and each measurement was repeated at least five times. Masses were determined with an analytical balance with a 0.1-mg precision.

Eq. 3.3 was used to calculate the materials' porosity. Skeletal densities (ρ_{sk}) were determined by helium pycnometry with an Anton Paar Ultrapyc 5000 Micro pycnometer.

$$porosity\ (\%) = \left(1 - \frac{\rho_{ap}}{\rho_{sk}}\right) \times 100 \quad (3.3)$$

3.3.3.3 Specific surface area

Specific surface areas were determined using nitrogen adsorption isotherms with a Micromeritics ASAP 2020 instrument, employing the Brunauer-Emmett-Teller (BET) approach. All samples were degassed under vacuum at 70 °C for 5 h before analysis. Biomass-based aerogels and cryogels were analyzed in triplicate, while samples prepared from neat LM pectin were analyzed in duplicate.

3.3.3.4 Morphology

Morphological features were observed via Scanning Electron Microscopy (SEM) using a Tescan Maia 3 microscope. The beam accelerating voltage was 3 kV. Prior to analysis, cryofractured surfaces were sputtered with a 14-nm platinum layer using a Q150T Quarum apparatus.

3.3.3.5 Attenuated Total Reflectance – Fourier-Transform Infrared Spectroscopy (ATR-FTIR)

ATR-FTIR spectra of mixed biomass cryogel and aerogels were collected using a Thermo Nicolet Avatar 370 spectrometer and 50 scans per sample. Wavenumber ranged from 4000 to 525 cm^{-1}, and the resolution was 2 cm^{-1}.

3.3.3.6 Intrinsic viscosity

The influence of the acid treatment on the neat LM pectin molecular weight was assessed from the intrinsic viscosity [η], determined using a capillary Ubbelhode viscometer (type I, with a 0.63-mm diameter capillary) and an iVisc system from LAUDA. Neat pectin and neat pectin aerogels were solubilized at 60 °C in 0.01 M NaCl and analyzed at 26.6 °C [177]. The average molecular weight (M_v) was estimated with Eq. 3.4:

$$[\eta] = K \times M_{\mathrm{v}}^{a} \qquad (3.4)$$

where K = 0.0234 and a = 0.8221 [177].

3.3.3.7 Mechanical testing

Uniaxial compression tests were carried out on mixed biomass and LM pectin samples (on both aerogels and cryogels) with a universal Instron machine, model 5569. A 500-N load cell was used, and the testing speed was 2 mm/min. Cylindrical specimens were polished to keep parallel top and bottom surfaces, and to ensure a height-to-diameter ratio of about 1:1. Sample diameters were 16-20 mm for aerogels and 25-26 mm for cryogels. At least 6 replicates were performed for each sample.

3.3.3.8 Thermal conductivity

The thermal conductivity of mixed biomass cryogel and aerogel samples was determined using a LaserComp Fox 150 heat flow meter customized for small samples at PERSEE/Mines Paris-PSL. Specimens had 22-26 mm in diameter and 4-6 mm in thickness. Measurements were performed in duplicate, at ambient pressure, and 20 °C. The device was calibrated with an Aspen Spaceloft® sample.

3.3.3.9 Biodegradation

The biodegradability of mixed biomass aerogels and cryogels was assessed by Biochemical Oxygen Demand (BOD) measurements, performed at the Istituto Italiano di Tecnologia (Genoa, Italy). Each sample was cut into small pieces, and about 25 mg of material was added to 432 mL of seawater collected from Porto Antico of Genoa, Italy. The experiments were conducted in duplicate, at room temperature and within 510 mL amber glass bottles, hermetically closed with the OxiTop® measuring heads. Sodium hydroxide tablets were added as a CO_2 scavenger to sequester the CO_2 produced during biodegradation. BOD was measured as a function of the decrease in pressure for 30 d. Raw oxygen consumption data (mg O_2/L) were corrected by subtracting the mean values of blank samples (seawater only). Obtained values were then normalized by the samples' mass (results were thus expressed as mg O_2/100 mg material).

Microcrystalline cellulose was used as a positive control, and biomass cast films were used as a non-porous sample. For the latter, prepared biomass suspensions (see Section 2.3) were poured into silicon molds until about 1 mm of height, followed by overnight oven-drying at 45 °C.

3.3.3.10 Bead size and shape

Organogel and aerogel beads' shape parameters and size distributions were determined from digital images taken over an LED light table and processed with the software ImageJ. At least 100 beads were measured for

each sample type. Size distributions were built using the equivalent diameter of the beads. Roundness and aspect ratio were calculated as described by Eq. 3.5 and Eq. 3.6, respectively:

$$roundness = \frac{4 \times A}{\pi \times a_{maj}^2} \qquad (3.5)$$

$$aspect\ ratio = \frac{a_{maj}}{a_{min}} \qquad (3.6)$$

where A is the cross-section area, and a_{maj} and a_{min} the major and minor axes lengths, respectively.

Beads size and shape were evaluated also by optical microscopy using a Keyence VHX 7000 microscope (20x magnification).

3.4 Results and discussions

3.4.1 Influence of biomass fraction and processing routes on aerogels' and cryogels' properties

Crack-free and homogeneous aerogel and cryogel monoliths were obtained from the different orange biomasses and processing routes (Figure 3.9a). Their volumetric shrinkage upon solvent exchange and drying, total shrinkage, apparent density, porosity, and specific surface area are presented in Figure 3.9b-e, and Tables B.1 and B.2 of Appendix B.

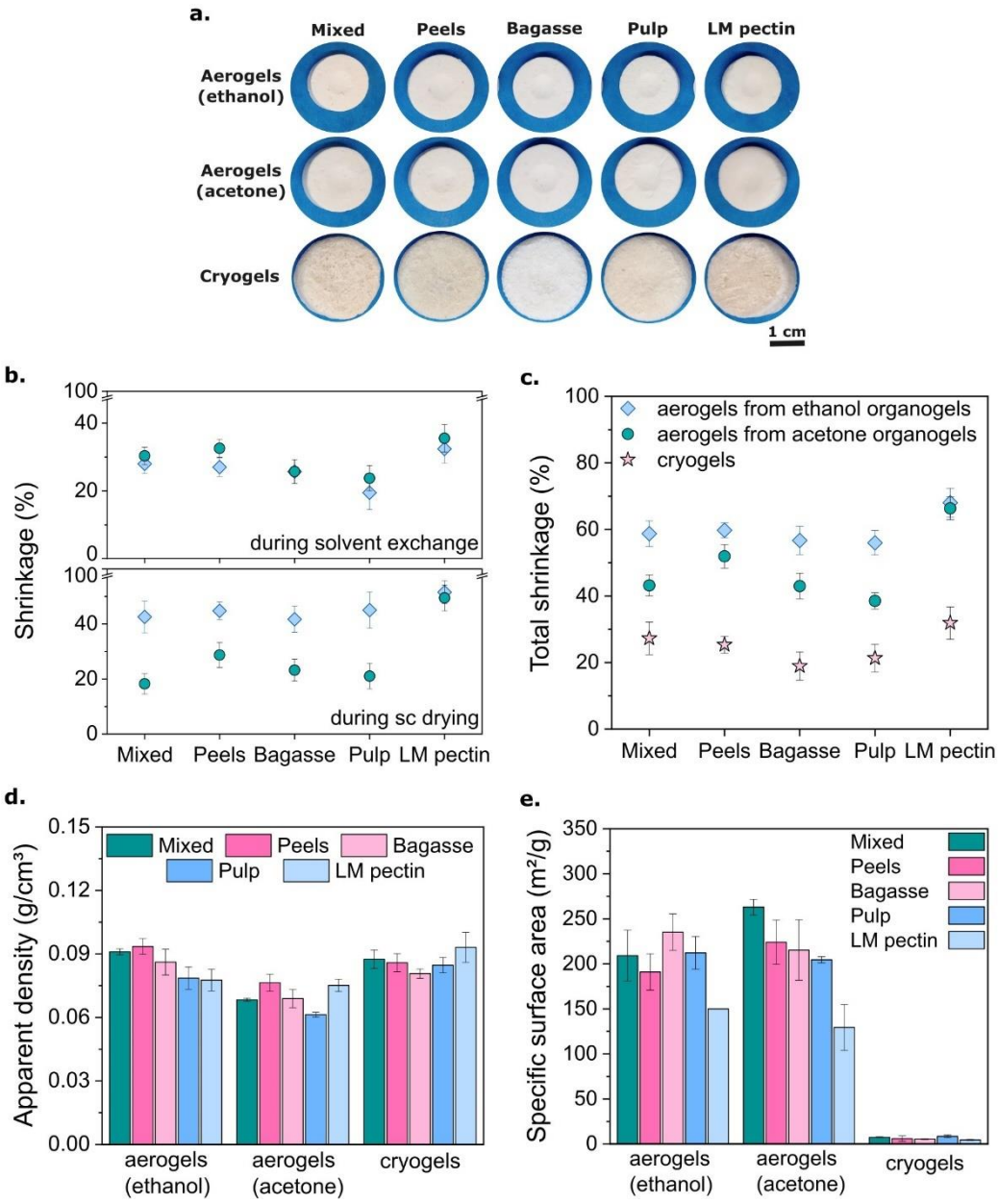

Figure 3.9: (a) Digital images of the porous materials produced, grouped by processing route and starting matter. (b) Volumetric shrinkage during solvent exchange and during supercritical drying for aerogel samples (same symbols as (c)), (c) total volumetric shrinkage, (d) apparent density, and (e) specific surface area of samples, grouped by process and starting matter. “Acetone” or “ethanol” correspond to non-solvent used. Supercritical drying is abbreviated as “sc” drying.

To prepare aerogels, non-solvent-induced phase separation was used to create a coagulated “wet” network from suspensions, followed by gradual solvent exchange, which led to volumetric shrinkage (19-33%, Figure 3.9b and Table B.1). This is a common behavior for polysaccharides like pectin, starch, chitosan and alginate [20]. Adding ethanol or acetone to polysaccharide solutions/gels leads to dehydration, polymer chains contraction, and thus material densification [178,179]. No significant influence of the non-solvent type on the shrinkage induced by solvent exchange was observed within experimental errors.

LM pectin aerogels experienced higher shrinkage during solvent exchange with acetone (36%) compared to those from pulp and bagasse (24-26%). A similar trend was observed with ethanol as a non-solvent, although differences did not have statistical significance. As reported in Section 2.4.2.3, pulp and bagasse suspensions had higher viscosities and insoluble fractions with greater swelling degrees, which likely improved their resistance to shrinkage. In turn, the citric acid pre-treatment reduced LM pectin’s molecular weight from 131 to 104 kg/mol (for commercial pectin vs. pectin aerogel, respectively). The reduced chain entanglements due to degradation, coupled with the absence of insoluble fibers, probably led to a weaker LM pectin gel network.

Shrinkage during supercritical drying was higher when using ethanol than when using acetone as the non-solvent, resulting in higher total shrinkage (Figure 3.9b and c). This was previously observed for neat pectin aerogels and attributed to the closer Hansen solubility parameters of acetone to that of supercritical CO_2 (19.9 and 5-8 $MPa^{1/2}$, respectively) compared to ethanol (26.5 $MPa^{1/2}$) [27,180]. Regarding the different starting matter, the shrinkage after supercritical drying showed the same trend as after solvent exchange.

When considering the entire preparation procedures, cryogels shrank less than aerogels, 19-32% vs. 39-68%, respectively (Figure 3.9c and Table B.1). While the shrinkage of aerogels stems from both solvent exchange and supercritical drying as discussed above, shrinkage during the preparation of cryogels may have occurred due to bound water removal and skeleton

contraction upon freezing. Previous studies have reported similar shrinkage after freeze-drying for carboxymethylcellulose (15-30%) [38], cellulose (14-27%) [32], and cellulose nanofibers (ca. 30%) [181]; but lower for ionically gelled LM pectin (10-13%) [25], and negligible for retrograded starch [45] and chitosan hydrogels [182].

All porous materials boasted very low densities (0.061-0.094 g/cm³) and high porosities (94-96%) (Figure 3.9d and Table B.2). Interestingly, LM pectin-based samples had similar apparent densities as those produced from orange biomasses. Hence, the higher volumetric shrinkage outweighed the absence of insoluble, and probably less porous, fibers. Between the different biomasses, there was also no significant influence of biomass type on density for the same drying procedures and non-solvent. Processing routes had statistically relevant, yet small, differences: aerogels from acetone organogels had lower densities (0.061-0.076 g/cm³) than those from ethanol (0.078-0.094 g/cm³). Cryogels had the lowest shrinkage (19-32% vs. 39-68% for aerogels), but not the lowest density (0.081-0.093 g/cm³) (Figure 3.9d and Table B.2). Their lower shrinkage might have been outweighed by the presence of the citric acid used during the pre-treatment and its mass contribution to the cryogels' density. As discussed in Section 3.4.2.1, citric acid was likely washed out during solvent exchange during aerogel production.

Aerogels presented similar specific surface areas regardless of the type of the non-solvent used (Figure 3.9e and Table B.2), and similar morphologies were observed in SEM images (Figure 3.10a and b). All aerogels from orange biomasses boasted high specific surface areas (191 to 263 m²/g) despite having high insoluble content (see Section 2.4.2.3). For all-cellulose aerogel composites (i.e. having non-dissolved fibers), the presence of non-swollen fibers decreased the specific surface area [134]. However, this was not the case for orange waste biomass-based aerogels. The reason was that non-dissolved particles and fibers were swollen in the suspension and remained porous after solvent exchange and drying, while being surrounded by a nanostructured pectin-based fibrillar network, as revealed by SEM observations (Figure 3.10a and b). The continuous phase morphology was remarkably similar to the LM

pectin aerogels' texture (Figure 3.10a and b), further supporting the assumption that it was composed mainly of pectin, while cellulose and hemicellulose remained mostly insoluble, as discussed in Chapter 2 (Section 2.4.2.3).

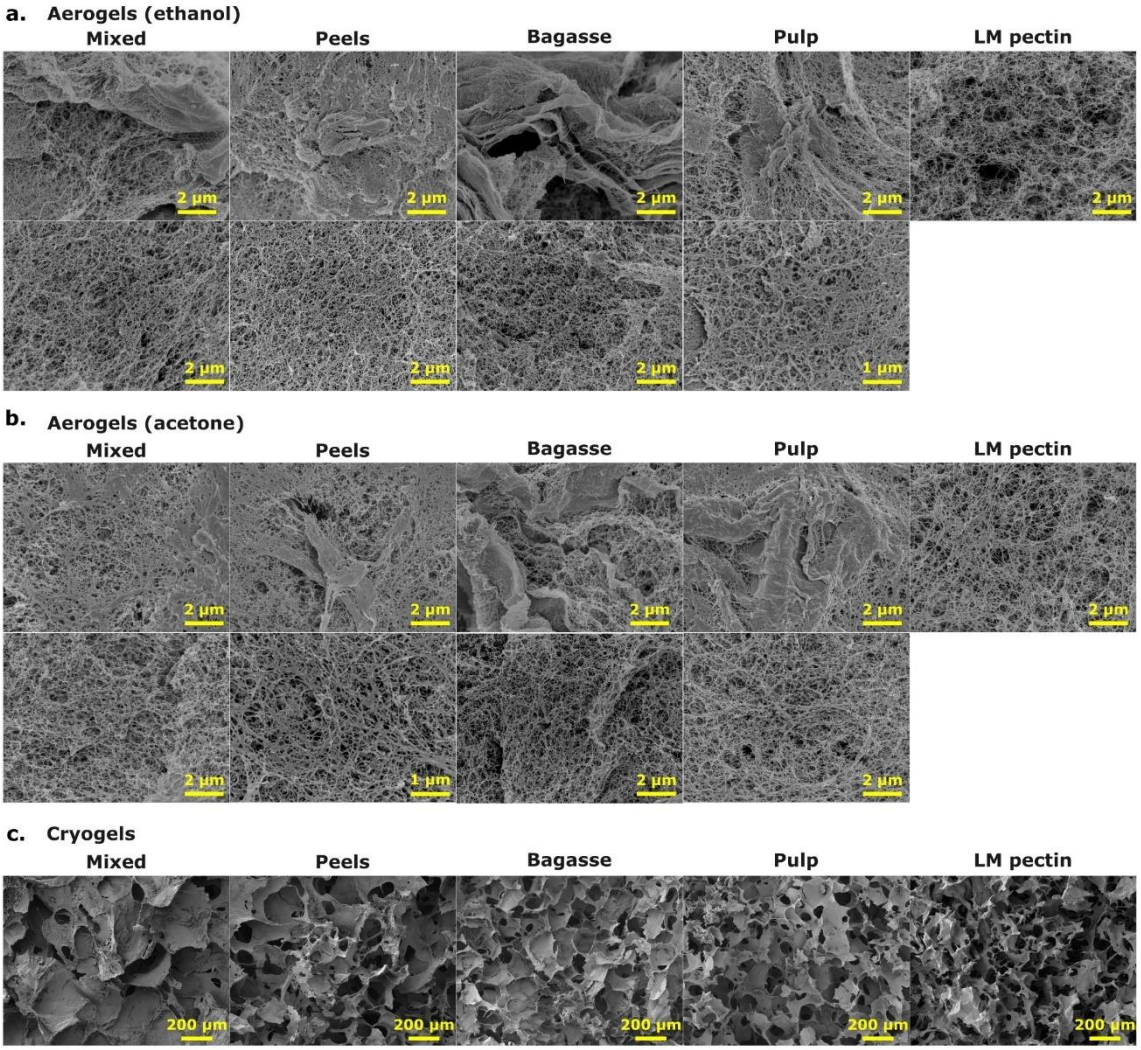

Figure 3.10: SEM micrographs, grouped by starting matter process route: (a) aerogels from (a) ethanol and (b) acetone organogels, and (c) cryogels. For orange waste-based aerogels, insoluble fractions are shown in the upper row and the pectic matrix in the bottom row.

LM pectin aerogels had lower specific surface areas (130-150 m^2/g) due to chain degradation during the acid pre-treatment. A decreased surface area due to the lowered molecular weight of the polymer was also reported for hyaluronic acid-based aerogels [183]. In addition, a partially damaged network

was observed for the LM pectin aerogel produced using ethanol as non-solvent (Figure 3.10a). Therefore, the acid hydrolysis had a decisive impact on the aerogel properties: on one hand, it allowed the swelling and fibrillation of non-dissolved parts and the production of homogeneous samples from orange biomass; on the other hand, it decreased pectin's molecular weight.

Larger pores measuring dozens to hundreds of micrometers were observed in cryogels (Figure 3.10c), leading to very low specific surface areas (5-8 m^2/g, Figure 3.9e and Table B2). Their whole morphology consisted of an assembly of flake-like pore walls, as a result of the ice-templating. SEM observations (Figure 3.10c) showed that while insoluble fibers remained partially porous after supercritical drying; they were compacted due to the ice crystals' growth during freezing, and the resulting morphologies of cryogels were nearly the same regardless of the starting matter.

Overall, morphological features and surface areas of aerogels were not strongly influenced by different biomass fractions and the type of non-solvent. Thus, the orange mixed biomass was selected to further evaluate the effects of the drying method on the materials' mechanical properties, thermal conductivities, and biodegradation. Ethanol was kept as a non-solvent.

3.4.2 Influence of the drying procedure on aerogels' and cryogels' mechanical properties, thermal conductivity and biodegradation

3.4.2.1 ATR-FTIR

Before discussing the properties of aerogels and cryogels, it is important to consider that the solvent exchange process carried out during the production of aerogels may have washed out the citric acid, a least partially, while for cryogels it was likely retained in the final material's structure. This was hypothesized to impact their apparent density (see Section 3.4.1) and suggested by ATR-FTIR results. The normalized spectra of mixed biomass-based aero and cryogels are presented in Figure 3.11.

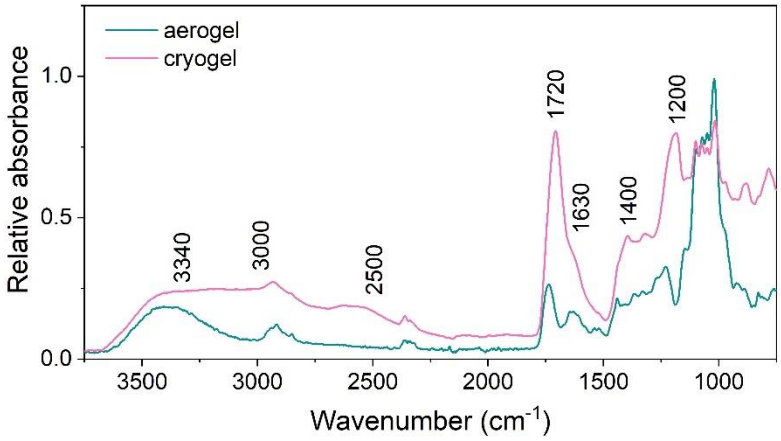

Figure 3.11: FTIR spectra of the orange mixed biomass-based cryogel and aerogel.

The O-H stretching region (3400-2500 cm^{-1}) was broader and had higher intensity for the cryogel spectrum when compared to that of the aerogel. This can be ascribed to the contribution of the stretching vibration of the O-H groups of citric acid (3340-3000 cm^{-1}). O-H vibrations of alcohol groups from polysaccharides' backbones and citric acid occur at higher wavenumbers (ca. 3400 cm^{-1}), while those from carboxylic acids (COOH) happen at lower wavenumbers (2500-3300 cm^{-1}). Although pectin has COOH moieties as well, citric acid contributed to the more intense absorbance in this region. Moreover, it has great affinity with water, which increases water contribution to its bands in this region (3490 and 3240 cm^{-1}) [184]. The presence of citric acid can also be observed by the increased absorbance in the bands associated with C=O stretching from ester and carboxylate groups (1720 and 1630 cm^{-1}), their weaker symmetrical stretching (ca. 1400 cm^{-1}), and C-O stretching (ca. 1200 cm^{-1}) [16,140,185,186]. Water bending vibrations at 1650 cm^{-1} may have led to the apparent "merging" of the 1720 and 1630 cm^{-1} signals in the cryogel spectrum [184]. FTIR results evidenced the presence of citric acid in the cryogels.

3.4.2.2 Mechanical properties

The mechanical behavior of aerogels and cryogels based on mixed biomass and LM pectin was examined through uniaxial compression testing.

Samples did not crack under compression and were compacted until the maximum strain possible. The resulting stress-strain curves (Figure 3.12) presented the typical shape exhibited by porous materials, consisting of three characteristic stages: (i) a linear region where elastic deformation and pore wall bending occurs, from which the compressive elastic modulus can be determined; (ii) a stress “plateau” region, that occurs due to plastic deformation (buckling of pore walls); and (iii) a stress increase with strain, reflecting the densification stage due to pore collapse [187–189].

The yield stress and yield strain mark the transition from the elastic regime to plasticity, and are determined at the intersection point of stages (i) and (ii) tangent lines [190]. It was not possible to calculate compressive modulus, yield stress and yield strain for LM pectin aerogels, as the elastic region was very small [187].

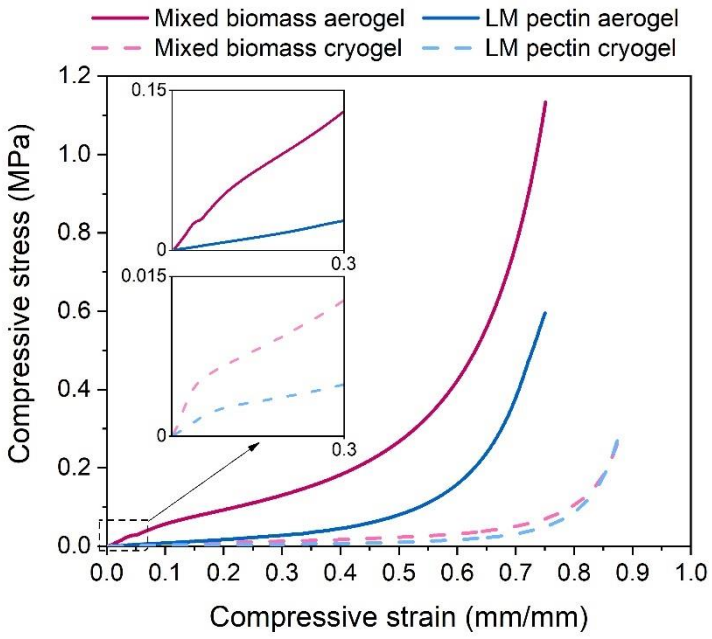

Figure 3.12: Compressive stress-strain curves of aerogels and cryogels from mixed biomass and LM pectin.

Elastic moduli (E), yield stresses (σ_y), and yield strains (ε_y) are presented in Table 3.1. Density strongly influences the mechanical behavior of porous materials [187,191]. Hence, E and σ_y were normalized to the specimens’

average apparent density (measured after polishing, see Section 3.3.3.7), resulting in the corresponding specific properties (E/ρ_{ap} and σ_y/ρ_{ap}, respectively), which are also reported in Table 3.1.

Table 3.1: Apparent density, absolute and specific mechanical properties of aerogels and cryogels from orange mixed biomass and LM pectin.

	ρ_{ap} (cm³/g)	E (MPa)	σ_y (MPa)	ε_y (%)	E/ρ_{ap} (MPa.cm³/g)	σ_y/ρ_{ap} (MPa.cm³/g)
Mixed biomass aerogel	0.067 ± 0.004	0.80 ± 0.08	0.04 ± 0.01	11.1 ± 0.9	12 ± 1	0.7 ± 0.2
LM pectin aerogel	0.052 ± 0.005	-	-	-	-	-
Mixed biomass cryogel	0.095 ± 0.003	0.16 ± 0.05	0.005 ± 0.001	8 ± 1	2 ± 1	0.05 ± 0.01
LM pectin cryogel	0.110 ± 0.003	0.04 ± 0.01	0.0021 ± 0.0006	9 ± 2	0.4 ± 0.1	0.02 ± 0.01

Cryogels were substantially more ductile than aerogels, exhibiting larger plastic deformation stages (up to ~70% vs. ~30-40%, respectively) (Figure 3.12). The compressive modulus of aerogels was substantially higher than that of cryogels; given their comparable densities, their specific modulus was 6 times higher than that of cryogels (2 vs. 12 MPa.cm³/g) (Table 3.1). Yield stresses and yield strains were similar for both types of cryogels (from LM pectin and mixed biomass), and lower when compared to the mixed biomass aerogel (0.005-0.002 vs. 0.04 MPa, and 8-9 vs. 11%) (Table 3.1).

These results could be attributed to the fact that aerogels were prepared via non-solvent induced phase separation, giving rise to a continuous network of entangled polymer chains. Cryogels, in turn, were made by directly freezing suspensions. The ice crystals' solidification fronts segregate polymer chains and insoluble particles, ultimately compressing them between their boundaries

and resulting in the “flake-like assembly” morphology of cryogels (see Figure 3.10), rather than a strong interconnected network. The finer and highly branched networks obtained by supercritical drying may have enabled better load distribution [192]. In addition to the predominant morphological effect, the observed differences could also be related to the plasticizing effect of citric acid, retained in the cryogels, as discussed in the previous Section. Although citric acid may be used as a cross-linker for hydroxyl-rich polymers by participating in esterification reactions, non-reacting “free” citric acid molecules may act as plasticizers. This behavior has been reported for pectin films [193], thermoplastic starch [194], and for polyvinyl alcohol/starch- [195] and soybean polysaccharides-based films [196] when citric acid concentrations was above 5%.

When comparing the use of mixed biomass with LM pectin as starting matter, the elastic modulus was notably increased for cryogels (0.16 vs. 0.04 MPa) (Table 3.1). A mechanical reinforcement effect was expected from the presence of well-dispersed insoluble fibers with good adhesion to the continuous phase. Although a quantitative comparison between aerogels was hindered due to the small elastic region for the LM pectin aerogel, the reinforcement effect was manifested by the higher stresses presented by the mixed biomass aerogel throughout the whole deformation range when compared to the LM pectin aerogel’s mechanical response (Figure 3.12).

Neat LM pectin aerogels with similar mechanical properties (E/ρ_{ap} = 13 MPa.cm³/g and σ_y/ρ_{ap} = 0.8 MPa.cm³/g) to those of orange mixed biomass-based aerogels were reported for specific preparation conditions (2% pectin, pH=2, in the presence of Ca^{2+} (R=0.2)) [153]. In contrast, acid-gelled pectin aerogels (2-6% pectin, pH = 0.5) showed substantially higher specific modulus and yield stresses (45-108 MPa.cm³/g and 2-5 MPa.cm³/g, respectively) [22] than the mixed biomass aerogels. Mixed biomass cryogels presented mechanical behavior and elastic modulus comparable to those reported for neat pectin cryogels, in which network formation was promoted by Ca^{2+} and/or tert-butanol/water solutions (E/ρ_{ap} = 3-4 MPa.cm³/g) [23], and had superior modulus and larger deformation before pore collapse (2 vs. 0.8-1.5 MPa.cm³/g, and ca.

70 vs. 10%, respectively) than cryogels composed of self-assembled hemp fibers [171]. It should be highlighted that results in the literature vary significantly, and comparisons are complicated due to multiple factors, including differences in density, morphology, pectin cross-linking to varying extents and via different mechanisms, as well as different processing conditions.

3.4.2.3 Thermal conductivity

The thermal conductivity (λ) of aerogels and cryogels produced from orange mixed biomass was also evaluated. The obtained results are shown in Table 3.2, along with those reported in the literature for neat pectin-based porous materials, as thermal conductivity of pectin-rich biomasses have not been reported (one reason is that only aerogel powders, and not monoliths, have been produced [42]). The ultimate thermal conductivity is composed of the contributions of different heat transfer mechanisms, namely: gas phase conduction, solid phase conduction, irradiation, and convection. The latter is negligible for solids with pores smaller than 1 mm. Radiative heat is also considered irrelevant at ambient pressure and temperature, and for optically thick materials [26,188].

Table 3.2: Thermal conductivity of cryogels and aerogels from mixed biomass and neat pectin from literature.

Starting matter	Preparation	Drying method	ρ_{ap} (g/cm³)	λ (mW/m.K)	Ref.
Mixed biomass (orange)	4%, direct coagulation	supercritical drying (non-solvent ethanol)	0.091 ± 0.001	25.0 ± 0.4	This work
		freeze-drying	0.088 ± 0.004	37.3 ± 0.1	
Apple pectin (DE = 58%)	2-3%, pH=2-3, direct coagulation	supercritical drying (non-solvents ethanol and acetone)	0.04–0.11	14.8–23.4	[54]

Citrus pectin (DE = 35%)	2-6%, pH=1-3, direct coagulation or gelled with Ca^{2+}	supercritical drying (non-solvent ethanol)	0.031–0.182	14.7–24.7	[26]
Citrus (DE = 54%) and apple pectin (DE = 72%)	5-6%, pH=0.3, acid-gelled	supercritical drying (non-solvent ethanol)	0.050–0.128	13.3–18.0	[22]
Citrus pectin	3% in NaCl solutions, directional freezing	freeze-drying	~0.034–~0.057	32–49 (axial) 20–26 (radial)	[44]
Pectin/clay	1-7% pectin/1-7% clay	freeze-drying	0.059–0.096	45.2–75.5	[197]

Neat pectin aerogels produced under certain conditions (pH, gelling or non-gelling, concentration, etc.) boasted superinsulating properties, i.e., their thermal conductivity was lower than that of the air at ambient conditions (25 mW/m.K) [22,26,54]. The superinsulation phenomenon originates from the material's low density and, most importantly, from the conductivity of the gas confined within pores smaller than 70 nm, which corresponds to the average mean free path of air molecules at ambient temperature and pressure (Knudsen effect) [22,188]. In these conditions, the gas conductivity within the aerogel is lower than that of free gas (in this case, air).

Mixed biomass aerogels fell at the boundary of the thermal superinsulation range, presenting an average thermal conductivity of 25 mW/m.K. A wide range of pore sizes was observed in both the pectic matrix and insoluble fibers (~20 to 400 nm) (see Figure 3.13a). For superinsulating neat pectin aerogels (λ = 15-20 mW/m.K), mesoporosity was favored by weaker networks (formed mainly via non-solvent-induced phase separation of

solutions), resulting in higher shrinkage while still preventing collapse [26]. As discussed previously, the insoluble fibers may have helped the biomass-based gels “resist” shrinkage and, as a consequence, the pectic matrix had bigger pores than neat pectin [22,26,54]. Moreover, the insoluble fractions consisted of both porous and denser regions, contributing directly to increased solid-phase conduction. Nonetheless, this is a particularly promising result, given that these aerogels were produced from bulk waste biomass, yet they exhibited nearly superinsulating properties.

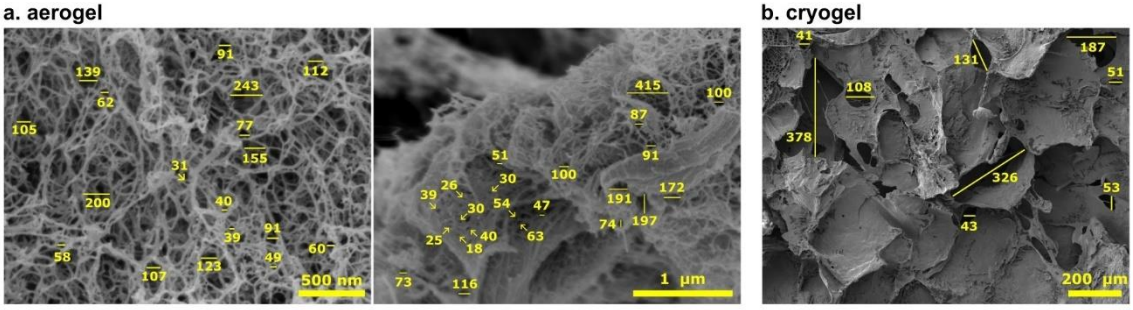

Figure 3.13: SEM images and pore sizes of (a) aerogel (in nm) and (b) cryogel (in µm) samples based on orange mixed biomass.

Cryogels from mixed biomass presented a thermal conductivity of 37.3 mW/m.K, which was comparable to that of expanded polystyrene (EPS) (0.032-0.037 W/m·K) [31], and higher than their aerogel counterparts due to their much larger pores (30-400 µm, see Figure 3.13b) [44,188]. Anisotropic neat pectin cryogels had similar thermal conductivities when measured in the axial direction (i.e., parallel to the directional freezing) but lower in the radial direction [44] (Table 3.2), at which the pore size was smaller than those herein observed. Isotropic pectin cryogels reinforced with clay exhibited higher conductivity compared to the orange biomass-based ones from this work [197].

3.4.2.4 Biodegradation

The biodegradation of cryogel and aerogel samples based on orange mixed biomass in seawater was evaluated by Biochemical Oxygen Demand (BOD), which expresses the amount of oxygen consumed by microorganisms

as they metabolize the biopolymer sample, using it as an energy and carbon source [198]. Therefore, higher BOD values express higher biodegradation extents. An orange mixed biomass cast film was used as a reference of a non-porous material, and microcrystalline cellulose (MCC) was used as the positive control, due to its known high biodegradability, to ensure suitable microbial activity for the biodegradation of polymeric samples [198,199]. Results are presented in Figure 3.14a.

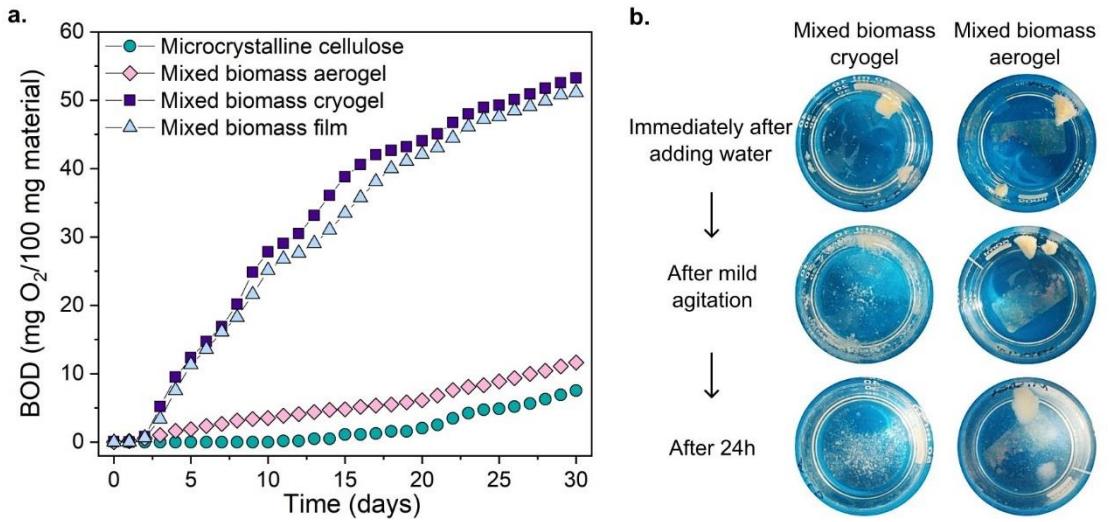

Figure 3.14: (a) Biochemical Oxygen Demand (BOD) evolution for microcrystalline cellulose and orange mixed biomass-based aerogel, cryogel and cast film samples. (b) Digital images of mixed biomass cryogel (left) and aerogel (right) in distilled water (at 1%).

MCC started to biodegrade after ten days and ultimately reached 7 mg O_2/100 mg. In contrast, all other samples initiated their biodegradation between the first and second days. While both cryogel and film samples reached BOD values between 50 and 60 mg O_2/100 mg, aerogels reached 5-15 mg O_2/100 mg, following a biodegradation kinetic closer to that of MCC. The different degradation behaviors between samples may be due to the different materials' properties and morphologies, induced by procedures used to prepare the materials, and their varying organic compositions. For instance, FTIR spectra suggested that citric acid was washed out from aerogels during the solvent

exchange procedure, but remained in the cryogel (Section 3.4.2.1) and presumably on the film as well.

The mixed biomass cryogel was readily dismantled into small particles when added to water, having its network morphology quickly disrupted, whereas the aerogel remained mostly swollen after one day (Figure 3.14b). Fragmentation into smaller particles likely contributed to the cryogel faster biodegradation [198,200]. This behavior may have resulted from the absence of a network formation prior to freeze-drying, as well as the presence of residual citric acid, increasing the materials' polarity and water absorption [198,201]. Acidic environments are known to be detrimental to bacterial growth [198], however, at the conditions used in this analysis, the citric acid concentration in the systems would be very low, 0.006% at the highest (see Section 3.3.3.9).

The nanometric pores of aerogels may have restricted microbial access to the internal parts of the material compared to the cast film sample, as bacteria typically have a few micrometers in size [202]. Microcrystalline cellulose, in turn, is highly crystalline; which also affects the accessibility of water molecules and enzymes secreted by microorganisms to the polymeric chains [203]. Solubilization kinetics and biodegradation analyses in non-aqueous media (e.g., soil), in which the pore morphology influence could be properly evaluated, could bring further clarification on the underlying mechanisms and factors governing the biodegradation of these materials.

3.4.3 Aerogel beads

Aerogel beads were produced from mixed biomass, demonstrating the feasibility of using orange juice waste to produce aerogels of different shapes. The biomass concentration was adjusted by diluting the original suspension to 3% to enable beads production, as the initial viscosity was too high for the setup used and led to clogging. Mixed biomass monolithic aerogels with the same biomass concentration were produced for comparison. Mixed biomass was used in all cases and the non-solvent was ethanol. Both are shown in Figure 3.15a, alongside the non-diluted mixed biomass aerogel (4%).

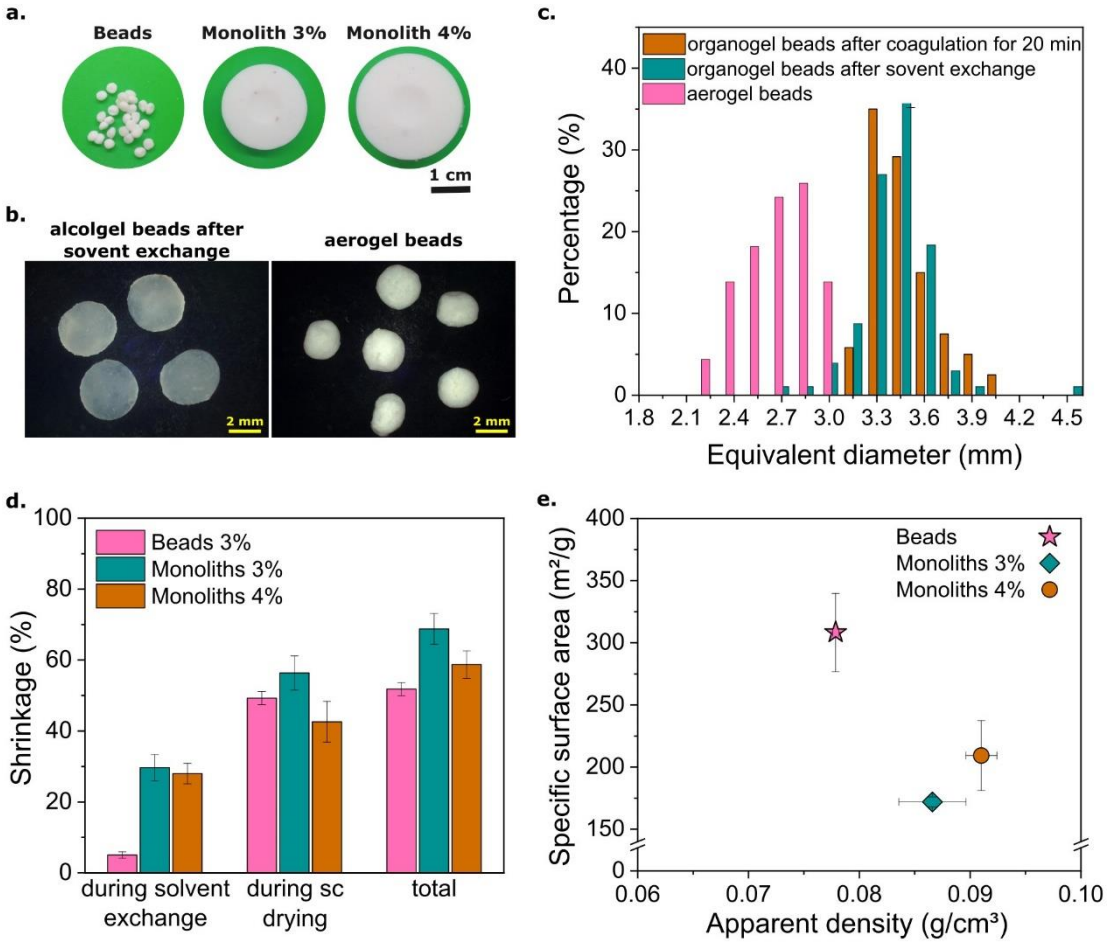

Figure 3.15: (a) Digital images of aerogel beads and monoliths, (b) optical micrographs, (c) size distributions, and (d) volumetric shrinkage of beads at different processing steps (here “during solvent exchange” corresponds to completed solvent exchange), and (e) specific surface area vs. apparent density of aerogel beads and monoliths at 3%, and monoliths at 4%. Mixed biomass was used in all cases and the non-solvent was ethanol. Supercritical drying is abbreviated as “sc” drying.

Producing beads enabled a faster solvent exchange procedure (from at least 3 d for monoliths to 2 d or less for beads). Table 3.3 shows the average equivalent diameter (D_{eq}), roundness (R_n) and aspect ratio (AR) of “freshly” coagulated organogel beads (measurements were performed 20 min after beads formation in the ethanol coagulation bath), organogel beads after complete solvent exchange, and aerogel beads (after supercritical drying). The equivalent diameter corresponds to the diameter of a circle having the same

area as the bead projection; roundness and aspect ratio were calculated with Eq. 3.5 and Eq. 3.6, respectively.

At all stages, beads had approximately spheric shapes, presenting R_n~0.9 and AR~1.1 (for perfect spheres, R_n=1 and AR=1) (Table 3.3). Organogel and aerogel beads are depicted in optical micrographs (Figure 3.15b). The average D_{eq} of aerogel beads was 2.7 mm, and respective size distributions are presented in Figure 3.15c.

Coagulated beads were collected 20 min after dripping the biomass suspension in ethanol for the size and shape assessments. This interval was used to ensure shape stability and bead integrity during collection. Negligible variation in D_{eq} occurred between beads coagulated for 20 min and after solvent exchange completion (Table 3.3). For alginate beads, it has been reported that nearly all shrinkage took place within 15 min in an ethanol-NaOH bath [178]. Possibly, shrinkage occurred during the first 20 min where the produced orange biomass-based beads were left still to avoid deformations during collection, underestimating the shrinkage during the solvent exchange procedure (5%, Figure 3.15d and Table B.3). Monitoring the whole shrinking process of beads requires specific tools.

Table 3.3: Average size (equivalent diameter, D_{eq}) and shape descriptors (roundness, R_n, and aspect ratio, AR) for beads after coagulation for 20 min, after solvent exchange and after supercritical drying.

	D_{eq} (mm)	**R_n**	**AR**
Organogel beads - After coagulation for 20 min	3.4 ± 0.2	0.90 ± 0.06	1.12 ± 0.08
Organogel beads - After solvent exchange	3.4 ± 0.2	0.89 ± 0.08	1.1 ± 0.1
Aerogel beads	2.7 ± 0.2	0.9 ± 0.06	1.12 ± 0.08

Aerogel beads presented higher surface area compared to their monolithic counterparts (ca. 300 vs. 170 m^2/g) and similar morphology, as observed by SEM (Figure 3.15d and 3.16). This is an interesting result as

similar properties were reported for cellulose aerogel monoliths and beads [204], but 3D-printed carboxymethyl cellulose aerogels exhibited twice the specific surface area of their molded monolithic counterparts [38]. Possibly, the different times required for the complete coagulation of monoliths and beads may have influenced the resulting organogel morphology (and, thus, that of the aerogel), but further investigations are needed to clarify their varying specific surface area. Beads' density, in contrast, was close to that of its monolithic counterpart (0.078 vs. 0.087 g/cm³, see Figure 3.15d and Table B.3).

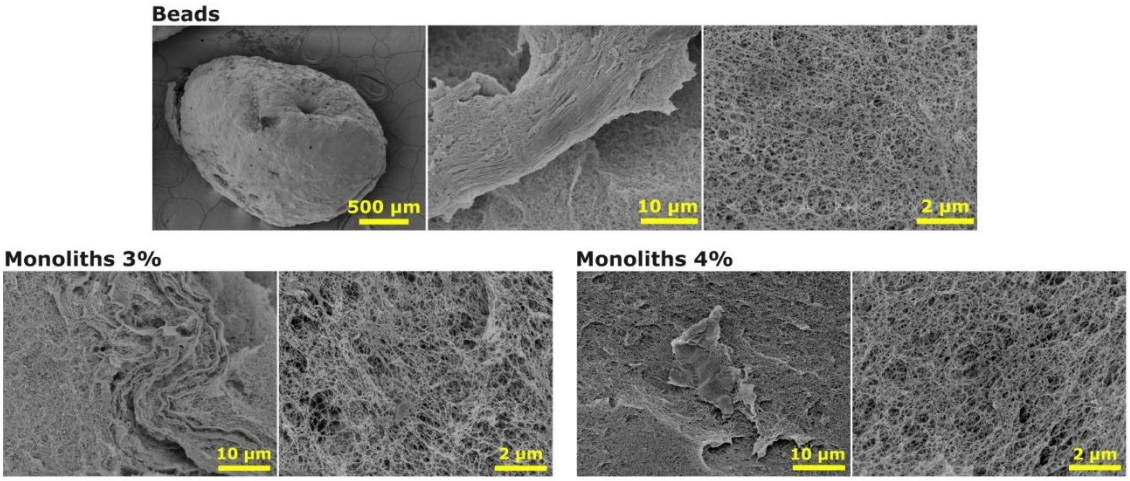

Figure 3.16: SEM images of aerogel beads and monoliths at 3%, and monoliths at 4%. Mixed biomass was used in all cases and the non-solvent was ethanol.

When comparing monolithic aerogels from 3% vs. 4% mixed biomass suspensions, results showed that a reduced concentration led to higher shrinkage during both solvent exchange and supercritical drying, as the network strength was reduced (Figure 3.15c). Greater shrinkage of lower concentration neat pectin solutions was previously reported and attributed to their reduced "resistance" to solvent exchange and drying [27]. The apparent density was reduced for the aerogel monolith made from a more diluted suspension, and accompanied by a slight decrease in surface area (Figure 3.15d).

3.5 Conclusions

Four types of orange biomass fractions obtained as waste from the juice processing chain (mixed, peels, bagasse, and pulp) were upcycled into lightweight (0.06-0.09 g/cm³) and highly porous (94-96%) materials using a “green” mild hydrolysis pre-treatment with citric acid. In addition to the influence of different biomasses as starting matter, various processing routes were explored.

Supercritical drying yielded high-surface-area monolithic aerogels (191-263 m²/g), composed by a fibrillar and nanostructured pectin network as a continuous phase, surrounding a dispersed and partially porous insoluble fraction. The non-solvent used before supercritical drying (ethanol or acetone) had a minor influence on the aerogel properties. Porous structures with large pores and flake-like pore walls were obtained by the freeze-drying route, resulting in materials with low surface areas (5-9 m²/g) and low specific elastic modulus (2 MPa.cm³/g). Aerogels exhibited superior mechanical properties (E/ρ_{ap} = 12 MPa.cm³/g) and a remarkably low thermal conductivity (25 mW/m.K), approaching superinsulating properties. Moreover, aerogels were quickly biodegraded in seawater, following the same kinetics as the positive control, microcrystalline cellulose. Cryogels had an even faster biodegradation.

The production of aerogel beads from orange biomass was also demonstrated. The dripping method was employed with an ethanol coagulating bath, using home-made setup. Nearly spherical beads were obtained with an average diameter of 2.7 mm. They presented a superior surface area (308 vs. 172 m²/g) compared to their monolithic counterparts, and a low density of 0.078 g/cm³.

In summary, the citric acid pre-treatment was an effective strategy to harness the high pectin content of orange biomasses and enable their processing into porous materials through different drying (supercritical drying vs. freeze-drying) and shaping procedures (molded monoliths vs. beads), yielding materials with tunable morphologies and properties. Nanostructured and high-surface-area aerogel monoliths and beads from bulk orange waste were reported for the first time, bearing nearly thermal superinsulating

properties and potential for many other applications (e.g., drug delivery, controlled release of soil nutrients or fertilizers, acoustic insulation, etc.).

CHAPTER 4 – ORANGE WASTE BIOMASS-DERIVED AEROGELS AND CRYOGELS AS SUSTAINABLE CARRIERS FOR PHASE-CHANGE MATERIALS

4.1 Introduction

As discussed in the previous Chapters, upcycling orange waste biomass from the juice industry into bio-based porous materials is a promising, yet unexplored strategy to valorize residues generated at an industrial scale [5,9]. Chapter 3 explored how this waste biomass can be processed via different routes to obtain porous materials with diverse properties, morphologies, and shapes. One promising application for porous materials is their use as carriers for functional substances, such as phase-change materials (PCMs). In a few words, phase-change materials (PCMs) are substances characterized by a high capacity to store or release thermal energy in the form of latent heat during phase transitions, which occur at nearly constant temperatures [69]. As a consequence, they have been investigated for thermal energy conversion and storage, thermal protection, and passive temperature control applications [62,69].

Organic PCMs are widely employed in both research and commercial applications by virtue of their low cost, high latent heat (up to ca. 270 J/g), wide range of phase-change temperatures (-5 to 80 °C), and chemical and thermal stabilities [65,205,206]. Most PCMs operate based on solid-liquid transitions, leading to molten PCM leakage and dimensional instability issues. The use of porous materials as “supporting” materials (i.e., carriers) has emerged as a feasible strategy to overcome these drawbacks. Their large pore volume enables high PCM loading ratios through simple and cost effective methods, such as melt impregnation [58,62]. Porous materials based on synthetic polymers (e.g., polyvinyl alcohol (PVA) [69,207] and polyimide [208,209]), neat biopolymers (e.g., sodium alginate [70,72], chitosan [70,71], starch [210], gelatin [211], (nano)cellulose [212–215] and its derivatives [216]), and their blends [217,218] have been investigated as potential carriers of PCMs. The use

of nanostructured porous networks from citrus waste has never been investigated as PCM carriers.

This Chapter explores aerogels and cryogels from upcycled orange waste biomass as carriers of PCMs. This study evaluates the influence of the porous carriers' morphology and their interactions with the PCM on the thermal behavior and leakage resistance of the resulting phase-change composites. Two organic PCMs bearing distinct physicochemical and thermal properties were selected: PEG 4000 and coconut oil.

4.2 Theoretical Background and Literature Review

4.2.1 Phase-change materials (PCMs)

Phase-change materials (PCMs) are substances that undergo phase transitions, typically from solid to liquid, that are associated with high latent heat values and occur within relatively narrow temperature ranges. As a consequence, they are capable of absorbing or releasing significant amounts of thermal energy at nearly constant temperatures. This makes them suitable for applications of passive thermal regulation systems for temperature-sensitive products (such as perishable foods, pharmaceuticals, and vaccines) transportation and storage, "heat sinks" for electronic devices, and smart textiles and materials for construction designed for improved thermal comfort [60,64–66,219].

PCMs constitute a physical method of thermal energy storage (TES), which can be classified into sensible and latent storage. In the former, the material stores/releases thermal energy while undergoing an increase/decrease in its internal energy, and consequently its temperature, via conventional heat transfer mechanisms (i.e., radiation, conduction, and convection) [60]. Sensible heat storage is the most commonly employed TES method. Examples include the use of water and rock beds for solar- and air-based heating systems, respectively [206]. Latent heat storage, on the other hand, relies on the material's phase transition and is generally more efficient (about 3-4 times

higher than sensible heat storage). It also offers the advantage of operating within well-defined temperature ranges [60,65].

As mentioned previously, PCMs rely primarily on the latent heat TES mechanism, although the sensible heat storage may also contribute to it to a lesser extent. Eq. 4.1 expresses the amount of heat (Q) stored/released by a PCM as a function of its mass (m), phase-change enthalpy (ΔH_t), specific heat capacity (C_p), and the phase-change, initial and final temperatures (T_t, T_i, and T_f, respectively) [60]. Figure 4.1 illustrates the operating mechanism of PCMs, including both sensible and latent heat storage.

$$Q = \int_{T_i}^{T_t} mC_p dT + m\Delta H_t + \int_{T_t}^{T_f} mC_p dT \qquad (4.1)$$

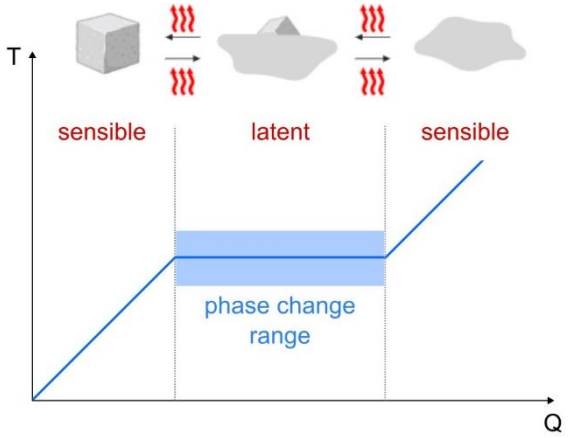

Figure 4.1: Schematic representation of the sensible and latent heat storage of a PCM.

Phase transformations are reversible processes, however, the persistence of a liquid phase below the melting temperature is a common occurrence. The difference between the melting and solidification temperatures of a substance is defined as the supercooling degree and considered an important parameter in the evaluation and selection of PCMs, in addition to their phase-change temperatures and enthalpies. Supercooling arises from the limited nucleation capacity of some PCMs, maintaining the material in a metastable state and delaying energy release. Strategies to mitigate this

shortcoming include the use of nucleating or thickening agents, formulating PCM blends, PCM encapsulation or impregnation, among others [60,65].

4.2.1.1 Confinement strategies

Most PCMs operate based on solid-liquid phase transformations, hence, leakage and dimensional instability are inherent challenges that must be addressed to enable their practical applications [58,62]. Different strategies have been used to overcome these drawbacks, which can rely on either chemical modification (e.g., cross-linking PCM molecules or grafting them into particles or polymeric chains) or their physical confinement. Methods for physically confining PCMs include (i) the simple use of containers (i.e., “macroencapsulation” into panels, capsules, tubes, etc. – see examples in Figure 4.2), which is the most common strategy used in commercially available PCMs [220]; (ii) encapsulating PCMs into micro or nanoparticles [221], fibers [222,223], and bulk materials (like films produced from blends or emulsions) [223–225] (some examples are shown in Figure 4.3); and (iii) their incorporation into porous materials, which act as supporting materials for the PCM through physical adsorption mechanisms [64,67,68].

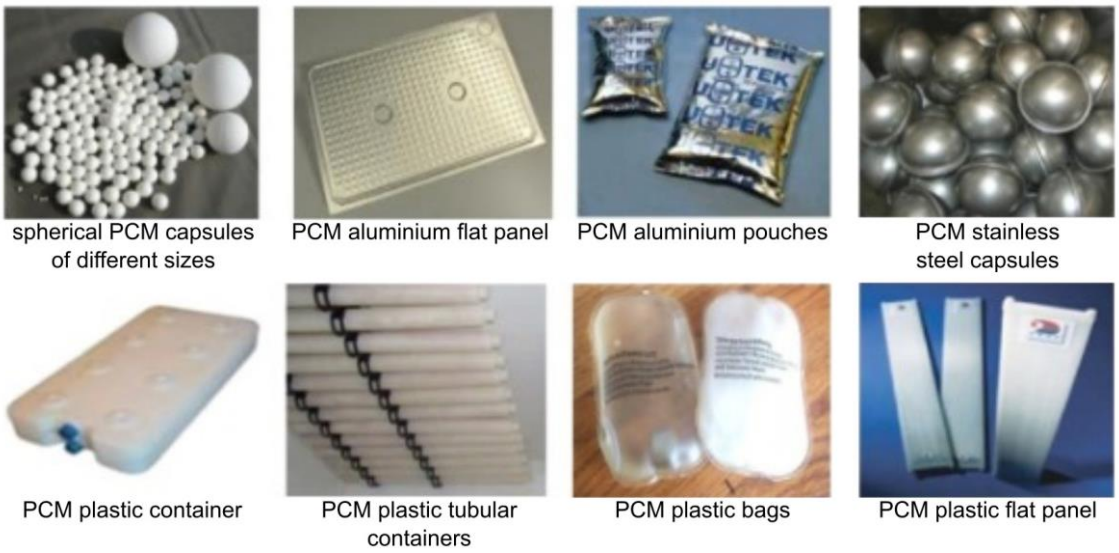

Figure 4.2: Examples of macroencapsulated PCMs. Reproduced from [220] with permission from Elsevier.

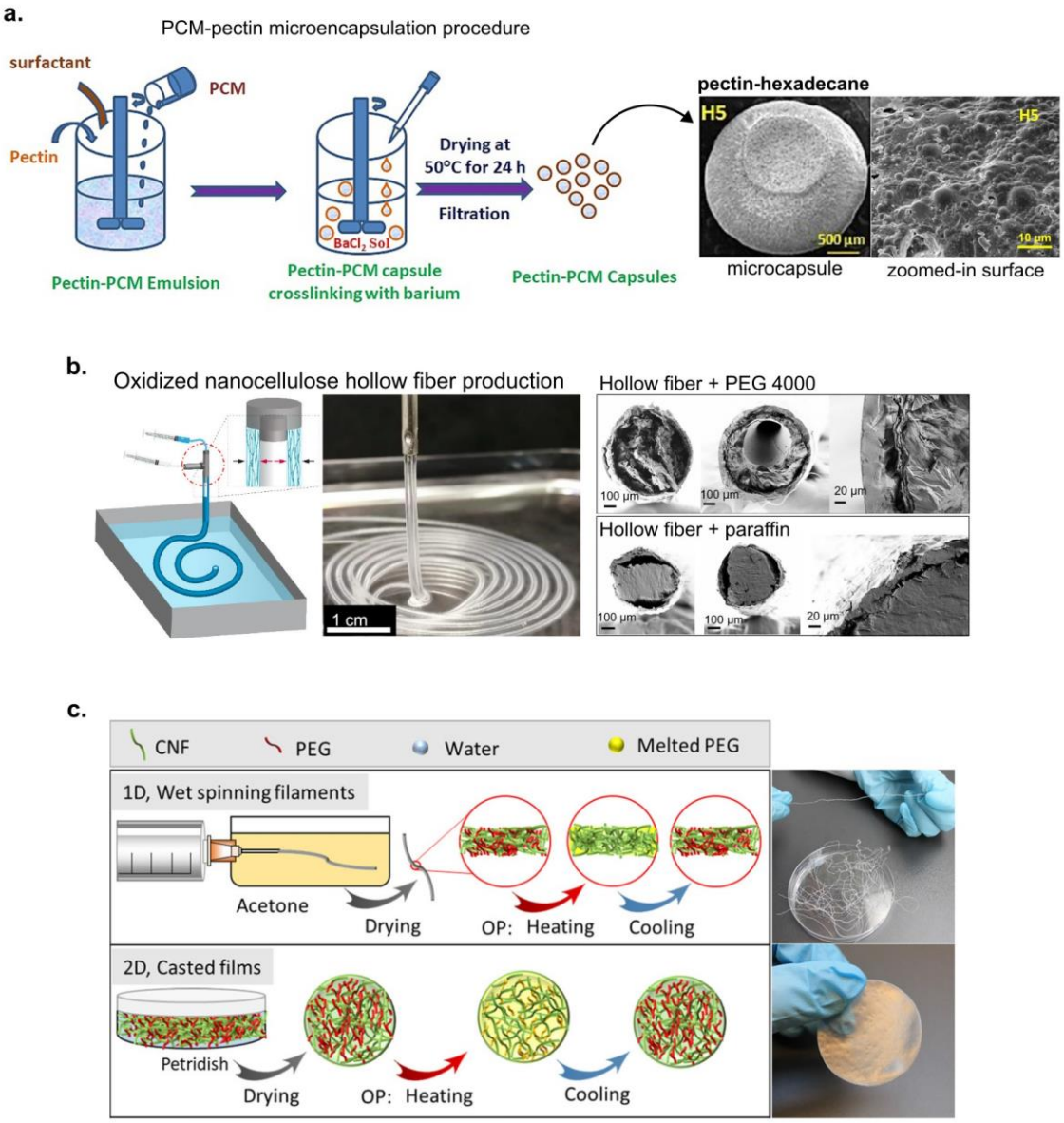

Figure 4.3: (a) PCM-pectin microcapsules preparation procedure (top) and morphology (bottom). Reproduced from [221] with permission from Elsevier. (b) Oxidized nanocellulose hollow fibers preparation (left) and their morphology after PCM impregnation (right). Reproduced from [222], licensed under CC BY 4.0. (c) Preparation of cellulose nanofibers/PEG filaments and films (left) and images of the resulting materials (right). Reproduced from [223], licensed under CC BY 4.0.

The use of porous materials as carriers for PCMs is considered a promising pathway to mitigate leakage and increase thermal stability, while

relying on simple preparation procedures (e.g., melt impregnation and vacuum-assisted melt impregnation) [49,62,83]. In addition, porous materials can be shaped into 3D structures, fibers, and beads prior to PCM impregnation [226,227]. Porous materials, like cryogels and aerogels, have been explored due to their high pore volume (> 90%), enabling the accommodation of large amounts of PCM inside their porous networks [62]. In this context, PCM leakage is mitigated by surface interactions and capillary forces acting inside the pores [59]. Therefore, porous materials bearing higher specific surface areas and smaller pores generally give rise to shape-stable phase-change composites with greater leakage resistance, and nanostructured materials are highlighted as notably promising PCM carriers. The presence of intermolecular interactions and chemical affinity between the components also enhances leakage resistance, while an open-pore network contributes to a more efficient PCM impregnation [62,69,70].

The loading ratio of PCMs into porous materials is usually expressed as the mass ratio between the PCM fraction and the whole phase-change composite (Eq. 4.2), while useful ways to assess the latent heat storage capacity of the obtained composites include calculating the latent heat efficiency and relative latent heat efficiency (Eq. 4.3 and Eq. 4.4, respectively). The former represents the proportion of the phase-change enthalpy (typically melting) of the phase-change composite relative to that of the neat PCM, whereas the latter accounts solely for the PCM fraction within the composite (Eq. 4.3 and 4.4).

$$loading\ ratio\ (\%) = \frac{m_f - m_i}{m_f} \times 100 \qquad (4.2)$$

where m_f is the mass of the phase-change composite and m_i the mass of the porous material before impregnation.

$$latent\ heat\ efficiency\ (\%) = \frac{\Delta H_{m,PCC}}{\Delta H_{m,PCM}} \times 100 \qquad (4.3)$$

$$relative\ latent\ heat\ efficiency\ (\%) = \left(\frac{\Delta H_{m,PCC}}{\Delta H_{m,PCM} \times LR}\right) \times 100 \qquad (4.4)$$

where $\Delta H_{m,PCM}$ is the melting enthalpy of the neat PCMs, $\Delta H_{m,PCC}$ the melting enthalpy of the phase-change composites, and LR the loading ratio (Eq. 4.2).

Porous materials can be loaded with PCMs via one-step (*in situ*) or two-step procedures [62]. For example, recent studies explored the incorporation of PEG (400 or 300) as a PCM into cellulose nanofibers (CNF) [212,228] and carboxymethyl chitosan/alginate-based cryogels [229] through one-step preparation methods. By mixing the biopolymer solutions/colloidal dispersions prior to freeze-drying, the PCM is confined within the pore walls (see examples on Figure 4.4b and c) or only partially fills the pores. Interestingly, one of these studies [212] compared this approach with the incorporation of PEG in the gel state (physical cross-linking was induced by HCl vapor), which provided higher melting enthalpy (93 vs. 45-65 J/g) attributed to a remarkably higher loading ratio (97%) (Figure 4.4e). Intermediary loading and thermal performance were achieved through physical cross-linking of the CNF-PEG mixture prior to freeze-drying (Figure 4.4f). The two-step route, in turn, involves the impregnation of already synthesized porous materials with a PCM, aiming to completely fill the pores with the PCM and achieve maximum loading into the porous carrier [62].

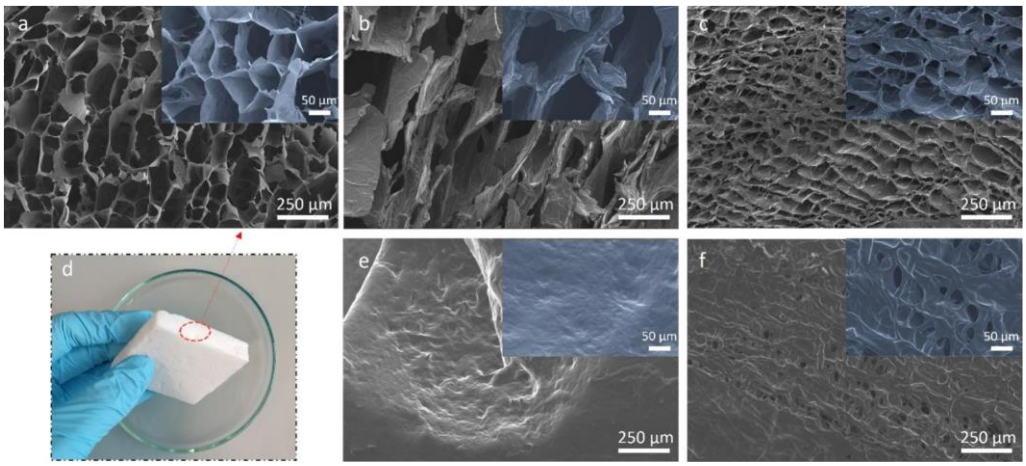

Figure 4.4: SEM observations of the (a) neat CNF cryogel and CNF-PEG cryogels prepared from dispersions containing (b) 80% and (c) 90% PEG:CNF. (d) Digital image of the neat CNF cryogel. Morphology of the (e) CNF-PEG

compound (90% PEG:CNF) dried after cross-linking, and the (d) the one prepared by PEG impregnation of the CNF hydrogel. Insets show the morphologies at a higher magnification. Reproduced from [212], licensed under CC BY 4.0.

4.2.1.2 Organic PCMs

PCMs can be classified as organic, inorganic, and eutectic (or hybrid). Examples of PCMs of each class, along with some examples of sensible heat storage materials (as discussed previously, Section 4.2.1), are presented in Figure 4.5. Inorganic PCMs include metal and metallic alloys, but salt hydrates are the most commonly used PCMs in this class for both research and commercial purposes [206]. They possess high latent heat values (up to 330 J/g), sharp melting peaks, and good thermal conductivity (ca. 0.5-0.7 W/mK). Nevertheless, some disadvantages include their corrosive nature, phase separation behavior (incongruent melting), and high supercooling degrees [65,206].

PHYSICAL THERMAL ENERGY STORAGE			
SENSIBLE HEAT STORAGE	LATENT HEAT STORAGE		
	ORGANIC	INORGANIC	EUTETIC
Water Themal oils Brine Rock beds Mansonry	Paraffins Polyethylene glycols Fatty acids Polyalcohols	Salt hydrates Metals	Organic-organic Organic-inorganic Inorganic-inorganic

Figure 4.5: Classification and examples of substances used for sensible heat storage and latent heat storage (PCMs) [65,206].

Organic PCMs, on the other hand, are widely available and generally inexpensive, while boasting high latent heat values (up to 270 J/g), phase-change temperatures suitable for various practical applications (−5 to 80 °C), congruent melting (i.e., without phase separation or compositional change), and thermal and chemical stability. This class includes paraffins, polyethylene glycols (PEGs), and fatty acids [65,205].

Paraffins (alkanes and their mixtures) and PEGs are derived from fossil-based feedstocks, and have a large range of melting temperatures that depend on their molecular weight (see Table 4.1) [205,206]. Although paraffins are the most widely used organic PCM [206], PEG has been increasingly investigated as a PCM confined by biomass- or biopolymer-based materials due to its capability it interact with OH-rich polymers through strong hydrogen bonds, thus, being compatible with those materials [69] (its chemical structure is presented in Figure 4.6a). In this context, mainly PEGs of higher molecular weight (e.g., PEG 4000 and PEG 6000) have been explored, as they present greater phase-change enthalpies and sharp melting peaks [49,68,77,230].

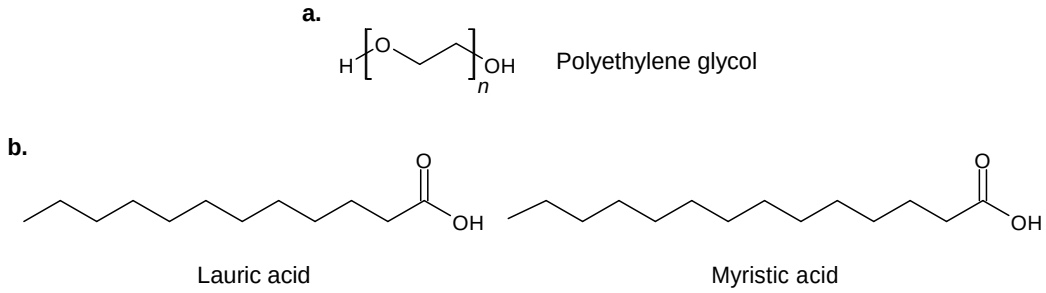

Figure 4.6: Chemical structures of (a) PEG, and (b) lauric and myristic acids.

Fatty acids, in contrast, are renewable PCMs (some examples are presented in Table 4.1). They are naturally found in vegetable oils such as coconut, soybean, and palm kernel oils [65,231]. Coconut oil is a promising alternative PCM, as it presents a melting temperature of approximately 25 °C, allowing its application in TESs at room temperature, in addition to a relatively high melting enthalpy (ca. 105 J/g) and reasonable thermal stability [231]. Coconut oil is a mixture of medium-chain saturated fatty acids in the form of triacylglycerols (fatty acid esters linked to a glycerol backbone). The main fatty acids in coconut oil are lauric acid (up to 51%) and myristic acid (17-21%), but lower amounts of caprylic, palmitic, capric acid, and others are also present (see Table 4.2) [231–233]. The structures of lauric and myristic acids are shown in Figure 4.6b.

Table 4.1: Melting temperature (T_m) and enthalpy (ΔH_m) of some paraffins (neat alkanes) [234], polyethylene glycols [205] and fatty acids [235].

PCM	Formula	T_m (°C)	ΔH_m (J/g)
Paraffins			
Tridecane	$C_{13}H_{28}$	-5	196
Tetradecane	$C_{14}H_{30}$	6	227
Pentadecane	$C_{15}H_{32}$	10	207
Hexadecane	$C_{16}H_{34}$	18	236
Heptadecane	$C_{17}H_{36}$	22	214
Octadecane	$C_{18}H_{38}$	28	244
Nonadecane	$C_{19}H_{40}$	32	222
Eicosane	$C_{20}H4_2$	37	248
Triacontane	$C_{30}H_{62}$	65	262
Tetracontane	$C_{40}H_{82}$	82	272
PEGs			
PEG 400	$HO(C_2H_2O)_nO$; M_w ~ 400	6	84
PEG 600	$HO(C_2H_2O)_nO$; M_w ~ 600	21	119
PEG 1000	$HO(C_2H_2O)_nO$; M_w ~ 1000	39	152
PEG 1500	$HO(C_2H_2O)_nO$; M_w ~ 1500	49	161
PEG 4000	$HO(C_2H_2O)_nO$; M_w ~ 4000	61	170
PEG 6000	$HO(C_2H_2O)_nO$; M_w ~ 6000	62	180
Fatty acids			
Capric acid	$CH_3(CH_2)_8{\cdot}COOH$	36	152
Eladic acid	$C_8H_7C_9\ H_{16}{\cdot}COOH$	47	218
Lauric acid	$CH_3(CH_2)_{10}{\cdot}COOH$	49	178
Myristic acid	$CH_3(CH_2)_{12}{\cdot}COOH$	58	199
Palmitic acid	$CH_3(CH_2)_{14}{\cdot}COOH$	55	163
Stearic acid	$CH_3(CH_2)_{16}{\cdot}COOH$	69	199

Table 4.2: Fatty acid composition of virgin coconut oil. Reproduced from [232], licensed under CC BY 3.0.

Fatty acid	Content (%)
Caproic acid	0.7
Caprylic acid	9.2
Capric acid	6.4
Lauric acid	45.6
Myristic acid	16.6
Palmitic acid	8.2
Stearic acid	3.4
Arachidic acid	0.6
Lignoceric acid	0.5

Various bio-based porous materials have been explored as carriers for organic PCMs in the literature. These studies are reviewed in the next Section, with a special focus on pectin and citrus waste-sourced porous materials.

4.2.2 Bio-based porous materials as carriers for organic PCMs

Bio-based porous materials have been increasingly explored as carriers for organic PCMs due to their environmental appeal and abundant sources, while maintaining high porosities and thus high PCM loading ratios [236]. In this context, mainly two types of bio-based materials have been investigated: carbon porous materials and non-carbon biopolymer-based foams, such as cryogels for example. Both can be obtained either from neat biopolymers or “bulk” biomass. A third strategy is the delignification of cellulose-rich biomasses, like wood [76] and sorghum straw [237], capitalizing on the intrinsic hierarchical structure of plant tissues. However, this approach falls out of the scope of this work and will not be discussed in the following.

In the first approach, organic precursors (bulk biomass or bio-based porous materials, fabricated through the second strategy) are subjected to a pyrolysis process [62,236]. In some cases, the biomass waste is hydrothermally treated to produce a carbonaceous hydrogel, which is then dried [80]. The second approach relies on different drying procedures (mainly freeze-drying and oven-drying). Neat isolated biopolymers are typically dissolved (or dispersed, in the case of colloidal particles), and sometimes gelled, prior to drying [67,73,212,228]. Bulk biomass wastes have been directly dried (oven-dried [68,238] or freeze-dried [49,81]) or, sometimes, after being subjected to pre-treatments to facilitate processing (e.g., alkaline pre-treatment [77]). The different drying procedures and properties of the various porous materials have been discussed in Chapter 3.

Carbon-based networks are electrically and thermally conductive, enabling the confined PCM to store/release thermal energy at higher rates and making them promising candidates for electrothermal and photothermal conversion applications. Conversely, materials with low thermal conductivity

(like the non-carbon bio-based porous materials) are more suitable for thermal protection applications [62].

Several biomass wastes have been investigated as a source for producing carbon scaffolds for PCM confinement, examples include rice husks [239], pine cone and sawdust [240], watermelon rind [80], and also citrus residues, including orange [49,50,83], pomelo [81] and grapefruit peels [82]. Orange peels have been converted into potassium hydroxide (KOH)-activated biochar, featuring a surface area of 52 m^2/g and macropores of ca. 10-50 µm, for the encapsulation of myristic acid [83]. The PCM loading ratio was limited to 39%, leading also to a reduced thermal storage capacity (ΔH_m of 67 J/g at best). Xiao et al. [49] prepared porous carbon cryogels from orange peels via freeze-drying followed by pyrolysis. Afterwards, PEG 6000 was infiltrated into the resulting carbon foams at an 82% loading ratio (see Figure 4.7a), and the melting enthalpy of the impregnated PEG was slightly increased compared to the neat PEG (see relative latent heat efficiency, Table 4.3). In this study, the obtained orange peel carbon foam was decorated with silver nanoparticles to increase the thermal conductivity of the phase-change composites, leading to a subtle increase in the PEG loading ratio and melting enthalpies. Similar results were achieved for freeze-dried and pyrolyzed grapefruit peels, decorated or not with silver nanoparticles (PEG 6000 was also used as PCM) [82].

Suchorowiec and co-authors [50] added starch to the orange waste as a binder (0-20%) prior to freeze drying and pyrolysis. Starch incorporation at the lowest concentration (2.5%) led to a more homogeneous pore structure and thus more efficient confinement of PEG 6000, palmitic acid, and octacosane as PCMs. PEG-impregnated samples had negligible leakage after 1 h at 80 °C (ca. 1%), while for the other two PCMs leakage ranged from 9-31%. The authors attributed this to PEG's higher viscosity. The freeze drying-pyrolysis approach was also effective for paraffin impregnation into pomelo peel-based carbon cryogels (loading ratios of 88-96% and ΔH_m of 131-168 J/g) [81].

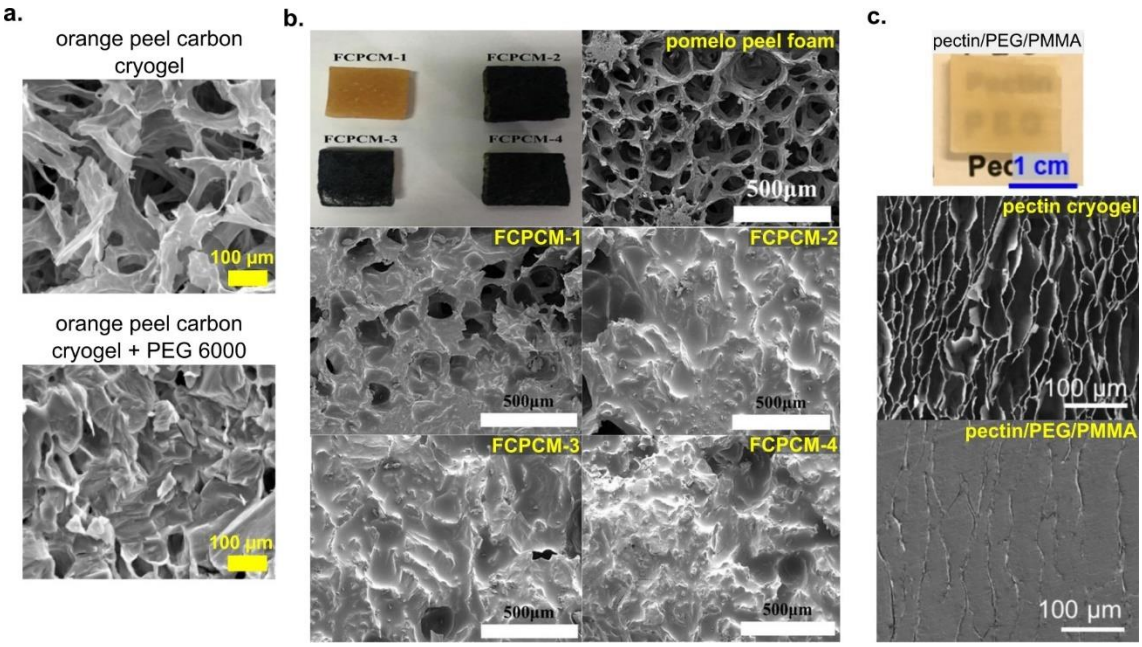

Figure 4.7: (a) SEM images of the orange peel-based carbon cryogel before (top) and after impregnation with PEG 6000 (bottom). Reproduced from [49] with permission from Elsevier. (b) Digital images (top right) and SEM images of the pomelo peel foam (top left) and pomelo peel-based phase-change composites: without MXene (FCPCM-1) and with MXene deposited from dispersions with 2, 4 and 6 mg/mL (FCPCM-2, 3 and 4, respectively). Reproduced from [68] with permission from Elsevier. (c) Digital image of the anisotropic pectin cryogel and the pectin/PEG/PMMA composite (top) and their respective morphologies. Reproduced from [74], licensed under CC BY 4.0.

The literature on non-carbon porous materials based on citrus biomass waste is even more limited. Foams obtained by directly oven-drying pomelo peels have been used to confine PEG 400 [68] and PureTemp®23 (composition not disclosed) [238]. In the first case [68], a coarse morphology (Figure 4.7b) and low specific surface area (5 m^2/g) were obtained. Consequently, 80% mass loss was observed after 10 h at 80 °C (above PEG 4000 melting temperature) due to liquid PCM leakage, which was decreased to 40% by decorating the pomelo peel foam with MXene sheets (Figure 4.7b). This modification also improved the PCM loading ratio (from 87% to 96%) and latent heat efficiency (from 85% to 95%), which was ascribed to the increased amount of oxygen

atoms in the foam surface with the incorporation of MXene, enhancing its compatibility with PEG. The relative latent heat was the same for all samples, therefore, MXene did not alter the crystal structure of PEG 4000.

Biesuz et al. [238] evaluated a PCM (composition not disclosed) incorporated in oven-dried pomelo peel, resulting in a loading ratio of 84% and a latent heat efficiency of 71%. Once again, a coarse foam morphology was observed (pores of ca. 20-300 μm), but a denser layer was also present, leading to remarkably different leakage behavior depending on which layer was facing the filter paper placed below the sample during the analyses (95% with the porous section in contact with the paper vs. 10% with the dense layer in contact with the paper).

As for neat biopolymer-based porous carriers for PCMs, (nano)cellulose and its blends/composites stand out at the forefront of this field [212–215,217,228]. Other examples include cryogels based on chitosan [70,71], alginate [70,72], starch [210], gelatin [211], and carboxymethylcellulose [216]. Only a few studies have dealt with pectin-based porous carriers for oraganic PCMs. Wang and co-authors [67] produced cryogels from ionically gelled pectin with dispersed MXene nanosheets, in which dodecylamine was confined as a PCM. The latent heat efficiency was 62% in the absence of MXene and increased to up to 84% after its incorporation. Impregnation provided a lower decrease in the melting enthalpy after 50 heating-cooling cycles. MXene further improved this aspect, in addition to conferring higher thermal conductivity and photo-thermal energy conversion ability to the composites. The same research group later explored the effects of clay incorporation into Ca^{2+}-cross-linked pectin cryogels, this time, followed by pyrolysis [73]. Clay incorporation and carbonization led to increased photo-thermal energy conversion, but decreased heat storage efficiency and stability upon thermal cycling. Finally, leakage resistance for up to 60 min at 70 °C (the dodecylamine T_m was 35 °C) of the composites was claimed by the authors (visually demonstrated).

In a different approach, anisotropic pectin cryogels were loaded with PEG 1000 mixed with methyl methacrylate, which was polymerized post-impregnation, creating a variable-transmittance phase-change composites

(Figure 4.7c) [74]. The presence of poly(methyl methacrylate) and the pectic network impaired PEG crystallization. Accordingly, the latent heat was only 48 J/g for the pectin/PEG/PMMA composite, while that of neat PEG was 147 J/g. The studies herein discussed, dealing with phase-change composites derived from citrus waste- and pectin-based porous carriers, are summarized in Table 4.3.

Table 4.3: Summary of articles on citrus waste-based porous materials as carriers for organic PCMs. LR is the loading ratio, ε the latent heat efficiency, and ε_r the relative latent heat efficiency (Eq. 4.2, Eq. 4.3 and Eq. 4.4, respectively).

Biomass **Material preparation** **PCM**	**LR (%)**	**Leakage test**	**ε (%)**	**ε_r (%)**	**Ref.**
Orange peels Dried (60 °C, 48 h), activated with KOH and pyrolyzed at 600 °C **Myristic acid**	33-39	Visually evaluated	33-44	-	[83]
Orange peels Freeze-dried, pyrolyzed at 800 °C, and decorated with silver nanoparticles **PEG 6000**	82-85	Visually evaluated (90 °C, 20 min)	88	105-107	[49]
Orange waste (not specified) Mixed with starch solutions (0-20% starch to orange waste), freeze-dried and pyrolyzed at 600 °C **PEG 6000, palmitic acid (PA), octacosane (OC)**	PEG 89-93 PA 87-91 OC 86-91	PEG 1% PA 9-35% OC 11-31% (80 °C, 1 h)	PEG 89-94 PA 89-99 OC 86-96	-	[50]
Grapefruit peels Freeze-dried, pyrolyzed at 800 °C, and decorated with silver nanoparticles **PEG 6000**	83-84	Visually evaluated (90 °C, 9 min)	82-84	98-99	[82]
Pomelo albedo Freeze-dried and pyrolyzed (650-850 °C) **Paraffin**	88-96	Visually evaluated (80 °C, 45 min)	81-100	-	[81]
Pomelo peels	87-96	40-80%	85-95	98	[68]

Oven dried and decorated with MXene nanosheets **PEG 4000**		(80 °C, 10 h)			
Pomelo peel Oven-dried (180 °C, 30 min) **PureTemp®23**	84	95%*; 10%** (80 °C, 14 days)	71*	-	[238]
Pectin Dissolution in the presence of $CaCl_2$ and MXene, and freeze-dried **Dodecylamine**	-	-	62-84	-	[67]
Pectin Dissolution in the presence of $CaCl_2$ and clay, freeze-dried and pyrolyzed (600 °C) **Dodecylamine**	-	Visually evaluated (75 °C, 1 h)	65-84%	-	[73]
Pectin Directionally frozen and freeze-dried **PEG 1000**/PMMA	48	-	33%	-	[74]

* porous part turned down
** dense layer turned down

4.2.3 Concluding remarks

The freeze-drying method has been the primary approach explored for producing bio-based porous materials, either from neat biopolymers [70–72,210–215] or bulk biomasses [49,50,77,81,82], to confine organic PCMs. Aerogels from citrus waste have never been explored as PCM carriers, despite having remarkable potential for the development of leakage-proof phase-change composites, as capillary forces can be enhanced by their nanostructured networks [62]. In addition, few studies have directly compared different organic PCMs confined within bio-based porous carriers [50,69].

In this Chapter, aerogels derived from orange waste biomass are evaluated as carriers for organic PCMs, and compared with their cryogel counterparts and neat pectin aerogels. A two-step preparation method was selected as it enables the PCM infiltration into the carriers' pore volume, resulting in remarkably high loading ratios (82-96%) [68,77,81,207]. PEG 4000 and coconut oil were chosen as organic PCMs. While the former is a fossil-

based PCM frequently studied in the literature [68,77,230], coconut oil is an emerging bio-based alternative with a more hydrophobic character [231]. Both were impregnated into orange waste biomass-based porous materials presenting different morphologies and shapes, and the impact of the porous materials characteristics on the PCMs thermal performance and leakage resistance was investigated.

4.3 Materials and Methods

4.3.1 Materials

Orange (*Citrus sinensis*, variety Pera Rio) waste biomass fractions were donated by JBT Company (Araraquara, Brazil): peels, bagasse, and pulp (see details in Section 2.3.1). According to results obtained on orange waste-based suspensions' stability in Chapter 2 and as used to make aerogels and cryogels in Chapter 3, each fraction was washed twice with tap water, dried, ground and sieved (mesh 35, 500 µm) (details are described in Section 2.3.2). Orange biomass fractions were then mixed at their respective proportions to obtain the mixed orange waste biomass (56% peels, 28% bagasse and 16% pulp). Individual fractions were not used in this Chapter.

Commercial low-methoxy (LM) pectin (GENU pectin type LM-102 AS) was donated by CP Kelco (Limeira, Brazil) and used as received. The degree of esterification was 30%, as informed by the manufacturer. Absolute ethanol (99%; Fisher), anhydrous citric acid (Synth), virgin coconut oil (La Tourangelle), and PEG 4000 (Sigma-Aldrich) were also used.

4.3.2 Porous materials preparation and characterization

To prepare the suspensions used as precursors for producing aerogels and cryogels, mixed biomass was hydrolyzed in 5% citric acid solutions at a 4% concentration, at 90 °C, for 2 h. Three types of porous materials based on orange mixed biomass were made: monolithic cryogels, monolithic aerogels

and aerogel beads. LM pectin monolithic aerogels were also made for comparison.

- Cryogel monoliths were obtained by freeze-drying suspensions. After removing bubbles with mild centrifugation (24 *g*, 2-3 min), samples were frozen at -5 °C, and freeze-dried with a Cryotec Cosmos 80 machine at -80 °C for 72 h.
- Orange mixed biomass aerogel monoliths were made from the suspensions via non-solvent induced phase separation (i.e., by adding ethanol as non-solvent on the top of suspension), solvent exchange with ethanol, and drying with supercritical CO_2. Aerogel preparation procedures are presented in detail in Section 3.3.2.1.
- Orange mixed biomass aerogel beads were prepared by the dripping method using with a home-made setup to control the flow rate, and distance between the needle tip and the coagulation bath, respectively set at 70 mL/min and approximately 1 cm. A blunt-tip needle with an internal diameter of 1.37 mm was used. Ethanol was employed in the coagulation bath (8 cm of height) and for solvent exchange, prior to drying with supercritical CO_2. Details are described in Section 3.3.2.1.
- LM pectin aerogel monoliths were prepared using the same procedure as for orange mixed biomass aerogel monoliths.

The porosity, morphology, and specific surface area of the porous materials used as carriers for the organic PCMs were assessed as described in Section 3.3.3.

4.3.3 Phase-change composites preparation

All types of porous materials prepared were impregnated with two organic PCMs: PEG 4000 (synthetic, hydrophilic, and with a higher melting point) and coconut oil (natural, hydrophobic, and with a lower melting point). The porous materials were placed inside beakers and covered with the PCMs at temperatures above their melting temperature, 75 °C for PEG 4000 and 35°C for coconut oil, under vacuum. Aerogel and cryogel monoliths were impregnated with PEG for 15 h and with coconut oil for 2 h. Beads, in contrast, required less

time: 7 h for PEG and 1 h for coconut oil. Impregnation times were determined visually, as the non-impregnated regions remained white and opaque, whereas those efficiently impregnated (at the macroscopic scale) had a translucent aspect above the PCM melting temperature. Excess molten PCM was removed from the carriers' surface with paper.

4.3.4 Phase-change composites characterization

4.3.4.1 Loading ratio and shrinkage

Volumetric shrinkage during impregnation was calculated by Eq. 4.5:

$$shrinkage\ (\%) = \frac{V_i - V_f}{V_i} \times 100 \qquad (4.5)$$

where V_i and V_f correspond to the sample volume before and after the PCM impregnation, respectively. The volume was calculated from height and diameter measurements with a 0.001 mm precision caliper, in triplicate, for monoliths; and via digital image processing for aerogel beads. Digital images were taken over a LED light table and processed with the software ImageJ. At least and 125 beads were evaluated for each sample set (impregnated with PEG or coconut oil).

The loading ratio was calculated with Eq. 4.2 (presented in Section 4.2.1.1), in triplicate, and expressed as the mass ratio of PCMs over the mass of the phase-change composites. The theoretical loading rate, estimated from samples' porosity and PCM density, was calculated with Eq. 4.6, and corrected for the volumetric shrinkage with Eq. 4.7.

$$theoretical\ loading\ ratio\ (\%) = \left(\frac{P \times \rho_{PCM}}{P \times \rho_{PCM} + \rho_{ap}}\right) \times 100 \qquad (4.6)$$

$$corrected\ theoretical\ loading\ ratio\ (\%) = \left(\frac{P \times (1-S) \times \rho_{PCM}}{P \times (1-S) \times \rho_{PCM} + \rho_{ap}}\right) \times 100 \qquad (4.7)$$

where P and ρ_{ap} were the porosity and apparent density of the porous materials before impregnation with the PCM, S the shrinkage samples underwent during PCM impregnation (Eq. 4.5), and ρ_{PCM} the density of the molten PCMs: 1.085 g/cm³ was used for PEG 4000 (assuming it has the same density as reported for PEG 3000 at 70 °C [241]), and 0.908 g/cm³ for coconut oil (value at 40 °C [242]).

4.3.4.2 Differential Scanning Calorimetry (DSC)

Thermal behavior and properties of the neat PCMs and phase-change composites were evaluated by DSC (Q200, TA Instruments). Samples of 6-8 mg were subjected to a first heating scan to erase their thermal history, followed by a cooling ramp and a second heating. All ramps were carried out using a heating/cooling rate of 10 °C/min and under a 50 mL/min nitrogen flow. Temperatures ranged from 10 to 90 °C for PEG 4000 and its phase-change composites, and from -40 to 50 °C for coconut oil and its phase-change composites. At least 3 replicates were performed for each sample.

Melting and crystallization enthalpies (ΔH_m and ΔH_c, respectively) were calculated from their corresponding peak areas normalized by the samples' mass. The latent heat efficiency and the relative latent heat efficiency were calculated using Eq. 4.3 and Eq. 4.4, respectively.

4.3.4.3 Leakage tests

The mass loss over time as a result of molten PCM leakage was monitored. Samples were left standing over filter paper for 6 h inside an oven (at 75 °C for the PEG composites, and at 35 °C for the coconut oil composites), and periodically weighed with a digital balance with a 0.1 mg precision.

4.3.4.4 Thermal stability

Thermogravimetric analyses (TGA) were carried out on 16-18 mg samples of neat PCMs and their corresponding phase-change composites,

using a Q50 equipment from TA Instruments. A temperature sweep from 30 to 600 °C was performed at a 20 °C/min rate, under a 60 mL nitrogen flow.

4.3.4.5 Infrared imaging

The thermal performance of the phase-change composites was assessed by monitoring their temperature with an PI450i infrared camera from Optris, having a spectral range of 8 µm to 14 µm, and calibrated in the temperature range of -20 to 100 °C. Calibrations are performed with blackbody references across different temperatures and loaded into the Optris Pix Connect software, used to set and run the analyses. Monoliths were polished with sandpaper to ensure a consistent thickness (1.8-1.9 mm) and good contact with the hot plate. Beads (17-20 beads) were placed on the hot plate directly. In order to fully solidify the coconut oil, its phase-change composites were cooled down from room temperature (20 °C) by placing them inside polypropylene vials submerged in liquid nitrogen.

Samples were placed over a hot plate at 95 °C for PEG-based phase-change composites, and at 50 °C for those based on coconut oil. Their infrared images and temperatures (calculated from the infrared radiation emitted in each pixel and converted into a color scale) were recorded over time.

4.3.4.6 Morphology

The morphology of the non-impregnated carriers and PEG-based phase-change composites were examined with a Tescan Maia 3 Scanning Electron Microscope (SEM), using a beam accelerating voltage of 3 kV. Prior to analysis, cryofractured surfaces were sputtered with a 14-nm platinum layer using a Q150T Quarum apparatus. SEM analyses of the composites loaded with coconut oil were not feasible as sample metallization at room temperature was not possible due to coconut oil’s melting temperature (ca. 25 °C).

4.4 Results and Discussions

4.4.1 Characterization of porous carriers and phase-change composites

The properties of the porous materials used as PCM carriers (apparent density, porosity (Eq. 3.3), and specific surface area) are summarized in Table 4.4, and their morphologies are depicted in Figure 4.8. Carriers were made from orange biomass waste derived from the mixed biomass fraction only (here referred to as “mixed biomass”), and neat LM pectin aerogels were used as a reference.

Table 4.4: Apparent density, specific surface area and porosity of the porous carriers before PCM impregnation.

	Mixed biomass aerogel	**Mixed biomass cryogel**	**Mixed biomass aerogel beads**	**LM pectin aerogel**
Apparent density (g/cm^3)	0.091 ± 0.001	0.088 ± 0.004	0.0779 ± 0.0003	0.078 ± 0.005
Specific surface area (m^2/g)	209 ± 28	8 ± 1	308 ± 31	150 ± 0
Porosity (%)	94 ± 1	94 ± 5	95 ± 1	95 ± 6

All porous carriers presented similar densities and porosities (0.08-0.09 g/cm^3 and 94-95%, respectively), while their specific surface areas were different. Cryogel monoliths based on mixed biomass had substantially lower specific surface area than their aerogel counterparts (8 vs. 209 m^2/g), which stems from their respective morphologies: cryogels exhibited large pores with dozens to hundreds of microns of size; while aerogels boasted a nanostructured fibrillar pectin network, surrounding partially porous insoluble fibers and particles (Figure 4.8a and b). Mixed biomass-based aerogel beads had a similar pore structure as the aerogel monolith (Figure 4.8c), but higher specific surface area (308 m^2/g). Despite the absence of insoluble particles, LM pectin underwent chain degradation during the citric acid pre-treatment, resulting in an aerogel with reduced surface area (150 m^2/g), as discussed in Chapter 3.

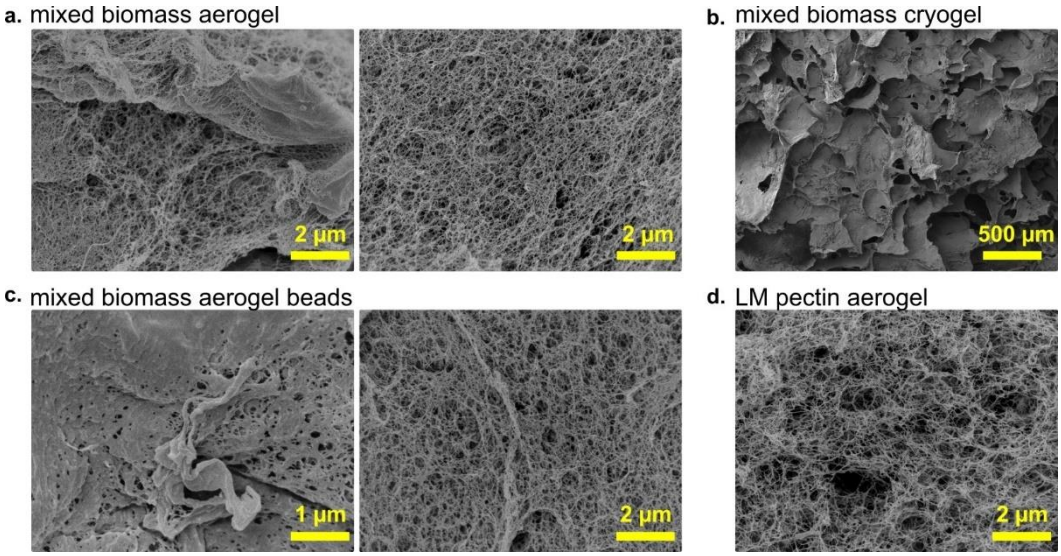

Figure 4.8: SEM images of the porous carriers before impregnation with the PCMs. (a) mixed biomass aerogel (insoluble fraction at the left and pectin matrix at the right), (b) mixed biomass cryogel, (c) mixed biomass (insoluble fraction at the left and pectin matrix at the right), and (d) LM pectin aerogel.

Phase-change composites were obtained after the impregnation of aerogel monoliths, cryogel monoliths, and aerogel beads with two organic PCMs, PEG and coconut oil (Figure 4.9). Impregnation conditions are provided in Section 4.3.3 and its duration depending on carrier shape is shown in Table 4.5. Phase-change composites from LM pectin aerogels were produced for comparison.

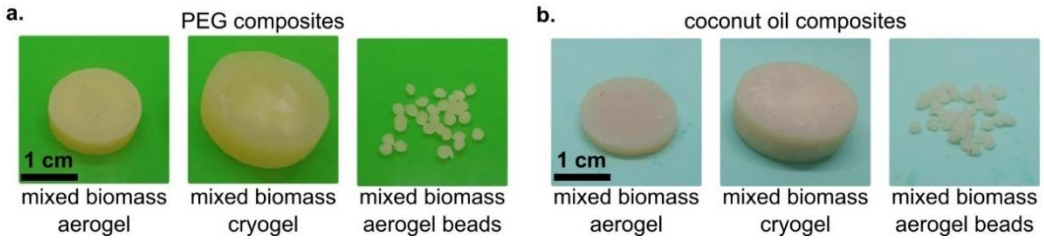

Figure 4.9: Digital images of the mixed biomass-based carriers loaded with (a) PEG and (b) coconut oil.

In a first approximation, impregnation times depended on the viscosity of the liquid, morphology and thickness of the porous carrier. PEG required 15 h to

be completely impregnated into the mixed biomass-based aerogels, and coconut oil only 2 h (Table 4.5). In the conditions used, molten PEG had a higher viscosity compared to coconut oil. According to the literature, PEG 3000 presented a viscosity of approximately 140 mPa.s at 80°C [241], while that of coconut oil was 28 mPa.s, at 38 °C [243]. All other monoliths were impregnated under the same conditions (mixed biomass cryogel and LM pectin aerogel), while aerogel beads were investigated for reduced impregnation times. Aerogel beads required about half the time to be entirely impregnated when compared to their monolithic counterparts: 7 h for PEG, and 1 h for coconut oil (Table 4.5).

Table 4.5: Impregnation time of the different PCMs into aerogel and cryogel monolithic carriers (mixed biomass aerogel, mixed biomass cryogel and LM pectin aerogel) and aerogel beads.

	Aerogel and cryogel monoliths	**Mixed biomass aerogel beads**
PEG 4000 (75 °C)	15 h	7 h
Coconut oil (35 °C)	2 h	1 h

During the impregnation with PCMs, porous carriers underwent different volumetric shrinkages (Eq. 4.5), as presented in Table 4.6. Concerning the PEG composites, those exhibiting higher surface areas underwent more pronounced volumetric shrinkage: 29-30% for mixed biomass aerogel monoliths and beads vs. 13 and 6% for LM pectin aerogels and mixed biomass cryogels, respectively. This could be ascribed to the increased capillary forces developed inside smaller pores. Carriers loaded with coconut oil exhibited lower shrinkage and smaller differences among themselves (7-16%). Coconut oil is expected to have reduced interactions with the biopolymer pore walls due to the aliphatic nature of its fatty acid chains, possibly reducing the influence of the capillary pressure within the pores.

To assess the PCM impregnation efficiency, the actual (LR) and theoretical loading ratios (LR_{th}) were calculated (Eq. 4.2 and Eq. 4.6, respectively) and presented in Table 4.6. The theoretical loading ratio

expresses the mass ratio of PCM to the phase-change composite if the pore volume of the carriers was entirely filled with PCM. Because the samples underwent volumetric shrinkage during impregnation, the theoretical loading ratio corrected for the final pore volume was also calculated (LR_{th}*, Eq. 4.7). It should be noted that although this correction was intended to compensate for the volume loss available for PCM loading, it represents an estimate, as the shrinkage occurred over time, gradually changing the pore volume during PCM impregnation.

Table 4.6: Shrinkage and loading ratios of the phase-change composites. LR_{th} and LR_{th}* are the theoretical loading ratios, the latter being corrected for the volumetric shrinkage.

	Mixed biomass aerogel	**Mixed biomass cryogel**	**Mixed biomass aerogel beads**	**LM pectin aerogel**
PEG composites				
Shrinkage (%)	29 ± 1	6 ± 2	30.4 ± 0.4	13 ± 1
LR (%)	85.5 ± 0.1	90.9 ± 0.4	90.1 ± 0.4	91.9 ± 0.7
LR_{th} (%)	92	92	93	93
LR_{th}* (%)	89	92	90	92
Coconut oil composites				
Shrinkage (%)	10 ± 3	13 ± 3	7.4 ± 0.1	16 ± 1
LR (%)	88.2 ± 0.7	88.3 ± 0.6	90 ± 2	89 ± 1
LR_{th} (%)	90	91	92	92
LR_{th}* (%)	89	89	91	90

All phase-change composites had a satisfactory loading ratio (85-92%, Table 4.6), comparable to those reported in the literature [49,68,77,81]. The lowest value, around 85%, was obtained for PEG-impregnated mixed biomass aerogels, most probably due to the long impregnation times and emergence of closed porosity, resulting from the gradual shrinkage. The effective PEG impregnation into the porous materials was confirmed by SEM images (Figure 4.10), which also shows the absence of clear phase boundaries, suggesting good adhesion between PEG and the biomass skeleton. Some cracks and voids are visible (blue arrows in Figure 4.10) and may have arisen from the volumetric contraction of PEG upon solidification after the impregnation

procedure. Coconut oil loading was efficient regardless of the pore structure and surface areas, reaching 88-90% (Table 4.6). Except for the PEG-impregnated mixed biomass aerogel monolith, the differences between the actual loading ratios and the theoretical ones, corrected for shrinkage, did not surpass 1%.

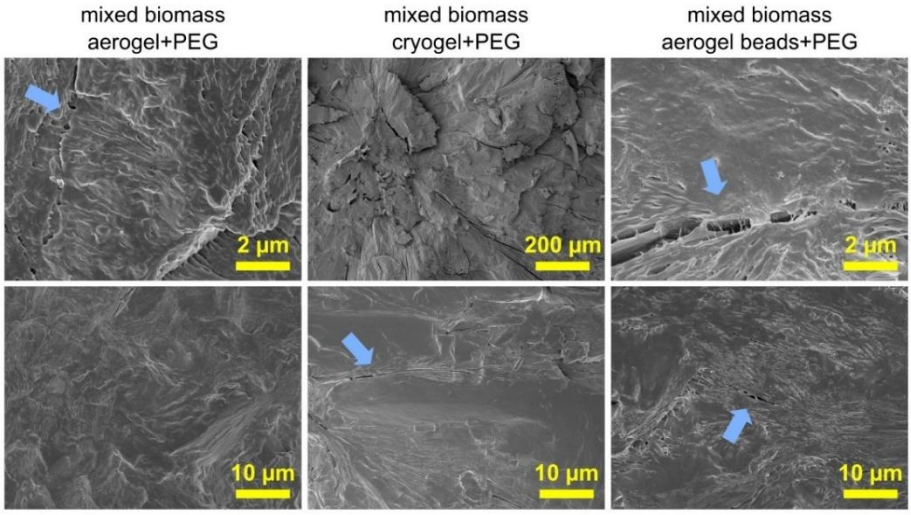

Figure 4.10: SEM images of mixed biomass-based carriers loaded with PEG. Blue arrows show cracks and voids.

4.4.2 Thermal stability

In addition to the leakage prevention, the PCM confinement inside porous structures is reported to provide increased thermal stability [59]. TGA analyses were performed to investigate how mixed biomass- and pectin-based carriers influenced PEG's and coconut oil's thermal stability. The obtained TG and DTG curves are presented in Figure 4.11.

All phase-change composites underwent a two-stage thermal decomposition: one associated with the biopolymer skeleton, at lower temperatures; and a second, associated with the PCMs (see Figure 4.11b and c). The PEG decomposition occurred in one sharp stage at 415 °C (Figure 4.11b), in accordance with the literature [207], and was slightly shifted to 417-419 °C when PEG was confined within the porous materials (see inset at the top right, Figure 4.11b). The onset of this decomposition peak, associated with

PEG, was delayed for the composites when compared to neat PEG (from ca. 262 to 353 °C) (see red arrow in the inset at the bottom right, Figure 4.11b). These results suggest that impregnating PEG into the porous carriers enhanced its thermal stability to a certain extent.

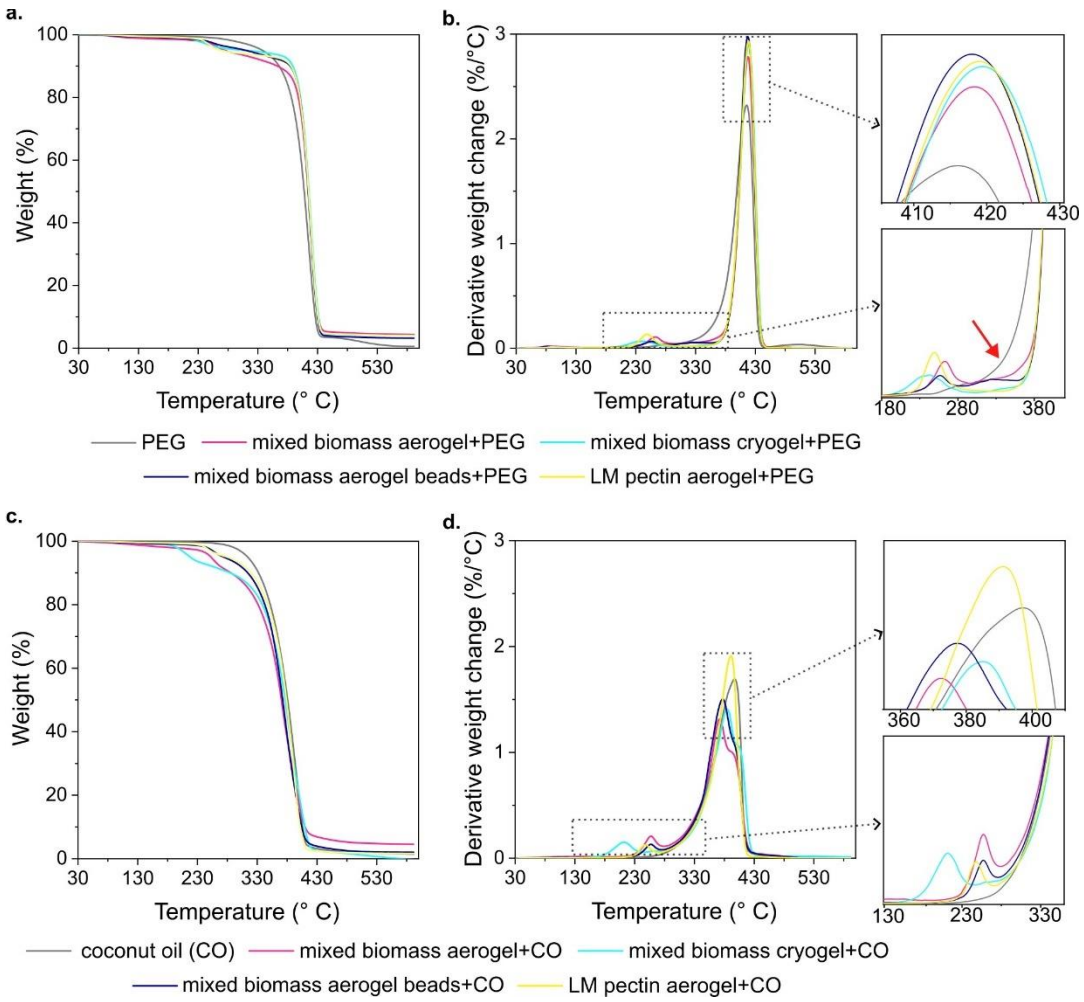

Figure 4.11: TG (left) and DTG (right) curves of (a,b) PEG and its composites, and (c,d) coconut oil and its composites. Enlarged insets of the DTG curves are presented, as indicated by the arrows.

More significant thermal protection has been achieved by confining PEG into other bio-based porous carriers, such as orange peel-based carbon cryogels [50] and *Miscanthus lutarioriparius* biochar [230], reflected by larger displacements of the decomposition peak to higher temperatures. Conversely, an effect of similar magnitude have also been reported for PVA/graphene

cryogels loaded with PEG 2000 [207]. A small decomposition peak at 190-300 °C also appears for the impregnated samples and corresponds to the overlapping decomposition of biopolymers present in the porous materials (pectin, hemicellulose, and cellulose) (Figure 4.11b) [17,135]. Lignin's decomposition was likely masked by PEG's peak. This first and smaller decompositon peak appeared at moderately lower temperatures when the carrier was the LM pectin aerogel (inset at the bottom right, Figure 4.11b), as pectin has inferior decomposition temperatures compared to hemicellulose and cellulose [17,135]. For the cryogel-based composite, this peak was more strongly displaced to lower temperatures, and centered at 240 °C. Possibly, this could be attributed to the presence of residual citric acid in the cryogels (as discussed in Chapter 3, Section 3.3.3.5), as its decomposition occurs at about 230 °C [196]. It could be also hypothesized that the presence of an acid promoted some degree of degradation of the biopolymers, resulting in polymer chains of lower molecular weight and earlier decomposition [106]. This behavior was also observed for the first decomposition stage of coconut oil composites, which could be attributed to the same possible factors.

Neat coconut oil presented a decomposition peak centered at 397 °C and broader than that of PEG (Figure 4.11d), as it consists of a mixture of different fatty acids [231]. The peak was dislocated towards lower temperatures (372-391 °C) after impregnation into the porous carriers, indicating that the thermal stability of coconut oil was reduced. The degradation peak associated to coconut oil was decomposed into two peaks for the mixed biomass-based porous materials (Figure 4.11d). Triacylglycerols are susceptible to hydrolysis, yielding free fatty acids [233], and results suggest that the presence of mixed biomass-based porous networks favored the thermal decomposition of coconut oil. Further research is needed to clarify the influence of the carriers on the thermal stability of coconut oil, as few studies have investigated similar systems [244,245].

4.4.3 Thermal behavior and latent heat storage performance

Neat PCMs and their phase-change composites were evaluated by DSC to assess their thermal behavior and latent heat thermal energy storage. “Aged” neat PCMs, simulating the impregnation procedure (75 °C during 15 or 7 h for PEG, and 35 °C during 2 or 1 h for coconut oil), were also analyzed to assess possible changes in the thermal behavior of neat PCMs stemming from the impregnation process. The obtained thermograms are presented in Figure 4.12.

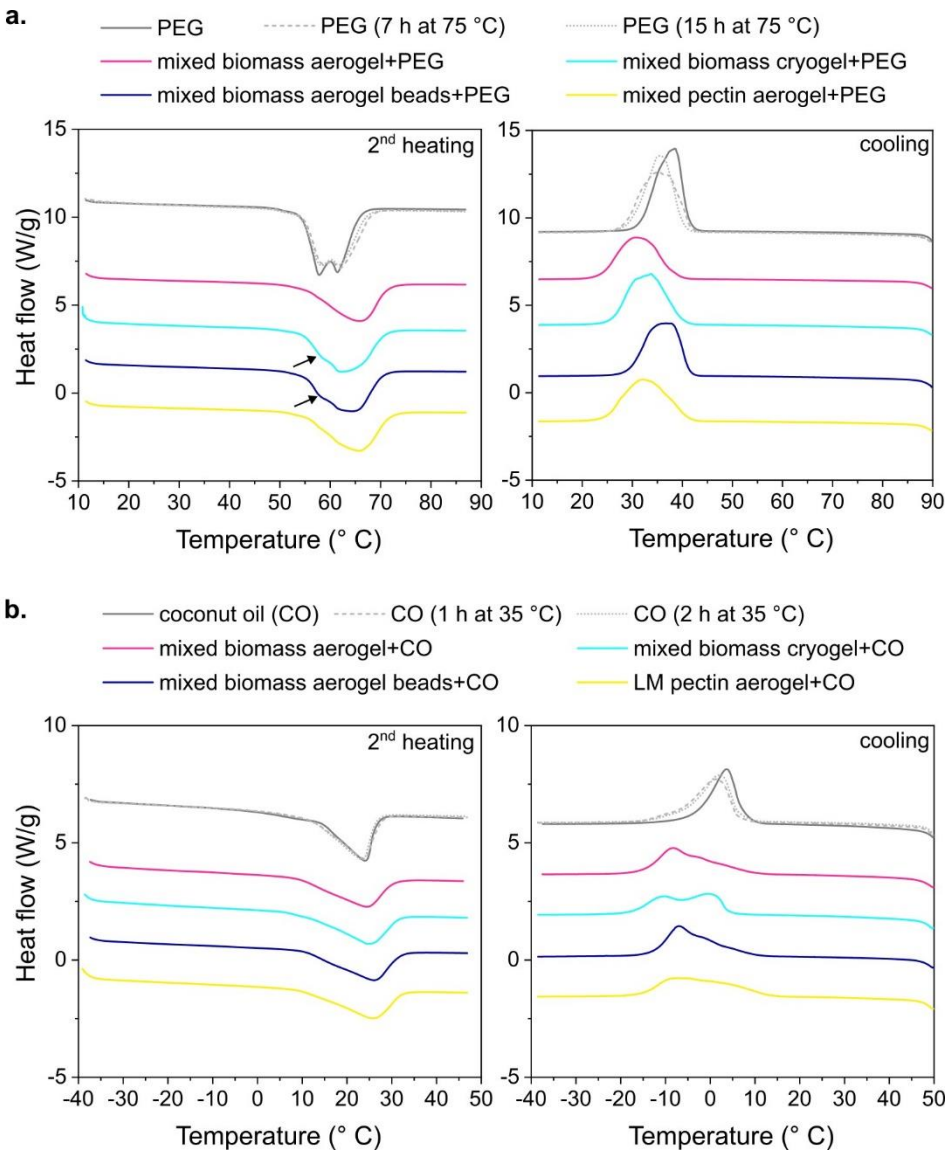

Figure 4.12: DSC thermograms (exo up) of (a) neat PEG and its composites, and (b) coconut oil (CO) and its composites.

PEG exhibited a double melting peak: the first one was at 58 °C (T_{m1}) and the second at 61 °C (T_{m2}), but only one crystallization peak at 38 °C (Figure 4.12a and Table 4.7). These results are in accordance with the literature [68,77]. The double melting behavior is attributed to the melt-recrystallization phenomenon, where the reorganization of more imperfectly packed crystals occurs during heating, before melting along with the more well-defined and stable ones, corresponding to the second peak [205,228].

Table 4.7: Thermal properties of PEG and its composites. ε is the latent heat efficiency, and ε_r the relative latent heat efficiency (Eq. 4.3 and Eq. 4.4, respectively).

Sample	T_{m1} (°C)	T_{m2} (°C)	ΔH_m (J/g)	T_c (°C)	ΔH_c (J/g)	ε (%)	ε_r (%)
PEG	57.8 ± 0.2	61.5 ± 0.2	192 ± 23	38.5 ± 0.2	188 ± 23	-	-
PEG (7 h at 75°C)	58.6 ± 0.5	61.9 ± 0.3	197 ± 28	35 ± 3	177 ± 10	-	-
PEG (15 h at 75°C)	58.2 ± 0.4	61.8 ± 0.4	187 ± 10	35.8 ± 0.9	183 ± 9	-	-
Mixed biomass aerogel+PEG	-	65.9 ± 0.4	147 ± 1	31 ± 1	142.2 ± 0.9	77	90
Mixed biomass cryogel+PEG	-	63 ± 1	165 ± 5	33.2 ± 0.7	160 ± 8	86	95
Mixed biomass aerogel beads+PEG	-	64 ± 1	162 ± 6	37 ± 2	156 ± 5	84	94
LM pectin aerogel+PEG	-	66 ± 1	155 ± 2	32 ± 1	151 ± 2	81	88

The thermal exposure of PEG at 75°C during 7 h and 15 h (equivalent to the impregnation procedure) led to subtle changes in the melting and crystallization behavior of PEG. The melting peak was slightly broadened, while the crystallization peak had a more pronounced widening and the crystallization temperature (T_c) decreased from 38 to 35-36 °C (Table 4.7). The reason of these changes could be a reduction of PEG molecular weight due to a possible

thermal degradation, and the presence of crystals with wider ranges of lamella thickness and “perfection” [205].

The T_c was reduced from 38 to 33-31 °C (except for the aerogel beads) with PEG impregnation into the carriers (Figure 4.12a and Table 4.7), reflecting a reduced nucleation capacity. Studies in the literature have claimed the opposite effect: that impregnation facilitated crystallization by promoting a heterogenous nucleation, although T_c variations reported were relatively small (1-2 °C) [207,216]. On the other hand, limited crystallization imposed by the physical confinement of PEG into biopolymer-based materials has also been reported. Examples include CNF-based cryogels [228] and films [246], and wheat bran cryogels [77].

Both melting and crystallization peaks were significantly broadened (as commonly observed in the literature [77,246]), revealing crystals’ size distribution widening due to impregnation. Zhang et al. [247] have shown the confinement effect on PEG crystals size using polarized light optical microscopy: neat PEG crystals were large and few, whereas PEG impregnated into pomelo peel flour presented multiple and smaller crystals with varying sizes.

PEG confinement within the porous materials led to the occurrence of one single melting peak, occurring at temperatures higher than those of neat PEG’s second peak (63-66 °C vs. 61 °C) (Figure 4.12a and Table 4.7). A shoulder was visible in the melting peak of some PEG-impregnated composites (mixed biomass cryogel+PEG and aerogel beads+PEG, see arrows in Figure 4.12a), suggesting that the observed single peak may have occurred due to the merging of the two neighboring peaks, as the first one was reduced and dislocated towards higher temperatures. This was unexpected due to the hampered crystallization observed during cooling. Hydrogen bonds between PEG and the biopolymers at the PCM-pore wall interfaces could have decreased the mobility of PEG molecules. Unlike long polymer chains, reduced mobility favors the crystallization of PEGs [205] and, as mentioned above, PEG recrystallizes during heating. This could explain the appearance of a small crystal population with higher melting temperatures and the reduction of the first

melting peak (less-stable crystals), despite the observed hindered crystallization during cooling (Figure 4.12 and Table 4.7). Notably, the cryogel sample (bearing the largest pores and lowest surface area) was the only one for which the T_{m2} increase was statistically non-significant. In summary, PEG crystallization was generally hindered by the physical confinement within the bio-based porous carriers, which also led to a broader distribution of crystals' dimensions that included a small fraction of more perfect and thermally stable crystals, likely stemming from recrystallization during heating. Further investigations are needed to fully understand the distinct thermal behavior of PEG upon confinement.

Displacements of both melting and crystallization temperatures in composites compared to neat PEG led to the increased levels of supercooling (from 23 °C for neat PEG to 27-35 °C for phase-change composites), which has negative effects for practical applications. The latent heat efficiency (latent heat of the phase-change composite relative to that of the neat PCM, Eq. 4.3) ranged from 77 to 86%, and was comparable to those reported in the literature [49,68,73,82]. The relative latent heat efficiency accounts solely for the PCM fraction of the phase-change composites (i.e., the latent heat efficiency corrected for the PCM loading ratio, Eq. 4.4) and ranged from 88 to 95% (Table 4.7), reflecting the limited crystallization caused by the PEG physical confinement, as discussed above. Nevertheless, the phase-change composites still exhibited relatively high melting enthalpies (147-165 J/g).

The thermal behavior of coconut oil and its composites is depicted in Figure 4.12b, and their thermal properties are presented in Table 4.8. Neat coconut oil presented single melting and crystallization peaks (at 24 °C and 3 °C, respectively), which were broader than those of PEG, as coconut oil is composed of fatty acids with varying chain lengths [231]. The "aging" of the neat coconut oil (simulating impregnation conditions) had a subtle influence on its thermal behavior. The crystallization peak was shifted and broadened (Figure 4.12b), but the variations on the associated thermal properties were not statistically significant (Table 4.8). The impregnation time was short, and a

previous study have reported that the thermal properties of virgin coconut oil are stable upon multiple thermal cycles [231].

Melting and crystallization peaks were broadened for the coconut oil composites and their corresponding enthalpies were reduced (from 114 to 93-94 J/g and 109 to 84-90 J/g, respectively), as commonly observed for many physically confined PCMs [73,77,83]. As discussed for PEG composites, this is related to the widening of crystal size and "perfection" distribution, and to the presence of non-melting biopolymers that constitute the porous carriers, respectively [77,246].

Table 4.8: Thermal properties of coconut oil (CO) and its composites.

Sample	T_m (°C)	ΔH_m (J/g)	T_{c1} (°C)	T_{c2} (°C)	ΔH_c (J/g)	ε (%)	ε_r (%)
CO	24.0 ± 0.2	114 ± 6	-	3.5 ± 0.4	109 ± 3	-	-
CO (1 h at 35°C)	23.7 ± 0.3	117 ± 11	-	1 ± 1	109 ± 10	-	-
CO (2 h at 35°C)	23.4 ± 0.3	117 ± 7	-	2.1 ± 0.8	110 ± 5	-	-
Mixed biomass aerogel+CO	24.6 ± 0.8	94 ± 7	-8 ± 1	-3.2 ± 0.8	88 ± 8	82	93
Mixed biomass cryogel+CO	25 ± 1	94 ± 2	-10 ± 1	1 ± 1	84 ± 4	82	93
Mixed biomass aerogel beads+CO	26.1 ± 0.8	94 ± 3	-7.0 ± 0.6	-2.2 ± 0.4	90 ± 4	82	92
LM pectin aerogel+CO	25.8 ± 0.8	93 ± 1	-7 ± 1	1 ± 3	88 ± 3	82	91

During the cooling of coconut oil composites, a lower-temperature peak (T_{c1}) appeared in addition to the one already observed for the neat PCM, which was shifted to inferior temperatures (from 3.5 to -3/-1°C). Restrained crystallization of coconut oil due to the physical confinement may have led to the formation of less stable polymorphs of vegetable fats and oils (namely, α and β'), and a reduction of the most stable form β, which has the highest melting temperature, giving rise to the observed double peak behavior [248]. Interestingly, all aerogel-based composite samples had a more prominent low-

temperature peak (at T_{m1}), whereas the cryogel had a higher fraction of the more stable crystals (melting at T_{m2}). This may be correlated to a reduced spatial restriction owing to cryogels' larger pores and lower surface area when compared to aerogels. The presumed presence of less stable polymorphs likely contributed to the intense broadening of the melting peak as well, due to peak superposition. Melting temperatures (T_m) did not vary within experimental errors.

Coconut oil composites showed similar latent heat efficiency (82%) and relative latent heat efficiency (91-93%) regardless of the type of porous carrier (see Table 4.8). Similar to PEG and its composites, the impregnation of coconut oil reduced its crystallization capacity, as reflected by the composites' relative latent heat efficiency of 91-93% (Table 4.8).

4.4.4 Leakage assessment

In addition to the thermal performance, leakage resistance is another fundamental aspect for the practical applications of phase-change composites. The efficiency of porous carriers with different textural properties on preventing leakage of molten PEG and coconut oil was evaluated, and the results are presented in Figure 4.13.

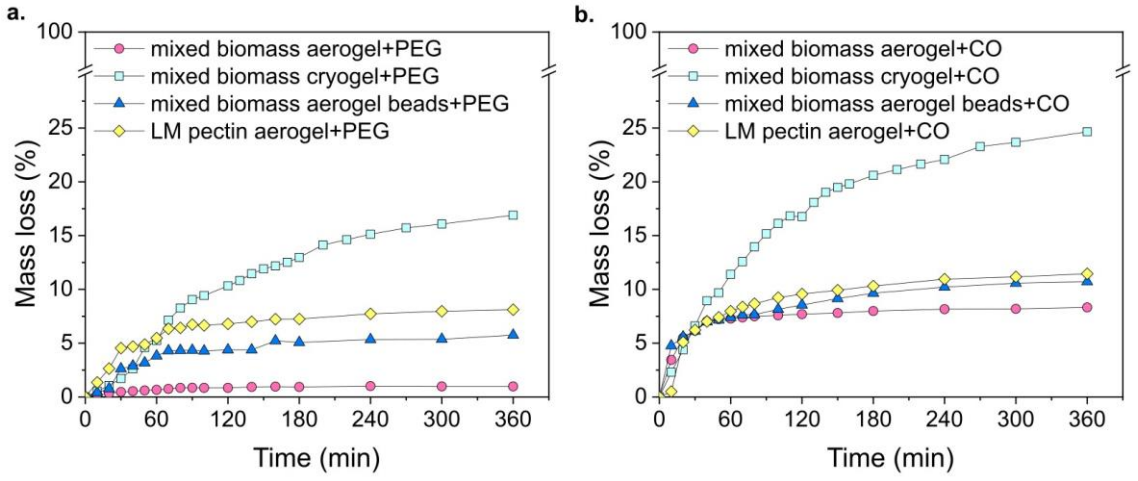

Figure 4.13: Mass loss as a function of time due to leakage of (a) PEG at 75 °C, and (b) coconut oil (CO) at 35 °C from their composites.

An initial stage of higher leakage rates is observed for all samples, having different magnitudes and durations. The mass loss rate gradually reduced and stabilized (except for cryogel-based composites), and the effectively confined PCM fraction was kept inside the porous networks by capillary forces [207]. Aerogel samples reached a relatively stable mass after ca.120-240 minutes, whereas cryogels continued to show significant mass variations after 6 h, although at decreased leakage rates. As a general trend, the aerogel-based composites exhibited much lower leakage for both PCMs when compared to the cryogel-based ones, due to their nanostructured morphology and higher specific surface area (150-300 m^2/g vs. 8 m^2/g, respectively).

The mixed biomass aerogel monolith had an outstanding low leakage of 1% when impregnated with PEG. Only a few articles in the field reported similar results, including carbon cryogels from orange peels and starch (0-20%) impregnated with PEG 6000 (0.3-0.9%) [50], watermelon rind-based carbon cryogels impregnated with mannitol (ca. 2%) [80], and PVA/graphene cryogels carrying PEG 2000 (0.5-1%) [207]). Authors attributed these results to the capillary forces and hydrogen bonding between carrier and PCM [80,207].

When coconut oil was used, the ultimate leakage percentage from the mixed biomass aerogel monolith increased to 8%, probably due to a lower affinity between both components. Nevertheless, this value is still below or comparable to results from the literature: bio-based porous materials as carriers for organic PCMs have been reported to undergo up to 20% of PCM mass loss due to leakage [50,68,69,77,80,207]. Other studies have reported phase-change composites which bear even poorer performances in terms of PCM leaching, reaching up to ca. 30-80% of mass loss [50,68].

Mixed biomass cryogels had an ultimate 17% mass loss due to PEG leakage and 25% for coconut oil, due to the combination of large pores and different compatibility levels with the PCMs. Mixed biomass aerogel beads and LM pectin aerogels exhibited intermediate leakage levels compared to those previously discussed. They showed similar performances between each other for both PCMs, with mass losses of 7–8% for PEG and 11% for coconut oil.

This was expected for LM pectin aerogel-based composites, as it had an intermediate specific surface area when compared to mixed biomass-based aerogels and cryogels. Aerogel beads, however, boasted the highest surface area. It was noticeable that the removal of excess PCM after impregnation was hampered by their size and shape; hence, it could be hypothesized that "additional" mass loss (compared to monolithic aerogels) may have arisen from the melting of PCM fractions adsorbed on the beads' surface rather than within their pores.

4.4.5 Latent heat storage performance by IR-imaging

As presented in Section 4.4.3, the latent heat storage performance of the phase-change composites was evaluated via DSC, however this method uses limited sample mass and volume. To further examine the behavior of the phase-change composites with low to moderate levels of leakage (the coconut oil-impregnated cryogel sample was excluded due to the intense leakage), IR-imaging was employed to monitor the materials' response to the temperature over time. Figure 4.14 presents the infrared temperature mapping of the phase-change composites placed on top of a hot plate (Figure 4.14a and c), and the estimated temperature *vs.* time graphs (Figure 4.14b and d). It is important to highlight that the temperature measurements of the hot plate are not accurate, as its surface consisted of uncoated metal, which have low infrared emissivity, resulting in underestimated temperatures [249]. This can be corrected in the camera's software; but, in this case, the metallic surface was not the primary concern, and the phase-change composites did not exhibit this issue, resulting in more reliable temperature estimates.

Images show that, at first, composites were still close to their initial temperatures (see images at 1 s, Figures 4.14a and c). As heat transfer occurred from the hot plate to the samples, their temperature started to rise as a result of the sensible heat storage until the melting temperature of the PCMs is reached (at approximately 30 s for all composites, Figure 4.14). After this point, the thermal energy from the hot plate is stored in the form of latent heat by the PCM, and the temperature remains approximately stable for different periods of

time depending on the sample. A “temperature plateau” is formed and reflects the occurrence of the PCMs’ phase transition. Once the PCM within the composites is completely molten, its temperature will start rising again (see images at 75-90 s for monoliths, and at about 50 s for beads, Figure 4.14a and c) [77,80].

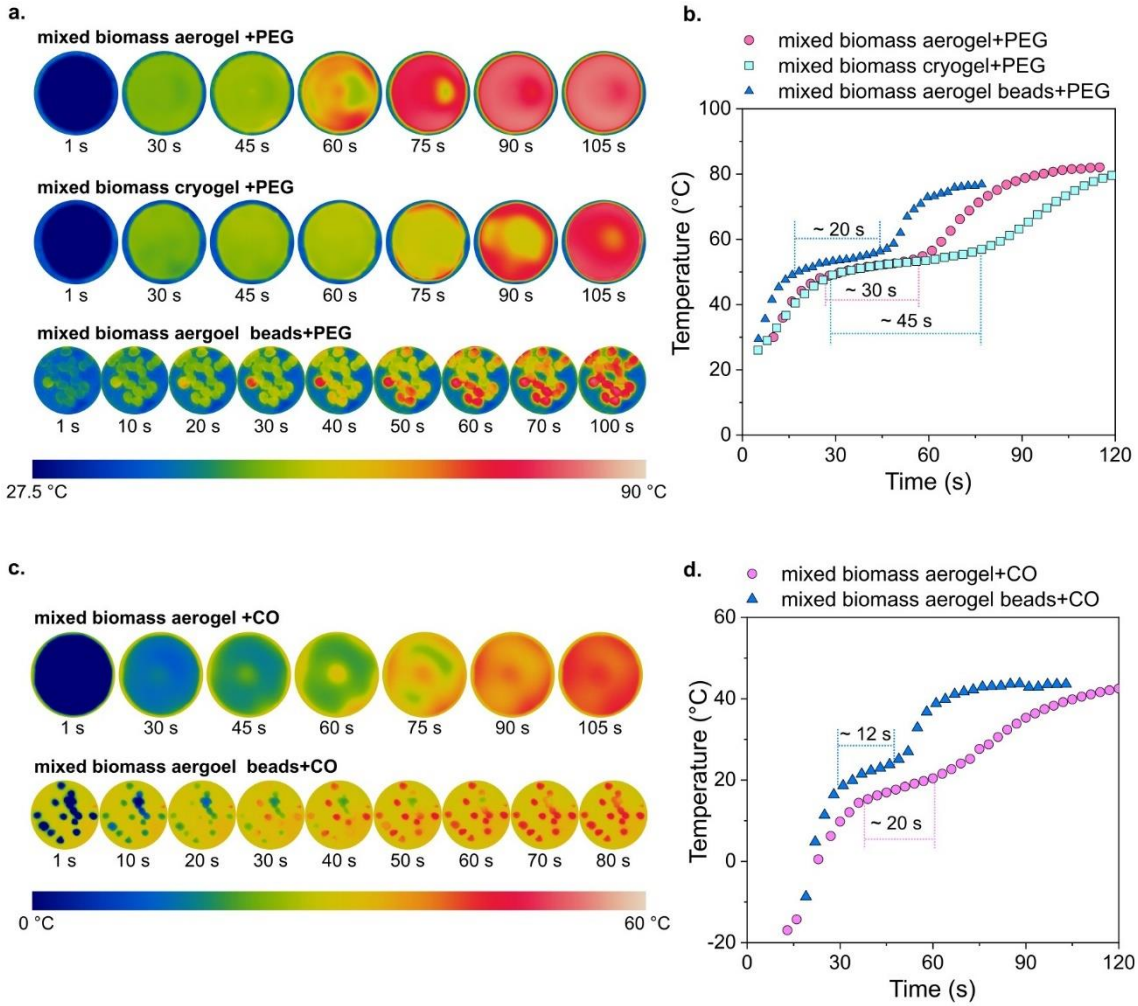

Figure 4.14: IR images (left) and temperature (right) over time for (a) PEG-based and (c) coconut oil (CO)-based phase-change composites. Temperature values were taken as an average of the visible area for monoliths and an average curve for the beads (8-10 were measured).

When impregnated with PEG, monolithic samples had similar masses (ca. 0.5 g) but different plateau lengths. The mixed biomass aerogel had a shorter plateau compared to its cryogel counterpart (30 s vs. 45 s, Figure

4.14b), due to its lower loading ratio (85% vs. 91%) and lower relative latent heat efficiency (90% vs. 95%). PEG-impregnated beads had a shorter plateau than monolithic samples, as its mass was significantly lower (ca. 0.1 g, each bead having 0.006 g on average). Nevertheless, plateau length reduction was moderate compared to the mass difference. Perhaps the heat transfer was hampered by the beads' geometry: they did not have a flat surface to ensure a good surface contact with the hot plate like monoliths had.

Samples loaded with coconut oil had shorter plateaus as it has inherently lower latent heat compared to PEG. Beads had a shorter plateau than the mixed biomass aerogel monolith, once again, likely due to their lower mass (ca. 0.1 g, each bead having 0.006 on average, vs. ca. 0.5 g) and spheric shape.

One study reported a plateau of about 500 s for PEG 4000-impregnated carboxymethylcellulose/montmorillonite cryogels, and the samples had more than 7 times the volume of the mixed biomass aerogels loaded with PCMs [216]. A 15 s plateau was observed, via IR-imaging, when sodium alginate/polypyrrole-modified corn straw fiber cryogels impregnated with PEG 2000 were heated using a xenon lamp as source [250]. However, the size and mass of the sample was not reported, hindering adequate comparisons. Another example includes plateaus of about 100 s for pyrolyzed *Miscanthus lutarioriparius* biomass/PEG 4000 composites [230] and 100-200 s for pomelo peel flour/PEG 6000 (neat and isocyanate-terminated PEG) [247], but once again the sample mass was not informed. Other examples that illustrated the thermal performance of phase-change composites via thermal imaging include PVA cryogel/PEG 2000 composites [207], watermelon rind carbon cryogel/mannitol composite [80], and TEMPO-oxidized CNF films blended with PEGs of different molecular weights (1000, 2000, and 4000); but the plateau region was not clearly defined, instead the temperature-time plots exhibited regions of reduced temperature change rates. Most studies did not report the samples' mass, which makes comparisons difficult. In addition, different setups may be used [212,223], which further hinders comparisons.

Nevertheless, results herein presented demonstrate the thermal performance of phase-change composites produced from orange waste-derived

carriers, highlighting their potential for thermal protection applications. They also underscore the influence of material size and shape on heat transfer kinetics, warranting careful consideration and further investigations.

4.5 Conclusions

Bio-based porous materials, aerogels and cryogels, from orange mixed waste biomass and neat LM pectin were explored as potential carriers for different organic PCMs, PEG 4000 and coconut oil. The effect of the porous carriers' properties, morphologies and shape on the performance of the resulting shape-stable phase-change composites was investigated. Impregnation times were influenced by the viscosity of the fluid, and by the carriers' shape and morphology. As intended, shorter times were required to completely impregnate aerogel beads when compared to their monolithic counterparts. Volumetric shrinkage occurred during the impregnation, and it was higher for porous carriers with finer morphologies (aerogels vs. cryogels), combined with higher compatibility between the porous carrier and the PCM (PEG/biomass vs. coconut oil/biomass). For instance, mixed biomass aerogel monoliths and beads had a 30% contraction vs. 6-13% for PEG-impregnated cryogels, and 7-15% for the coconut oil-impregnated samples. Loading ratios were high for all cases (85-92%) and very close to the theoretical values corrected for shrinkage (89-92%).

Pore size and PCM-carrier compatibility also influenced PCM leakage from the composites. Overall, aerogels combined with PEG showed the higher leakage resistance when compared with cryogels as carrier and coconut oil as the confined PCM. Mixed biomass monolithic aerogels impregnated with PEG exhibited a remarkable leakage resistance, allowing only 1% of the PCM to leach out. The other samples presented higher mass losses due to leakage (7-25%), although values were comparable to those reported in the literature.

The physical confinement of the PCMs introduced modifications in their melting and crystallization behaviors, broadening crystal size distributions and hindering crystallization. Nevertheless, this effect was moderate, resulting in a

relative latent heat efficiency of 88-95% and high melting enthalpies (147-165 J/g for PEG composites, and 93-94 J/g for coconut oil-based ones). Lastly, the passive temperature control capacity of the composites produced was observed via IR-imaging.

Finally, the potential of the porous materials developed in this work as shape-stable PCM-carriers for passive thermal regulation was demonstrated. The materials' pore morphology and interfacial interactions with the PCM strongly influenced the phase-change composites' shrinkage during the impregnation procedure, leakage resistance, and melting and crystallization behavior. Nanostructured orange waste-based carriers for PCMs were evaluated for the first time, and exhibited an effective capacity to prevent leakage. Still, further research is needed to improve their properties for practical applications and answer open questions.

CHAPTER 5 – GENERAL CONCLUSIONS

This thesis demonstrated the feasibility of converting orange biomass waste from the juice industry into porous materials, aerogels and cryogels. A citric acid pre-treatment was employed to leverage the high pectin content of citrus biomasses, resulting in aqueous suspensions and enabling their transformation into 3D materials. Distinct porous structures and properties were achieved through different processing routes and correlated with their performance as carriers for organic PCMs.

Chapter 2 addressed strategies to improve the kinetic stability biomass suspensions, a key requirement for producing homogeneous porous monoliths. The total orange waste (i.e., the “mixed” biomass) comprised three biomass fractions (peels, pulp, and bagasse), and was dispersed and hydrolyzed in citric acid solutions. The kinetic stability of mixed biomass suspensions was tailored by tuning preparation parameters (biomass washing or not, and biomass and citric acid concentrations). Washing the orange biomass waste with water reduced the content of low-molecular-weight compounds, such as soluble sugars, likely increasing the suspensions’ liquid phase viscosity and slowing down the insoluble fraction precipitation. Higher biomass concentrations led to increased suspension viscosity, insoluble content, and insoluble fraction’s water holding capacity (WHC). Improved stability was further associated with the formation of a “network” of swollen particles, which “entraps” the liquid phase and slows down phase separation. Greater citric acid content improved pectin extraction from the orange tissues and its solubilization into the liquid phase, thereby contributing to prolonged suspension stability.

One hypothesis of this thesis was that the biochemical composition of the biomass fractions would significantly influence the suspensions’ physical properties. Conditions yielding the highest kinetic stability (washing biomass with water, 4% biomass, and 5% citric acid) were employed to evaluate the influence of the biomass fraction type (mixed vs. its individual fractions: peels, bagasse, and pulp), and a less pronounced impact on the kinetic stability was observed. Peels-based suspensions were less stable than those containing bagasse and pulp fractions (93% vs. 99-100% after 72 h), which was correlated

to the fibrillated morphology and higher WHC of their insoluble fractions. The bagasse biomass fraction had the highest pectin and extractives contents and the lowest cellulose content, potentially facilitating pectin extraction to the liquid phase and insoluble fraction fibrillation. Pulp and peels had similar contents of extractives, pectin, and cellulose; however, the pulp's softer tissue compared to peels may have facilitated fibrillation.

Conditions leading to the best kinetic stability of the suspensions were adopted to proceed with the production of porous materials, as discussed in Chapter 3. For aerogel preparation, ethanol or acetone were employed to trigger non-solvent-induced phase separation and obtain organogels, which were then dried with supercritical CO_2. Aerogels with low density (0.6-0.9 g/cm³) and high specific surface area (190-260 g/m²) were obtained, all bearing a nanostructured pectin network matrix with dispersed and partially porous insoluble fractions. Cryogels were produced by freeze-drying biomass suspensions. They exhibited low density (0.08-09 g/cm³) and very low surface areas (5-9 m²/g), due to their large pores (up to 300 µm in diameter) resulting from ice-templating. The biomass fraction type had a minor influence on the textural properties of aerogels and cryogels.

The mechanical behavior, thermal conductivity, and biodegradation of aerogel and cryogel monoliths based on mixed biomass were further evaluated. Cryogels exhibited a markedly lower specific modulus compared to their aerogel counterparts (2 vs. 12 MPa.cm³/g), owing to their coarse pore morphology formed by assembled flake-like structures, and the reinforcing effect of the insoluble fraction on biomass-based materials was demonstrated. Aerogels exhibited an exceptionally low thermal conductivity of 25 mW/m.K, the same as that of air at ambient conditions, thereby positioning them at the frontier of superinsulating materials. Due to their very large macropores, cryogels presented a higher thermal conductivity (37 mW/m.K), yet comparable to that of conventional fossil-based foams like EPS. Both aerogels and cryogels were effectively biodegraded in seawater: aerogels at rates slightly above that of the microcrystalline cellulose (positive control), and cryogels significantly faster.

The feasibility of producing aerogel beads from mixed orange biomass was also demonstrated using the dripping method with ethanol as a coagulation bath. Resulting beads were nearly spherical, with an average diameter of 2.7 mm, and had a higher specific surface area when compared to their monolithic counterparts (308 vs. 172 m^2/g, respectively).

In Chapter 4, porous materials based on mixed orange waste biomass, bearing different morphologies and specific surface areas (aerogel and cryogel monoliths, and aerogel beads), were evaluated as carriers for two distinct organic PCMs, PEG 4000 and coconut oil. LM pectin aerogel monoliths were used as a reference. Loading ratios ranged from 85 to 92%, either approaching or matching the theoretical loading ratios corrected for the volume shrinkage that occurred during impregnation (89-92%). Findings demonstrated that both the pore size of the carrier and the PCM-carrier affinity were key aspects influencing PCM leakage. Cryogels had the highest mass loss due to PCM leakage (17% for PEG and 25% for coconut oil). In contrast, the orange biomass aerogel monolith loaded with PEG had the best performance, with only 1% of leakage after 6 h, and when loaded with coconut oil, leakage reached 8%. The latter was similar to the other aerogel samples (orange biomass aerogel beads and LM pectin aerogel monoliths) loaded with either PEG (7-9%) or coconut oil (11%). DSC analyses revealed that the PCMs crystallization was hindered by their physical confinement, and the distribution of crystals' "perfection" was broadened after impregnation. Nevertheless, the relative latent heat efficiency remained relatively high: 88-95% for PEG-based composites and 91-93% for coconut oil-based composites.

In summary, this thesis demonstrated the feasibility of upcycling industrial orange waste into porous materials with diverse pore structures and properties, underscoring the decisive role of preparation and processing parameters in tailoring the properties of precursors (suspensions) and final materials (aerogels and cryogels), respectively. This study further explored their performance as carriers for organic PCMs as a potential application. Findings presented herein may contribute to advancing citrus waste valorization strategies, and offer new insights into the combination of biomass-based porous

materials with organic PCMs for passive thermal regulation applications, opening new pathways for the design of sustainable and functional materials.

PERSPECTIVES AND FUTURE WORK

Based on the findings presented throughout this thesis, different challenges and perspectives for future works can be suggested:

- The composition of the liquid phase and insoluble fraction of the orange biomass suspensions could be further investigated to assess the extent of pectin extraction and solubilization into the liquid phase of the suspensions, as well as the possible presence of hemicellulose in it, which was not detected by spectroscopy techniques employed in this study (ATR-FTIR and FT-Raman). Advanced analytical techniques, like HPLC, could provide quantitative information and a deeper understanding of biochemical transformations occurring in the orange biomass waste during the citric acid pre-treatment.
- Other biomass pre-treatments could be explored. For instance, suspensions bearing insoluble fractions with fibrillated morphology boasted the highest kinetic stabilities, therefore, mechanical fibrillation could be explored as an alternative pre-treatment to avoid the use of heat and/or acid.
- One of the hypotheses of this work was that the citric acid pre-treatment would promote the formation of a pectin-rich liquid phase; which, upon drying, would form a cohesive matrix for the dispersed insoluble fraction. Cross-linking the soluble pectin (e.g., with polyvalent cations) could be a promising strategy to further tailor the morphology and properties of aerogels and/or cryogels based on orange biomass and other citrus wastes. For example, the cryogels obtained had markedly low elastic modulus. Cross-linking pectin could enhance their mechanical properties.
- Biopolymer- and biomass-based materials are known for their hydrophilicity. Hence, the water absorption of orange biomass waste-based porous materials and the evolution of their properties in humid environments warrants further investigations. Strategies to reduce their hydrophilic character could make them suitable for a wider range of applications (e.g., packaging, building).
- Drying with supercritical CO_2 and freeze-drying requires severe pressure conditions. Alternative approaches, such as evaporative drying, could be explored to improve scalability and reduce energy consumption.

- Results suggested the presence of residual citric acid in the obtained cryogels. Its action as a cross-linking agent for polysaccharides via esterification reactions could be investigated (e.g., via thermal treatments) for improved mechanical properties and reduced water uptake.
- The distinct biodegradation rates of orange waste biomass-based aerogels and cryogels in seawater require further clarification. Complementary studies could elucidate mechanisms and factors governing the biodegradation of these materials in seawater. Moreover, assessing biodegradation in other media, like soil and/or compost, could offer additional insights into the degradation behavior of these materials.
- Aerogel beads had significantly superior specific surface area than their monolithic counterparts, and the structural differences and mechanisms underlying this difference warrants further investigations.
- PCMs' melting and crystallization behaviors were altered by their impregnation into the porous carriers, acquiring more complex profiles. Changes in the thermal behavior of PCMs were attributed to their spatial confinement, and interactions at the interface may have also played a roll. Yet, the reasons for these changes are not fully understood. Crystal morphology and interfacial properties of the phase-change composites can be clarified with advanced techniques like atomic force microscopy (AFM)-based nanoidentation, which reveals localized nanomechanical properties fluctuations (e.g., interface thickness, lamella thickness).
- Evaluating the long-term performance of phase-change composites, such as the stability of their latent heat and phase-change temperatures over multiple thermal cycles and upon exposure to humid environments, could bring valuable insights for their practical applications.
- The porous materials from orange waste biomass can be investigated for other applications, beyond carriers for PCMs. For example, their thermal insulating capacity was demonstrated, and can be further enhanced. Other promising directions include the controlled release of drugs in the cosmetic and biomedical fields, the sustained delivery of fertilizers and nutrients in agriculture, and acoustic insulation.

In summary, this thesis presented new strategies for developing porous materials from orange biomass waste and explored their potential application in phase-change composites with mitigated leakage. Yet, several fundamental and practical aspects of this study remain open questions, warranting further investigations and opening multiple avenues for future research.

REFERENCES

[1] FAO. FAOSTAT Analytical Brief 96 - Agricultural Production Statistics 2010–2023.; 2024. Accessed: March 31, 2025. Available at <https://openknowledge.fao.org/server/api/core/bitstreams/df90e6cf-4178-4361-97d4-5154a9213877/content>.

[2] Sharma, K.; Mahato, N.; Cho, M. H.; et al. Converting citrus wastes into value-added products: Economic and environmently friendly approaches. Nutrition. 2017, v. 34, p. 29-46. doi:10.1016/j.nut.2016.09.006

[3] Teigiserova, D. A.; Tiruta-Barna, L.; Ahmadi, A.; et al. A step closer to circular bioeconomy for citrus peel waste: A review of yields and technologies for sustainable management of essential oils. Journal of Environmental Management. 2021, v. 280, p. 111832. doi:10.1016/j.jenvman.2020.111832

[4] Chavan, P.; Singh, A. K.; Kaur, G. Recent progress in the utilization of industrial waste and by- products of citrus fruit : A review. Journal of food process engineering. 2018, v. 41, n. 8, p. e12895. doi:10.1111/jfpe.12895

[5] Bertolo, M. R. V; Pereira, T. S.; dos Santos, F. V; et al. Citrus wastes as sustainable materials for active and intelligent food packaging: Current advances. Comprehensive Reviews in Food Science and Food Safety. 2025, v. 24, n. 2, p. e70144. doi:10.1111/1541-4337.70144

[6] Rivas, B.; Torrado, A.; Torre, P.; et al. Submerged Citric Acid Fermentation on Orange Peel Autohydrolysate. Journal of Agricultural and Food Chemistry. 2008, v. 56, n. 7, p. 2380-2387. doi:10.1021/jf073388r

[7] Berk, Z. By-products of the citrus processing industry. *In*: Berk, Z. (ed.) Citrus Fruit Processing. 1st ed. Academic Press; 2016:219-233. doi:10.1016/B978-0-12-803133-9.00010-2

[8] Otoni, C. G.; Azeredo, H. M. C.; Mattos, B. D.; et al. The Food–Materials Nexus: Next Generation Bioplastics and Advanced Materials from Agri-Food Residues. Advanced Materials. 2021, v. 33, n. 43, p. 2102520. doi:10.1002/adma.202102520

[9] Vieira, R. M.; de Freitas, C.; Beluomini, M. A.; et al. Exploring fruit waste

macromolecules and their derivatives to produce building blocks and materials. Reviews in Environmental Science and Bio/Technology. 2025, v. 24, n. 1, p. 167-189. doi:10.1007/s11157-024-09713-3

[10] Revathi, V.; Bora, S.; Afzia, N.; et al. Orange peel composition, biopolymer extraction, and applications in paper and packaging sector: A review. Sustainable Chemistry and Pharmacy. 2025, v. 43, p. 101908. doi:10.1016/j.scp.2025.101908

[11] Bátori, V.; Jabbari, M.; Åkesson, D.; et al. Production of Pectin-Cellulose Biofilms: A New Approach for Citrus Waste Recycling. International Journal of Polymer Science. 2017, v. 2017, p. 9732329. doi:10.1155/2017/9732329

[12] Bátori, V.; Lundin, M.; Åkesson, D.; et al. The effect of glycerol, sugar, and maleic anhydride on pectin-cellulose thin films prepared from orange waste. Polymers. 2019, v. 11, n. 3, p. 392. doi:10.3390/polym11030392

[13] Moaveni, R.; Ghane, M.; Soltani, P.; et al. Production of Polymeric Films from Orange and Ginger Waste for Packaging Application and Investigation of Mechanical and Thermal Characteristics of Biofilms. Applied Sciences. 2024, v. 14, n. 11, p. 4670. doi:10.3390/app14114670

[14] Karakuş, E.; Ayhan, Z.; Haskaraca, G. Development and characterization of sustainable-active-edible-bio based films from orange and pomegranate peel waste for food packaging: Effects of particle size and acid/plasticizer concentrations. Food Packaging and Shelf Life. 2023, v. 37, p. 101092. doi:10.1016/j.fpsl.2023.101092

[15] Quilez-Molina, A. I.; Mazzon, G.; Athanassiou, A.; et al. A novel approach to fabricate edible and heat sealable bio-based films from vegetable biomass rich in pectin. Materials Today Communications. 2022, v. 32, p. 103871. doi:10.1016/j.mtcomm.2022.103871

[16] Santos, L. B.; Silva, R. D.; Alonso, J. D.; et al. Bioplastics from orange processing byproducts by an ecoefficient hydrothermal approach. Food Packaging and Shelf Life. 2023, v. 38, p. 101114. doi:10.1016/j.fpsl.2023.101114

[17] Merino, D.; Simonutti, R.; Perotto, G.; et al. Direct transformation of

industrial vegetable waste into bioplastic composites intended for agricultural mulch films. Green Chemistry. 2021, v. 23, n. 16, p. 5956-5971. doi:10.1039/D1GC01316E

[18] Yaradoddi, J. S.; Banapurmath, N. R.; Ganachari, S. V.; et al. Bio-based material from fruit waste of orange peel for industrial applications. Journal of Materials Research and Technology. 2021, v. 17, p. 3186-3197. doi:10.1016/j.jmrt.2021.09.016

[19] Duarte, A. V.; Possari, L. T.; Gonçalves, L. M. G.; et al. Accelerating Degradable Composite Breakdown Using Citrus Processing Side Streams. ACS Sustainable Resource Management. 2024, v. 1, n. 2, p. 344-354. doi:10.1021/acssusresmgt.3c00108

[20] Budtova, T.; Aguilera, D. A.; Beluns, S.; et al. Biorefinery approach for aerogels. Polymers. 2020, v. 12, n. 12, p. 1-63. doi:10.3390/polym12122779

[21] Gerschenson, L. N.; Fissore, E. N.; Rojas, A. M.; et al. Pectins obtained by ultrasound from agroindustrial by-products. Food Hydrocolloids. 2021, v. 118, p. 106799. doi:10.1016/j.foodhyd.2021.106799

[22] Rudaz, C.; Courson, R.; Bonnet, L.; et al. Aeropectin: Fully Biomass-Based Mechanically Strong and Thermal Superinsulating Aerogel. Biomacromolecules. 2014, v. 15, n. 6, p. 2188-2195. doi:10.1021/bm500345u

[23] Nesic, A.; Meseldzija, S.; Onjia, A.; et al. Impact of Crosslinking on the Characteristics of Pectin Monolith Cryogels. Polymers. 2022, v. 14, p. 5252. doi:10.3390/polym14235252

[24] Tkalec, G.; Knez, Z.; Novak, Z. Fast production of high-methoxyl pectin aerogels for enhancing the bioavailability of low-soluble drugs. The Journal of Supercritical Fluids. 2015, v. 106, p. 16-22. doi:10.1016/j.supflu.2015.06.009

[25] Groult, S.; Buwalda, S.; Budtova, T. Pectin hydrogels, aerogels, cryogels and xerogels: Influence of drying on structural and release properties. European Polymer Journal. 2021, v. 149, p. 110386. doi:10.1016/j.eurpolymj.2021.110386

[26] Groult, S.; Budtova, T. Thermal conductivity/structure correlations in thermal super-insulating pectin aerogels. Carbohydrate Polymers. 2018, v. 196, n. 2018, p. 73-81. doi:10.1016/j.carbpol.2018.05.026

[27] Groult, S.; Budtova, T. Tuning structure and properties of pectin aerogels. European Polymer Journal. 2018, v. 108, n. November 2018, p. 250-261. doi:10.1016/j.eurpolymj.2018.08.048

[28] Tkalec, G.; Knez, Z.; Novak, Z. Formation of polysaccharide aerogels in ethanol. RSC Advances. 2015, v. 5, p. 77362-77371. doi:10.1039/C5RA14140K

[29] Wang, Y.; Su, Y.; Wang, W.; et al. The advances of polysaccharide-based aerogels: Preparation and potential application. Carbohydrate Polymers. 2019, v. 226, p. 115242. doi:10.1016/j.carbpol.2019.115242

[30] Zou, F.; Budtova, T. Polysaccharide-based aerogels for thermal insulation and superinsulation: An overview. Carbohydrate Polymers. 2021, v. 266, p. 118130. doi:10.1016/j.carbpol.2021.118130

[31] Zhao, S.; Malfait, W. J.; Guerrero-alburquerque, N.; et al. Biopolymer Aerogels and Foams: Chemistry, Properties, and Applications. Angewandte Chemie - International Edition. 2018, v. 57, n. 26, p. 7580-7608. doi:10.1002/anie.201709014

[32] Buchtová, N.; Budtova, T. Cellulose aero- , cryo- and xerogels: towards understanding of morphology control. Cellulose. 2016, v. 23, p. 2585-2595. doi:10.1007/s10570-016-0960-8

[33] Schwertfeger, F.; Frank, D.; Schmidt, M. Hydrophobic waterglass based aerogels without solvent exchange or supercritical drying. Journal of Non-Crystalline Solids. 1998, v. 225, p. 24-29. doi:10.1016/S0022-3093(98)00102-1

[34] Druel, L.; Budtova, T. Aerogel-like (low density and high surface area) cellulose monoliths and beads obtained without supercritical- or freeze-drying. Cellulose. 2023, v. 30, n. 13, p. 8339-8353. doi:10.1007/s10570-023-05349-8

[35] Zou, F.; Budtova, T. Starch Alcogels, Aerogels, and Aerogel-like Xerogels: Adsorption and Release of Theophylline. ACS Sustainable

Chemistry & Engineering. 2023, v. 11, n. 14, p. 5617-5625. doi:10.1021/acssuschemeng.2c07762

[36] Fumagalli, M.; Ouhab, D.; Boisseau, S. M.; et al. Versatile Gas-Phase Reactions for Surface to Bulk Esterification of Cellulose Microfibrils Aerogels. Biomacromolecules. 2013, v. 14, n. 9, p. 3246-3255. doi:10.1021/bm400864z

[37] Borisova, A.; Bruyn, M. De; Budarin, V. L.; et al. A Sustainable Freeze-Drying Route to Porous Polysaccharides with Tailored Hierarchical Meso- and Macroporosity. Macromolecular Rapid Communications. 2015, v. 36, p. 774-779. doi:10.1002/marc.201400680

[38] Yu, S.; Budtova, T. Creating and exploring carboxymethyl cellulose aerogels as drug delivery devices. Carbohydrate Polymers. 2024, v. 332, p. 121925. doi:10.1016/j.carbpol.2024.121925

[39] Nešić, A.; Gordić, M.; Davidović, S.; et al. Pectin-based nanocomposite aerogels for potential insulated food packaging application. Carbohydrate Polymers. 2018, v. 195, p. 128-135. doi:10.1016/j.carbpol.2018.04.076

[40] Guo, W.; Budtova, T.; Martinez, M. M. Upcycling stale bread into (meso)porous materials: Xerogels and aerogels. Food Hydrocolloids. 2025, v. 160, p. 110807. doi:10.1016/j.foodhyd.2024.110807

[41] Gaggero, G.; Subrahmanyam, R. P.; Schroeter, B.; et al. Organic Bio-Based Aerogel from Food Waste: Preparation and Hydrophobization. Gels. 2022, v. 8, n. 11, p. 691. doi:10.3390/gels8110691

[42] Gibowsky, L.; De Berardinis, L.; Plazzotta, S.; et al. Conversion of natural tissues and food waste into aerogels and their application in oleogelation. Green Chemistry. 2025, v. 27, p. 4713-4731. doi:10.1039/D4GC05703A

[43] Lozinsky, V. I.; Galaev, I. Y.; Plieva, F. M.; et al. Polymeric cryogels as promising materials of biotechnological interest. Trends in Biotechnology. 2003, v. 21, n. 10, p. 445-451. doi:10.1016/j.tibtech.2003.08.002

[44] Zou, F.; Cucharero, J.; Dong, Y.; et al. Maximizing sound absorption , thermal insulation , and mechanical strength of anisotropic pectin cryogels. Chemical Engineering Journal. 2023, v. 462, p. 142236. doi:10.1016/j.cej.2023.142236

[45] Zou, F.; Budtova, T. Tailoring the morphology and properties of starch aerogels and cryogels via starch source and process parameter. Carbohydrate Polymers. 2021, v. 255, p. 117344. doi:10.1016/j.carbpol.2020.117344

[46] Zou, F.; Bouvard, J. L.; Pradille, C.; et al. Ice-templated additive-free porous starches with tuned morphology and properties. European Polymer Journal. 2022, v. 176, p. 111403. doi:10.1016/j.eurpolymj.2022.111403

[47] Korhonen, O.; Budtova, T. All-cellulose composite aerogels and cryogels. Composites Part A: Applied Science and Manufacturing. 2020, v. 137, p. 106027. doi:10.1016/j.compositesa.2020.106027

[48] Ciuffarin, F.; Négrier, M.; Plazzotta, S.; et al. Interactions of cellulose cryogels and aerogels with water and oil: Structure-function relationships. Food Hydrocolloids. 2023, v. 140, p. 108631. doi:10.1016/j.foodhyd.2023.108631

[49] Xiao, S.; Zou, M.; Xie, Y.; et al. Nanosilver modified navel orange peel foam/polyethylene glycol composite phase change materials with improved thermal conductivity and photo-thermal conversion efficiency. Journal of Energy Storage. 2022, v. 56, p. 105976. doi:10.1016/j.est.2022.105976

[50] Suchorowiec, K.; Bieda, M.; Szatkowska, M.; et al. From Waste to Functional Material—Carbon Aerogels from Citrus Biomass Infiltrated with Phase Change Materials for Possible Application in Solar-Thermal Energy Conversion and Storage. Energies. 2025, v. 18, n. 4, p. 814. doi:10.3390/en18040814

[51] Wang, H.; Wang, P.; Kasapis, S.; et al. Aerogel-based oil sorbents derived from pomelo (Citrus grandis L.) peels as potential gel matrices for food applications: Formation, properties and in-vitro oral processing. Journal of Food Engineering. 2025, v. 394, p. 112532. doi:10.1016/j.jfoodeng.2025.112532

[52] Li, L.; Jin, Z.; Wang, C.; et al. Valorization of Food Waste: Utilizing Natural Porous Materials Derived from Pomelo-Peel Biomass to Develop

Triboelectric Nanogenerators for Energy Harvesting and Self-Powered Sensing. ACS Applied Materials & Interfaces. 2024, v. 16, n. 29, p. 37806-37817. doi:10.1021/acsami.4c02319

[53] Imran, M.; Islam, A.; Ismail, F.; et al. 3D porous superoleophilic/hydrophobic grapefruit peel aerogel for efficient removal of emulsified-oil from water. Journal of Environmental Chemical Engineering. 2023, v. 11, n. 2, p. 109324. doi:10.1016/j.jece.2023.109324

[54] Effraimopoulou, E.; Jaxel, J.; Budtova, T.; et al. Hydrophobic Modification of Pectin Aerogels via Chemical Vapor Deposition. Polymers. 2024, v. 16, n. 12, . doi:10.3390/polym16121628

[55] Asim, N.; Badiei, M.; Alghoul, M. A.; et al. Biomass and Industrial Wastes as Resource Materials for Aerogel Preparation: Opportunities, Challenges, and Research Directions. Industrial and Engineering Chemistry Research. 2019, v. 58, n. 38, p. 17621-17645. doi:10.1021/acs.iecr.9b02661

[56] Nešić, A.; Cabrera-Barjas, G.; Dimitrijević-Branković, S.; et al. Prospect of polysaccharide-based materials as advanced food packaging. Molecules. 2020, v. 25, n. 1, . doi:10.3390/molecules25010135

[57] Chen, H. B.; Chiou, B. S.; Wang, Y. Z.; et al. Biodegradable pectin/clay aerogels. ACS Applied Materials and Interfaces. 2013, v. 5, n. 5, p. 1715-1721. doi:10.1021/am3028603

[58] Ren, Y.; Jin, F.; Yang, L.; et al. Emerging porous supporting materials for form-stable organic phase change materials. Sustainable Materials and Technologies. 2025, v. 45, p. e01440. doi:10.1016/j.susmat.2025.e01440

[59] Yazdani McCord, M. R.; Baniasadi, H. Advancements in form-stabilized phase change materials: stabilization mechanisms, multifunctionalities, and applications—a comprehensive review. Materials Today Energy. 2024, v. 41, p. 101532. doi:10.1016/j.mtener.2024.101532

[60] Pielichowska, K.; Pielichowski, K. Phase change materials for thermal energy storage. Progress in Materials Science. 2014, v. 65, p. 67-123. doi:10.1016/j.pmatsci.2014.03.005

[61] Okogeri, O.; Stathopoulos, V. N. What about greener phase change

materials? A review on biobased phase change materials for thermal energy storage applications. International Journal of Thermofluids. 2021, v. 10, p. 100081. doi:10.1016/j.ijft.2021.100081

[62] Liu, P.; Chen, X.; Li, Y.; et al. Aerogels Meet Phase Change Materials: Fundamentals, Advances, and Beyond. ACS Nano. 2022, v. 16, n. 10, p. 15586-15626. doi:10.1021/acsnano.2c05067

[63] Sun, M.; Wang, Q.; Di, H. A review of lignocellulosic biomass-based shape-stable composite phase change materials. Journal of Energy Storage. 2023, v. 73, p. 109114. doi:10.1016/j.est.2023.109114

[64] Tauseef-ur-Rehman; Muhammad, H. M.; Janjua, M. M.; et al. A critical review on heat transfer augmentation of phase change materials embedded with porous materials/foams. International Journal of Heat and Mass Transfer. 2019, v. 135, p. 649-673. doi:10.1016/j.ijheatmasstransfer.2019.02.001

[65] Dash, L.; Mahanwar, P. A. A review on organic phase change materials and their applications. International Journal of Engineering Applied Sciences and Technology. 2021, v. 5, n. 9, p. 268-284.

[66] Hyun, D. C.; Levinson, N. S.; Jeong, U.; et al. Emerging Applications of Phase-Change Materials (PCMs): Teaching an Old Dog New Tricks. Angewandte Chemie International Edition. 2014, v. 53, n. 15, p. 3780-3795. doi:10.1002/anie.201305201

[67] Wang, L. Q.; Liang, W. D.; Wang, C. J.; et al. Dodecylamine/Ti3C2-pectin form-stable phase change composites with enhanced light-to-thermal conversion and mechanical properties. Renewable Energy. 2021, v. 176, p. 663-674. doi:10.1016/j.renene.2021.05.136

[68] Sheng, X.; Dong, D.; Lu, X.; et al. MXene-wrapped bio-based pomelo peel foam/polyethylene glycol composite phase change material with enhanced light-to-thermal conversion efficiency, thermal energy storage capability and thermal conductivity. Composites Part A. 2020, v. 138, p. 106067. doi:10.1016/j.compositesa.2020.106067

[69] Yang, L.; Yang, J.; Tang, L. sheng; et al. Hierarchically Porous PVA Aerogel for Leakage-Proof Phase Change Materials with Superior Energy

Storage Capacity. Energy & Fuels. 2020, v. 34, p. 2471-2479. doi:10.1021/acs.energyfuels.9b04212

[70] Yin, G. Z.; Yang, X. M.; López, A. M.; et al. Sodium alginate and Chitosan aided design of form-stable Polyrotaxane based phase change materials with ultra-high latent heat. International Journal of Biological Macromolecules. 2022, v. 222, p. 429-437. doi:10.1016/j.ijbiomac.2022.09.149

[71] Tian, W.; Zheng, X.; Xiao, Y.; et al. A novel photovoltaic-thermoelectric hybrid system with an anisotropic shape-stale phase change composites. Journal of Energy Storage. 2024, v. 104, p. 114676. doi:10.1016/j.est.2024.114676

[72] Zhou, J.; Du, G.; Hu, J.; et al. The establishment of Boron nitride@sodium alginate foam/polyethyleneglycol composite phase change materials with high thermal conductivity, shape stability, and reusability. Chinese Journal of Chemical Engineering. 2023, v. 54, p. 11-21. doi:10.1016/j.cjche.2022.04.001

[73] Wang, L.; Liang, W.; Liu, Y.; et al. Carbonized clay pectin-based aerogel for light-to-heat conversion and energy storage. Applied Clay Science journal. 2022, v. 224, p. 106524. doi:10.1016/j.clay.2022.106524

[74] Dong, Y.; Zou, F.; Vapaavuori, J. Variable-transmittance bio-based phase change composites based on the photothermal property of pectin. Carbohydrate Polymers. 2024, v. 343, p. 122416. doi:10.1016/j.carbpol.2024.122416

[75] Jiang, L.; Lei, Y.; Liu, Q.; et al. Facile preparation of polyethylene glycol/wood-flour composites as form-stable phase change materials for thermal energy storage. Journal of Thermal Analysis and Calorimetry. 2020, v. 139, n. 1, p. 137-146. doi:10.1007/s10973-019-08394-3

[76] Yang, H.; Wang, S.; Wang, X.; et al. Wood-based composite phase change materials with self-cleaning superhydrophobic surface for thermal energy storage. Applied Energy. 2020, v. 261, p. 114481. doi:10.1016/j.apenergy.2019.114481

[77] Zhang, X.; Dong, M.; Shi, J.; et al. Construction of Wheat Bran Biomass

Porous Aerogel by Starch Pasting for Fabrication of Phase Change Composites with High Latent Heat Storage and Temperature Regulation. Energy & Fuels. 2023, v. 37, n. 8, p. 6110-6121. doi:10.1021/acs.energyfuels.3c00447

[78] Zhang, X.; Shi, J.; Wang, Q.; et al. The spider web of modified wheat bran captured PEG to form stabilized phase change composites for temperature regulation and waste heat storage. Journal of Energy Storage. 2024, v. 77, p. 109877. doi:10.1016/j.est.2023.109877

[79] Xie, Y.; Xi, L. MXene quantum dots modified pitaya peel-based composite phase change material with excellent thermal properties for building energy efficiency applications. Construction and Building Materials. 2024, v. 449, p. 138392. doi:10.1016/j.conbuildmat.2024.138392

[80] Liu, H.; Qian, Z.; Wang, Q.; et al. Development of Renewable Biomass-Derived Carbonaceous Aerogel/Mannitol Phase-Change Composites for High Thermal-Energy-Release Efficiency and Shape Stabilization. ACS Applied Energy Materials. 2021, v. 4, n. 2, p. 1714-1730. doi:10.1021/acsaem.0c02864

[81] Ji, Z.; Abdalkarim, S. Y. H.; Li, H.; et al. Waste pomelo peels-derived ultralow density 3D-porous carbon aerogels: Mechanisms of “Soft-rigid” structural formation and solar-thermal energy storage conversion. Solar Energy Materials and Solar Cells. 2023, v. 259, p. 112453. doi:10.1016/j.solmat.2023.112453

[82] Xie, Y.; Xiao, S.; Chen, W.; et al. Shape-stabilized nanosilver-modified grapefruit peel-based porous carbon composite phase change material with high thermal conductivity, photothermal conversion performance and thermal management capability. Journal of Energy Storage. 2024, v. 83, p. 110819. doi:10.1016/j.est.2024.110819

[83] Mandal, S.; Ishak, S.; Lee, D. E.; et al. Shape-stabilized orange peel/myristic acid phase change materials for efficient thermal energy storage application. Energy Reports. 2022, v. 8, p. 9618-9628. doi:10.1016/j.egyr.2022.07.143

[84] Wang, C.; Cheng, C.; Jin, T.; et al. Review on bio-based shape-stable

phase change materials for thermal energy storage and utilization. Journal of Renewable and Sustainable Energy. 2022, v. 14, n. 5, p. 52701. doi:10.1063/5.0102005

[85] Gaur, A.; Tiwari, S.; Kumar, C.; et al. Bio-waste orange peel and polymer hybrid for efficient energy harvesting. Energy Reports. 2020, v. 6, p. 490-496. doi:10.1016/j.egyr.2020.02.020

[86] Kalajahi, S. E. M.; Alizadeh, A.; Hamishehkar, H.; et al. Orange Juice Processing Waste as a Biopolymer Base for Biodegradable Film Formation Reinforced with Cellulose Nanofiber and Activated with Nettle Essential Oil. Journal of Polymers and the Environment. 2022, v. 30, n. 1, p. 258-269. doi:10.1007/s10924-021-02195-2

[87] Gautreau, M.; Durand, S.; Paturel, A.; et al. Impact of cell wall non-cellulosic and cellulosic polymers on the mechanical properties of flax fibre bundles. Carbohydrate Polymers. 2022, v. 291, p. 119599. doi:10.1016/j.carbpol.2022.119599

[88] Berk, Z. Morphology and chemical composition. *In*: Berk, Z. (ed.) Citrus Fruit Processing. Academic Press; 2016:9-54. doi:10.1016/B978-0-12-803133-9.00002-3

[89] Tütem, E.; Sözgen Başkan, K.; Karaman Ersoy, Ş.; et al. Orange. *In*: Jaiswal, A. (ed.) Nutritional Composition and Antioxidant Properties of Fruits and Vegetables. 1st ed. Academic Press; 2020:353-376. doi:10.1016/B978-0-12-812780-3.00022-2

[90] Berk, Z. Production of single-strength citrus juices. *In*: Berk, Z. (ed.) Citrus Fruit Processing. 1st ed. Academic Press; 2016:127-185. doi:10.1016/B978-0-12-803133-9.00008-4

[91] Akyildiz, A.; Ağçam, E. Citrus Juices Technology. *In*: Malik, A.; Erginkaya, Z.; Ahmad, S.; Erten, H. (eds.) Food Processing: Strategies for Quality Assessment. 1st ed. Springer New York; 2014:37-103. doi:10.1007/978-1-4939-1378-7_3

[92] Pasandide, B.; Khodaiyan, F.; Mousavi, Z.; et al. Pectin extraction from citron peel: optimization by Box–Behnken response surface design. Food Science and Biotechnology. 2018, v. 27, n. 4, p. 997-1005.

doi:10.1007/s10068-018-0365-6

[93] Merino, D.; Quilez-molina, A. I.; Perotto, G.; et al. A second life for fruit and vegetable waste: a review on bioplastic films and coatings for potential food protection applications. Green Chemistry. 2022, v. 24, n. 12, p. 4703-4727. doi:10.1039/d1gc03904k

[94] Pereira, B. S.; de Freitas, C.; Vieira, R. M.; et al. Brazilian banana, guava, and orange fruit and waste production as a potential biorefinery feedstock. Journal of Material Cycles and Waste Management. 2022, v. 24, n. 6, p. 2126-2140. doi:10.1007/s10163-022-01495-6

[95] Vieira, R. M.; Gonçalves, A. R.; Brienzo, M. Comprehensive chemical characterization study of three major fruit residues from São Paulo State (Brazil): banana pseudostem, orange bagasse, and guava seed cake. Journal of Material Cycles and Waste Management. 2024, v. 26, n. 6, p. 3554-3570. doi:10.1007/s10163-024-02057-8

[96] Sinnott, M. L. Carbohydrate Chemistry and Biochemistry: Structure and Mechanism. 1st ed. RSC Publishing; 2007.

[97] Bajpai, P. Biomass composition. *In*: Bajpai, P. (ed.) Biomass to Energy Conversion Technologies: The Road to Commercialization. 1st ed. Elsevier; 2020:31-40. doi:10.1016/B978-0-12-818400-4.00004-9

[98] Henriksson, G. Lignin. *In*: Ek, M.; Gellerstedt, G.; Henriksson, G. (eds.) Volume 1 Wood Chemistry and Biotechnology. Vol 1. DeGruyter; 2009:121-145. doi:10.1515/9783110213447

[99] Wan Chik, M. A.; Yusof, R.; Shafie, M. H.; et al. The versatility of pectin: a comprehensive review unveiling its recovery techniques and applications in innovative food products. Journal of Food Measurement and Characterization. 2024, v. 18, n. 7, p. 6101-6123. doi:10.1007/s11694-024-02632-5

[100] Licona-Aguilar, Á. I.; Torres-Huerta, A. M.; Domínguez-Crespo, M. A.; et al. Reutilization of waste biomass from sugarcane bagasse and orange peel to obtain carbon foams: Applications in the metal ions removal. Science of The Total Environment. 2022, v. 831, p. 154883. doi:10.1016/j.scitotenv.2022.154883

[101] Pundir, A.; Sil, A. Orange peel derived hierarchical porous carbon/sulfur composite cathode material for Li–S battery. Biomass and Bioenergy. 2024, v. 180, p. 106999. doi:10.1016/j.biombioe.2023.106999

[102] Vaez, S.; Karimi, K.; Mirmohamadsadeghi, S.; et al. An optimal biorefinery development for pectin and biofuels production from orange wastes without enzyme consumption. Process Safety and Environmental Protection. 2021, v. 152, p. 513-526. doi:10.1016/j.psep.2021.06.013

[103] Taghavi Kevij, H.; Salami, M.; Mohammadian, M.; et al. Mechanical, physical, and bio-functional properties of biopolymer films based on gelatin as affected by enriching with orange peel powder. Polymer Bulletin. 2021, v. 78, n. 8, p. 4387-4402. doi:10.1007/s00289-020-03319-9

[104] Bezerra, P. H. S.; Souza-Santos, Y. J.; Pallone, E. M. J. A.; et al. Development of Sodium Alginate Bioplastic Reinforced with Dried Orange Juice By-Product for Use in Packaging. Polymers. 2024, v. 16, n. 23, p. 3382. doi:10.3390/polym16233382

[105] Luchese, C. L.; Pavoni, J. M. F.; Tessaro, I. C. Influence of the incorporation form of waste from the production of orange juice in the properties of cassava starch-based films. Food Hydrocolloids. 2021, v. 117, p. 106730. doi:10.1016/j.foodhyd.2021.106730

[106] Quilez-Molina, A. I.; Oliveira-Salmazo, L.; Amezúa-Arranz, C.; et al. Evaluation of the acid hydrolysis as pre-treatment to enhance the integration and functionality of starch composites filled with rich-in-pectin agri-food waste orange peel. Industrial Crops and Products. 2023, v. 205, p. 117407. doi:10.1016/j.indcrop.2023.117407

[107] Pagliarini, E.; Minichiello, C.; Sisti, L.; et al. From food waste to eco-friendly functionalized polymer composites: Investigation of orange peels as active filler. New Biotechnology. 2024, v. 80, p. 37-45. doi:10.1016/j.nbt.2024.01.001

[108] Veeman, D.; Subramaniyan, M. K.; Surendhar, G. J.; et al. A Novel Material for Sustainable Environment: Processing, Additive Manufacturing, and Characterization. Journal of Materials Engineering

and Performance. 2024, v. 33, n. 14, p. 7368-7377. doi:10.1007/s11665-023-08458-4

[109] Sambudi, N. S.; Lin, W. Y.; Harun, N. Y.; et al. Modification of Poly(lactic acid) with Orange Peel Powder as Biodegradable Composite. Polymers. 2022, v. 14, n. 19, p. 4126. doi:10.3390/polym14194126

[110] Shunmugam, M. N.; Sankaranarayanan, S.; Pandiarajan, N.; et al. Enhancing Mechanical Properties of PLA Filaments through Orange Peel Powder Reinforcement: Optimization of 3D Printing Parameters. Applied Science and Engineering Progress. 2024, v. 17, n. 4, p. 7536. doi:10.14416/j.asep.2024.08.011

[111] Koutoulis, A. S.; Giannakas, A. E.; Lazaridis, D. G.; et al. Preparation and Characterization of PLA-Based Films Fabricated with Different Citrus Species Peel Powder. Coatings. 2024, v. 14, n. 10, p. 1311. doi:10.3390/coatings14101311

[112] Rathinavel, S.; Saravanakumar, S. S. Development and Analysis of Poly Vinyl Alcohol/Orange peel powder biocomposite films. Journal of Natural Fibers. 2021, v. 18, n. 12, p. 2045-2054. doi:10.1080/15440478.2019.1711285

[113] Motezuki, J. E. Compósitos Poliméricos Biodegradáveis Obtidos Pela Transformação de Resíduos Cítricos Agroindustriais. Universidade Federal de São Carlos; 2018.

[114] Ghasemizad, S.; Pirsa, S.; Amiri, S.; et al. Optimization and Characterization of Bioactive Biocomposite Film Based on Orange Peel Incorporated with Gum Arabic Reinforced by Cr2O3 Nanoparticles. Journal of Polymers and the Environment. 2022, v. 30, p. 2493–2506. doi:10.1007/s10924-021-02357-2

[115] Merino, D.; Bellassi, P.; Paul, U. C.; et al. Assessment of chitosan/pectin-rich vegetable waste composites for the active packaging of dry foods. Food Hydrocolloids. 2023, v. 139, n. May 2023, p. 108580. doi:https://doi.org/10.1016/j.foodhyd.2023.108580

[116] Gao, F.; Qiu, Z.; Hou, Y.; et al. Novel aerogel of aminated MXene composite orange peel biomass for ultra-high capacity of V(V) adsorption.

Colloids and Surfaces A: Physicochemical and Engineering Aspects. 2024, v. 697, p. 134472. doi:10.1016/j.colsurfa.2024.134472

[117] Pung, T.; Jitchum, V.; Srisang, S.; et al. Carbonaized carbon aerogels derived from pomelo peels for sorption of some organic solvents. Agriculture and Natural Resources. 2024, v. 58, n. 1, p. 81-88. doi:10.34044/j.anres.2024.58.1.09

[118] Shi, G.; Qian, Y.; Tan, F.; et al. Controllable synthesis of pomelo peel-based aerogel and its application in adsorption of oil/organic pollutants. Royal Societu Open Science. 2019, v. 6, p. 181823. doi:10.1098/rsos.181823

[119] Valoppi, F.; Wang, Y. J.; Alt, G.; et al. Valorization of Native Soluble and Insoluble Oat Side Streams for Stable Suspensions and Emulsions. Food and Bioprocess Technology. 2021, v. 14, p. 751-764. doi:10.1007/s11947-021-02602-5

[120] Lin, J.; Tang, Z. sheng; Brennan, C. S.; et al. Thermomechanically micronized sugar beet pulp: Dissociation mechanism, physicochemical characteristics, and emulsifying properties. Food Research International. 2022, v. 160, n. October 2022, p. 111675. doi:10.1016/j.foodres.2022.111675

[121] Yin, Z.; Wang, Z.; He, Z.; et al. Effect of particle size and microstructure on the physical properties of soybean insoluble dietary fiber in aqueous solution. Food Bioscience. 2021, v. 41, n. June 2021, p. 100898. doi:10.1016/j.fbio.2021.100898

[122] Pung, T.; Ponglong, N.; Panich-pat, T. Fabrication of Pomelo-Peel Sponge Aerogel Modified with Hexadecyltrimethoxysilane for the Removal of Oils/Organic Solvents. Water, Air, & Soil Pollution. 2022, v. 233, p. 283. doi:10.1007/s11270-022-05766-8

[123] Hiemenz, P. C.; Rajagopalan, R. Principles of Colloid and Surface Chemistry. 3rd ed. Marcel Dekker; 1997.

[124] Ptaszek, P.; Basu, S. Influence of Fibers and Particle Size Distribution on Food Rheology. *In*: Ahmed, J. (ed.) Advances in Food Rheology and Its Applications. 1st ed. Woodhead Publishing; 2016:177-208.

doi:10.1016/B978-0-08-100431-9.00008-5

[125] Su, D.; Zhu, X.; Wang, Y.; et al. Effect of high-pressure homogenization on rheological properties of citrus fiber. LWT. 2020, v. 127, p. 109366. doi:10.1016/j.lwt.2020.109366

[126] Huang, J.; Liao, J.; Qi, J.; et al. Structural and physicochemical properties of pectin-rich dietary fiber prepared from citrus peel. Food Hydrocolloids. 2021, v. 110, p. 106140. doi:10.1016/j.foodhyd.2020.106140

[127] Bengtsson, H. The Physicochemical and Sensory Properties of Fruit and Vegetable Fibre Suspensions - The Effect of Fibre Processing and Its Addition to Low-Fat Sausages. Lund University; 2009.

[128] Bruno, E.; Lupi, F. R.; Martin-Piñero, M. J.; et al. Influence of different dispersing systems on rheological and microstructural properties of citrus fiber suspensions. LWT. 2021, v. 152, p. 112270. doi:10.1016/j.lwt.2021.112270

[129] Zhang, Y.; Liao, J.; Qi, J. Functional and structural properties of dietary fi ber from citrus peel a ff ected by the alkali combined with high-speed homogenization treatment. LWT - Food Science and Technology. 2020, v. 128, p. 109397. doi:10.1016/j.lwt.2020.109397

[130] Lupi, F. R.; Puoci, F.; Bruno, E.; et al. The effects of process conditions on rheological properties of functional citrus fibre suspensions. Food and Bioproducts Processing. 2020, v. 121, p. 54-64. doi:10.1016/j.fbp.2020.01.018

[131] Su, D.; Zhu, X.; Adhikari, B.; et al. Effect of high-pressure homogenization on the rheology, microstructure and fractal dimension of citrus fiber-oil dispersions. Journal of Food Engineering. 2020, v. 277, p. 109899. doi:10.1016/j.jfoodeng.2019.109899

[132] Qi, J. ru; Song, L. wen; Zeng, W. qi; et al. Citrus fiber for the stabilization of O/W emulsion through combination of Pickering effect and fiber-based network. Food Chemistry. 2021, v. 343, p. 128523. doi:10.1016/j.foodchem.2020.128523

[133] Sluiter, J.; Sluiter, A.; Scarlata, C.; et al. Determination of Structural Carbohydrates and Lignin in Biomass: Laboratory Analytical Procedure

(LAP) (Revised August 2012). Published online, 2008p. 18. Available at <https://www.nrel.gov/docs/gen/fy13/42618.pdf>.

[134] Korhonen, O.; Sawada, D.; Budtova, T. All-cellulose composites via short-fiber dispersion approach using NaOH–water solvent. Cellulose. 2019, v. 26, n. 8, p. 4881-4893. doi:10.1007/s10570-019-02422-z

[135] Castro, R. I.; Morales-Quintana, L. Study of the cell wall components produced during different ripening stages through thermogravimetric analysis. Cellulose. 2019, v. 26, n. 5, p. 3009-3020. doi:10.1007/s10570-019-02305-3

[136] Vallejo, F.; Larrosa, M.; Escudero, E.; et al. Concentration and Solubility of Flavanones in Orange Beverages Affect Their Bioavailability in Humans. Journal of Agricultural and Food Chemistry. 2010, v. 58, n. 10, p. 6516-6524. doi:10.1021/jf100752j

[137] Sharma, K.; Mahato, N.; Lee, Y. R. Extraction, characterization and biological activity of citrus flavonoids. 2019, v. 35, n. 2, p. 265-284. doi:10.1515/revce-2017-0027

[138] Panwar, D.; Saini, A.; Panesar, P. S.; et al. Unraveling the scientific perspectives of citrus by-products utilization: Progress towards circular economy. Trends in Food Science & Technology. 2021, v. 111, p. 549-562. doi:10.1016/j.tifs.2021.03.018

[139] Ortiz-Sanchez, M.; Cardona Alzate, C. A.; Solarte-Toro, J. C. Orange Peel Waste as a Source of Bioactive Compounds and Valuable Products: Insights Based on Chemical Composition and Biorefining. Biomass. 2024, v. 4, n. 1, p. 107-131. doi:10.3390/biomass4010006

[140] Vieira, R. M.; Sanvezzo, P. B.; Branciforti, M. C.; et al. Effects of Particle Size on the Preparation of Biomass Samples for Structural Characterization. Bioenergy Research. 2023, v. 16, n. 4, p. 2192-2203. doi:10.1007/s12155-023-10587-6

[141] Szymańska-Chargot, M.; Pękala, P.; Siemińska-Kuczer, A.; et al. A determination of the composition and structure of the polysaccharides fractions isolated from apple cell wall based on FT-IR and FT-Raman spectra supported by PCA analysis. Food Hydrocolloids. 2024, v. 150, n.

December 2023, . doi:10.1016/j.foodhyd.2023.109688

[142] Szymanska-Chargot, M.; Zdunek, A. Use of FT-IR Spectra and PCA to the Bulk Characterization of Cell Wall Residues of Fruits and Vegetables Along a Fraction Process. Food Biophysics. 2013, v. 8, n. 1, p. 29-42. doi:10.1007/s11483-012-9279-7

[143] Kostryukov, S. G.; Malov, N. A.; Masterova, Y. Y.; et al. On the Possibility of Quantitative Determination of Lignin and Cellulose in Plant Materials Using IR Spectroscopy. Russian Journal of Bioorganic Chemistry. 2023, v. 49, n. 7, p. 1628-1635. doi:10.1134/S106816202307083X

[144] Chylińska, M.; Szymańska-Chargot, M.; Zdunek, A. Imaging of polysaccharides in the tomato cell wall with Raman microspectroscopy. Plant Methods. 2014, v. 10, n. 1, p. 14. doi:10.1186/1746-4811-10-14

[145] Chylińska, M.; Szymańska-Chargot, M.; Zdunek, A. FT-IR and FT-Raman characterization of non-cellulosic polysaccharides fractions isolated from plant cell wall. Carbohydrate Polymers. 2016, v. 154, p. 48-54. doi:10.1016/j.carbpol.2016.07.121

[146] Demina, T. S.; Minaev, N. V; Akopova, T. A. Polysaccharide-based aerogels fabricated via supercritical fluid drying: a systematic review. Polymer Bulletin. 2024, v. 81, n. 15, p. 13331-13356. doi:10.1007/s00289-024-05359-x

[147] Nguyen, N. T. T.; Nguyen, T. T. T.; Nguyen, D. T. C.; et al. Fruit waste-derived aerogels for the removal of dyes, heavy metals and oils in water: a review. Environmental Chemistry Letters. 2024, v. 22, n. 1, p. 419-443. doi:10.1007/s10311-023-01667-2

[148] Kistler, S. S. Coherent Expanded-Aerogels. The Journal of Physical Chemistry. 1932, v. 36, n. 1, p. 52-64. doi:10.1021/j150331a003

[149] Kistler, S. S. Coherent Expanded Aerogels and Jellies. Nature. 1931, v. 127, n. 3211, p. 741. doi:10.1038/127741a0

[150] Steiner, S. A.; Pierre, A. C. The Story of Aerogel. *In*: Aegerter, M. A.; Leventis, N.; Koebel, M.; Steiner III, S. A. (eds.) Springer Handbook of Aerogels. Springer International Publishing; 2023:1-50. doi:10.1007/978-3-030-27322-4_1

[151] IUPAC. Compendium of Chemical Terminology. International Union of Pure and Applied Chemistry. doi:10.1351/goldbook.B00661

[152] Gelas, L.; Budtova, T. From Cellulose Solutions to Aerogels and Xerogels: Controlling Properties for Drug Delivery. Biomacromolecules. 2024, v. 25, n. 11, p. 7421-7432. doi:10.1021/acs.biomac.4c01074

[153] Groult, S. Pectin-Based Aerogels: Advanced Materials for Thermal Insulation and Drug Delivery Applications. Université Paris sciences et lettres; 2019.

[154] Budtova, T. Cellulose II aerogels: a review. Cellulose. 2019, v. 26, n. 1, p. 81-121. doi:10.1007/s10570-018-2189-1

[155] Mendez, D. A.; Schroeter, B.; Martínez-abad, A.; et al. Pectin-based aerogel particles for drug delivery: Effect of pectin composition on aerogel structure and release properties. Carbohydrate Polymers. 2023, v. 306, p. 120604. doi:10.1016/j.carbpol.2023.120604

[156] Suttiruengwong, S.; Konthong, S.; Pivsa-Art, S.; et al. Fabrication and characterization of porous pectin-based aerogels for drug delivery. Carbohydrate Polymer Technologies and Applications. 2024, v. 7, p. 100499. doi:10.1016/j.carpta.2024.100499

[157] Lee, D.; Noh, J.; Moon, S. Y.; et al. Pectin Nanoporous Structures Prepared via Salt-Induced Phase Separation and Ambient Azeotropic Evaporation Processes. Biomacromolecules. 2024, v. 25, n. 3, p. 1709-1723. doi:10.1021/acs.biomac.3c01230

[158] Dong, Y.; Li, H.; Zou, F.; et al. Structure-properties correlations in low-methylated pectin hydrogels and aerogels crosslinked by divalent ions. International Journal of Biological Macromolecules. 2025, v. 285, p. 137980. doi:10.1016/j.ijbiomac.2024.137980

[159] Groult, S.; Buwalda, S.; Budtova, T. Tuning bio-aerogel properties for controlling theophylline delivery. Part 1: Pectin aerogels. Materials Science & Engineering C. 2021, v. 126, p. 112148. doi:10.1016/j.msec.2021.112148

[160] Jiang, Y. H.; Pang, X. N.; Deng, Y. J.; et al. An Alginate Hybrid Sponge with High Thermal Stability: Its Flame Retardant Properties and

Mechanism. Polymers. 2019, v. 11, n. 12, p. 1973. doi:10.3390/polym11121973

[161] Dranca, F.; Mironeasa, S. Green Extraction of Pectin from Sugar Beet Flakes and Its Application in Hydrogels and Cryogels. Gels. 2024, v. 10, n. 4, p. 228. doi:10.3390/gels10040228

[162] Ma, Y.; Bi, J.; Wu, Z.; et al. Understanding the mechanism of saccharides type and concentration affecting texture of freeze-dried pectin-CMC cryogels through experiment and molecular dynamic simulation. International Journal of Biological Macromolecules. 2025, v. 292, p. 139263. doi:10.1016/j.ijbiomac.2024.139263

[163] Wang, R.; Li, Y.; Shuai, X.; et al. Development of Pectin-Based Aerogels with Several Excellent Properties for the Adsorption of Pb2+. Foods. 2021, v. 10, n. 12, p. 3127. doi:10.3390/foods10123127

[164] Chen, Z.; Zhan, B.; Li, S.; et al. Bubble-enhanced ultralight aerogels derived from pectin for oil absorption. Cellulose. 2025, v. 32, n. 7, p. 4435-4448. doi:10.1007/s10570-025-06523-w

[165] Wu, W.; Wu, Y.; Lin, Y.; et al. Facile fabrication of multifunctional citrus pectin aerogel fortified with cellulose nanofiber as controlled packaging of edible fungi. Food Chemistry. 2022, v. 374, p. 131763. doi:10.1016/j.foodchem.2021.131763

[166] Chaux-Gutiérrez, A. M.; Pérez-Monterroza, E. J.; Cattelan, M. G.; et al. Active Packaging Incorporating Cryogels Loaded with Pink Pepper Essential Oil (Schinus terebinthifolius Raddi) for Strawberry Preservation. Processes. 2025, v. 13, n. 4, p. 1179. doi:10.3390/pr13041179

[167] Ma, Y.; Bi, J.; Feng, S.; et al. Higher molecular weight pectin inhibits ice crystal growth and its effect on the microstructural and physical properties of pectin cryogels. Carbohydrate Polymers. 2024, v. 340, p. 122312. doi:10.1016/j.carbpol.2024.122312

[168] Ma, Y.; Bi, J.; Yi, J.; et al. Modulation of ice crystal formation behavior in pectin-sucrose hydrogel by freezing temperature: Effect on ice crystal morphology and drying properties. Drying Technology. 2023, v. 41, n. 11, p. 1-12. doi:10.1080/07373937.2023.2184829

[169] Nguyen, P. T. T.; Do, N. H. N.; Goh, X. Y.; et al. Recent Progresses in Eco-Friendly Fabrication and Applications of Sustainable Aerogels from Various Waste Materials. Waste and Biomass Valorization. 2022, v. 13, n. 4, p. 1825-1847. doi:10.1007/s12649-021-01627-3

[170] Thai, Q. B.; Nguyen, S. T.; Ho, D. K.; et al. Cellulose-based aerogels from sugarcane bagasse for oil spill-cleaning and heat insulation applications. Carbohydrate Polymers. 2020, v. 228, p. 115365. doi:10.1016/j.carbpol.2019.115365

[171] Lyu, P.; Xia, L.; Liu, X.; et al. Self-cleaning superhydrophobic aerogels from waste hemp noil for ultrafast oil absorption and highly efficient PM removal. Separation and Purification Technology. 2023, v. 306, p. 122503. doi:10.1016/j.seppur.2022.122503

[172] Dai, H.; Huang, Y.; Zhang, H.; et al. Direct fabrication of hierarchically processed pineapple peel hydrogels for efficient Congo red adsorption. Carbohydrate Polymers. 2020, v. 230, n. 2, p. 115599. doi:10.1016/j.carbpol.2019.115599

[173] Li, W.; Li, Z.; Wang, W.; et al. Green approach to facilely design hydrophobic aerogel directly from bagasse. Industrial Crops & Products. 2021, v. 172, p. 113957. doi:10.1016/j.indcrop.2021.113957

[174] Liu, Z.; Wu, J.; Xia, J.; et al. Characterization of lignocellulose aerogels fabricated using a LiCl/DMSO solution. Industrial Crops & Products. 2019, v. 131, p. 293-300. doi:10.1016/j.indcrop.2019.01.057

[175] Zhang, M.; Liao, Y.; Han, N.; et al. Upcycling Industrial Biomass Wastes Into Aerogels Using Zinc Chloride Salt Hydrates. Advanced Sustainable Systems. 2025, v. 9, n. 4, p. 2400688. doi:10.1002/adsu.202400688

[176] Chen, M.; Zhang, X.; Zhang, A.; et al. Direct preparation of green and renewable aerogel materials from crude bagasse. Cellulose. 2016, v. 23, n. 2, p. 1325-1334. doi:10.1007/s10570-015-0814-9

[177] Masuelli, M. A. Mark-Houwink Parameters for Aqueous-Soluble Polymers and Biopolymers at Various Temperatures. Journal of Polymer and Biopolymer Physics Chemistry. 2014, v. 2, n. 2, p. 37-43. doi:10.12691/jpbpc-2-2-2

[178] Ferrero, F.; Campagna, P.; Piccrnini, N. Shrinking Kinetics of Calcium Alginate Beads in Alcoholic Soda. Chemical Engineering Communications. 1982, v. 15, n. 1-4, p. 197-206. doi:10.1080/00986448208911069

[179] Kurita, O.; Murakami, K.; Fujiwara, T. Chemical modification of polysaccharides by the use of intramolecular associations in polar organic solvents. Polymer Bulletin. 2010, v. 65, n. 5, p. 443-454. doi:10.1007/s00289-009-0219-8

[180] Zhang, M.; Dou, M.; Wang, M.; et al. Study on the solubility parameter of supercritical carbon dioxide system by molecular dynamics simulation. Journal of Molecular Liquids. 2017, v. 248, p. 322-329. doi:https://doi.org/10.1016/j.molliq.2017.10.056

[181] Baraka, F.; Ganesan, K.; Milow, B.; et al. Cellulose nanofiber aerogels: effect of the composition and the drying method. Cellulose. 2024, v. 31, n. 16, p. 9699-9713. doi:10.1007/s10570-024-06191-2

[182] Chartier, C.; Buwalda, S.; Berghe, H. Van Den; et al. Tuning the properties of porous chitosan : Aerogels and cryogels. International Journal of Biological Macromolecules. 2022, v. 202, p. 215-223. doi:10.1016/j.ijbiomac.2022.01.042

[183] Aguilera-bulla, D.; Legay, L.; Buwalda, S. J.; et al. Crosslinker-Free Hyaluronic Acid Aerogels. Biomacromolecules. 2022, v. 23, p. 2838-2845. doi:10.1021/acs.biomac.2c00207

[184] Tsioptsias, C.; Panagiotou, A.; Mitlianga, P. Thermal Behavior and Infrared Absorbance Bands of Citric Acid. Applied Sciences. 2024, v. 14, n. 18, p. 8406. doi:10.3390/app14188406

[185] Groen, H.; Roberts, K. J. Nucleation, Growth, and Pseudo-Polymorphic Behavior of Citric Acid As Monitored in Situ by Attenuated Total Reflection Fourier Transform Infrared Spectroscopy. The Journal of Physical Chemistry B. 2001, v. 105, n. 43, p. 10723-10730. doi:10.1021/jp011128l

[186] Bichara, L. C.; Lanús, H. E.; Ferrer, E. G.; et al. Vibrational Study and Force Field of the Citric Acid Dimer Based on the SQM Methodology. Advances in Physical Chemistry. 2011, v. 2011, n. 1, p. 347072.

doi:10.1155/2011/347072

[187] Mattos, B. D.; Zhu, Y.; Tardy, B. L.; et al. Versatile Assembly of Metal–Phenolic Network Foams Enabled by Tannin–Cellulose Nanofibers. Advanced Materials. 2023, v. 35, n. 12, p. 2209685. doi:10.1002/adma.202209685

[188] Lavoine, N.; Bergström, L. Nanocellulose-based foams and aerogels: processing, properties, and applications. Journal of Materials Chemistry A. 2017, v. 5, n. 31, p. 16105-16117. doi:10.1039/C7TA02807E

[189] Yu, S.; Pradille, C.; Budtova, T. Mechanical properties of carboxymethyl cellulose aerogels and cryogels. Cellulose. Published online, 2025. doi:10.1007/s10570-025-06647-z

[190] Martoïa, F.; Cochereau, T.; Dumont, P. J. J.; et al. Cellulose nanofibril foams: Links between ice-templating conditions, microstructures and mechanical properties. Materials & Design. 2016, v. 104, p. 376-391. doi:10.1016/j.matdes.2016.04.088

[191] Buchtová, N.; Pradille, C.; Bouvard, J. L.; et al. Mechanical properties of cellulose aerogels and cryogels. Soft Matter. 2019, v. 15, n. 39, p. 7901-7908. doi:10.1039/C9SM01028A

[192] Xiong, W.; Abdusalamov, R.; Itskov, M.; et al. Analysis of the microstructural connectivity and compressive behavior of particle aggregated silica aerogels. Proceedings in Applied Mathematics and Mechanics. 2024, v. 24, n. 1, p. e202300224. doi:10.1002/pamm.202300224

[193] Shafie, M. H.; Yusof, R.; Naharudin, I.; et al. Effect of different molar ratios of choline chloride–citric acid monohydrate in deep eutectic solvents as plasticizers for Averrhoa bilimbi pectin films. Journal of Food Measurement and Characterization. 2022, v. 16, n. 5, p. 3832-3843. doi:10.1007/s11694-022-01479-y

[194] Shi, R.; Zhang, Z.; Liu, Q.; et al. Characterization of citric acid/glycerol co-plasticized thermoplastic starch prepared by melt blending. Carbohydrate Polymers. 2007, v. 69, n. 4, p. 748-755. doi:10.1016/j.carbpol.2007.02.010

[195] Shi, R.; Bi, J.; Zhang, Z.; et al. The effect of citric acid on the structural properties and cytotoxicity of the polyvinyl alcohol/starch films when molding at high temperature. Carbohydrate Polymers. 2008, v. 74, n. 4, p. 763-770. doi:10.1016/j.carbpol.2008.04.045

[196] Liu, J.; Dong, Y.; Zheng, X.; et al. Citric acid crosslinked soluble soybean polysaccharide films for active food packaging applications. Food Chemistry. 2024, v. 438, p. 138009. doi:10.1016/j.foodchem.2023.138009

[197] Lu, Y.; Wu, H.; Chen, Q.; et al. Facile preparation of fracture-free pectin/clay aerogel monoliths. Materials Research Innovations. 2016, v. 8917, p. S2-46-S2-51. doi:10.1179/1432891714Z.0000000001060

[198] Bastioli, C. Handbook of Biodegradable Polymers. Smithers Rapra Press; 2005.

[199] Miyaji, K.; Zhou, C.; Maeda, A.; et al. Biodegradation of various forms of cellulose and chitin in natural waters with different salinity. Polymer Degradation and Stability. 2023, v. 215, p. 110423. doi:10.1016/j.polymdegradstab.2023.110423

[200] García-Depraect, O.; Lebrero, R.; Rodriguez-Vega, S.; et al. Biodegradation of bioplastics under aerobic and anaerobic aqueous conditions: Kinetics, carbon fate and particle size effect. Bioresource Technology. 2022, v. 344, p. 126265. doi:10.1016/j.biortech.2021.126265

[201] Rangel-Marrón, M.; Mani-López, E.; Palou, E.; et al. Effects of alginate-glycerol-citric acid concentrations on selected physical, mechanical, and barrier properties of papaya puree-based edible films and coatings, as evaluated by response surface methodology. LWT. 2019, v. 101, p. 83-91. doi:10.1016/j.lwt.2018.11.005

[202] Otoni, C. G.; Figueiredo, J. S. L.; Capeletti, L. B.; et al. Tailoring the Antimicrobial Response of Cationic Nanocellulose-Based Foams through Cryo-Templating. ACS Applied Bio Materials. 2019, v. 2, n. 5, p. 1975-1986. doi:10.1021/acsabm.9b00034

[203] Haq, F.; Kiran, M.; Khan, I. A.; et al. Exploring the pathways to sustainability: A comprehensive review of biodegradable plastics in the circular economy. Materials Today Sustainability. 2025, v. 29, p. 101067.

doi:10.1016/j.mtsust.2024.101067

[204] Negrier, M.; El Ahmar, E.; Sescousse, R.; et al. Upcycling cellulose waste textile into aerogel beads via prilling technique. Cellulose. 2024, v. 31, n. 2, p. 823-839. doi:10.1007/s10570-023-05659-x

[205] Paberit, R.; Rilby, E.; Göhl, J.; et al. Cycling Stability of Poly(ethylene glycol) of Six Molecular Weights: Influence of Thermal Conditions for Energy Applications. ACS Applied Energy Materials. 2020, v. 3, n. 11, p. 10578-10589. doi:10.1021/acsaem.0c01621

[206] Khan, Z.; Khan, Z.; Ghafoor, A. A review of performance enhancement of PCM based latent heat storage system within the context of materials, thermal stability and compatibility. Energy Conversion and Management. 2016, v. 115, p. 132-158. doi:10.1016/j.enconman.2016.02.045

[207] Yin, L.; Xie, D.; Gong, K.; et al. Phase Change Materials Encapsulated in Coral-Inspired Organic − Inorganic Aerogels for Flame-Retardant and Thermal Energy Storage. ACS Applied Nano Materials. 2023, v. 6, p. 8752−8762. doi:10.1021/acsanm.3c01128

[208] Zheng, Z.; Liu, H.; Wu, D.; et al. Polyimide/MXene hybrid aerogel-based phase-change composites for solar-driven seawater desalination. Chemical Engineering Journal. 2022, v. 440, p. 135862. doi:10.1016/j.cej.2022.135862

[209] Zheng, Z.; Shi, T.; Liu, H.; et al. Polyimide/phosphorene hybrid aerogel-based composite phase change materials for high-efficient solar energy capture and photothermal conversion. Applied Thermal Engineering. 2022, v. 207, p. 118173. doi:10.1016/j.applthermaleng.2022.118173

[210] Liu, S.; Quan, B.; Yang, Y.; et al. Shape stable phase change composites based on MXene/biomass-derived aerogel for solar–thermal energy conversion and storage. Journal of Energy Storage. 2023, v. 67, p. 107592. doi:10.1016/j.est.2023.107592

[211] Li, S.; Zhang, W.; Zhou, L.; et al. Reversible assembled gelatin aerogel-based phase change materials for light-to-thermal conversion and management. Journal of Energy Storage. 2024, v. 75, p. 109769. doi:10.1016/j.est.2023.109769

[212] Heidari, N. A.; Hamdami, N.; Siqueira, G.; et al. Valorizing brewery industry waste in nanocellulose cryogel-PEG composites for cold chain packaging. Carbohydrate Polymers. 2025, v. 349, p. 123031. doi:10.1016/j.carbpol.2024.123031

[213] Ren, J.; Tan, R.; Huang, C.; et al. Self-assembled cellulose nanofibers/graphene aerogel-supported phase change composites with a three-dimensional network structure for enhanced solar-thermal energy conversion and storage. Journal of Colloid and Interface Science. 2025, v. 700, p. 138343. doi:10.1016/j.jcis.2025.138343

[214] Gao, H.; Ma, H.; Cui, J.; et al. Natural cellulose-based kapok fiber composite aerogel phase change materials with flame retardancy, fire warning, thermal energy storage and thermoelectric conversion. International Journal of Biological Macromolecules. 2025, v. 319, p. 145740. doi:10.1016/j.ijbiomac.2025.145740

[215] Wang, F.; Zhao, S.; Wei, G.; et al. Bacterial cellulose-based Janus energy storage phase change composite aerogel for efficient interfacial solar vapor generation. Separation and Purification Technology. 2025, v. 356, p. 129983. doi:10.1016/j.seppur.2024.129983

[216] Hu, H.; Wang, C.; Xie, S.; et al. Polyethylene glycol/carboxymethyl cellulose/montmorillonite composite phase change materials for thermal management. Journal of Energy Storage. 2025, v. 105, p. 114714. doi:10.1016/j.est.2024.114714

[217] Zou, S.; Xi, L. CNF/PVA aerogel-based eutectic composite phase change materials with high strength and form stability for energy efficient building applications. Journal of Energy Storage. 2025, v. 127, p. 117139. doi:10.1016/j.est.2025.117139

[218] Cheng, P.; Gao, H.; Chen, X.; et al. Flexible monolithic phase change material based on carbon nanotubes/chitosan/poly(vinyl alcohol). Chemical Engineering Journal. 2020, v. 397, p. 125330. doi:10.1016/j.cej.2020.125330

[219] Eller, C.; Rida, M.; Boudier, K.; et al. Climate-based analysis for the potential use of coconut oil as phase change material in buildings.

Sustainability. 2021, v. 13, n. 19, p. 10731. doi:10.3390/su131910731

[220] Zeinelabdein, R.; Omer, S.; Gan, G. Critical review of latent heat storage systems for free cooling in buildings. Renewable and Sustainable Energy Reviews. 2018, v. 82, p. 2843-2868. doi:10.1016/j.rser.2017.10.046

[221] Reddy, V. J.; Dixit, P.; Singh, J.; et al. Understanding the core-shell interactions in macrocapsules of organic phase change materials and polysaccharide shell. Carbohydrate Polymers. 2022, v. 294, p. 119786. doi:10.1016/j.carbpol.2022.119786

[222] Reyes, G.; Ajdary, R.; Yazdani, M. R.; et al. Hollow Filaments Synthesized by Dry-Jet Wet Spinning of Cellulose Nanofibrils: Structural Properties and Thermoregulation with Phase-Change Infills. ACS Applied Polymer Materials. 2022, v. 4, n. 4, p. 2908-2916. doi:10.1021/acsapm.2c00177

[223] Yazdani, M. R.; Ajdary, R.; Kankkunen, A.; et al. Cellulose Nanofibrils Endow Phase-Change Polyethylene Glycol with Form Control and Solid-to-gel Transition for Thermal Energy Storage. ACS Applied Materials & Interfaces. 2021, v. 13, n. 5, p. 6188-6200. doi:10.1021/acsami.0c18623

[224] Chen, M.; Fan, C.; Pan, N.; et al. Phase-Change Emulsion Stabilized by Lignin-Modified Cellulose Nanofiber and Its Application as Energy-Exchange Fluid. ACS Sustainable Chemistry & Engineering. 2024, v. 12, n. 22, p. 8521-8532. doi:10.1021/acssuschemeng.4c01900

[225] Liu, L.; Fan, X.; Zhang, Y.; et al. Novel bio-based phase change materials with high enthalpy for thermal energy storage. Applied Energy. 2020, v. 268, p. 114979. doi:10.1016/j.apenergy.2020.114979

[226] Zhao, J. L.; Luo, W. J.; Kim, J. K.; et al. Graphene Oxide Aerogel Beads Filled with Phase Change Material for Latent Heat Storage and Release. ACS Applied Energy Materials. 2019, v. 2, n. 5, p. 3657-3664. doi:10.1021/acsaem.9b00374

[227] Lyu, J.; Liu, Z. W.; Wu, X. H.; et al. Nanofibrous Kevlar Aerogel Films and Their Phase-Change Composites for Highly Efficient Infrared Stealth. ACS Nano. 2019, v. 13, n. 2, p. 2236-2245. doi:10.1021/acsnano.8b08913

[228] Baniasadi, H.; Abidnejad, R.; Cruz, C. D.; et al. Sustainable multifunctional foams for cold-chain packaging: Stabilizing polyethylene glycol with cellulose and pomegranate peel for antibacterial protection and temperature control. Sustainable Materials and Technologies. 2025, v. 43, p. e01312. doi:10.1016/j.susmat.2025.e01312

[229] Guo, D.; Zhang, Y.; Chen, K.; et al. Carboxymethyl chitosan-based form-stable phase change materials with ultra-low leakage and excellent low-temperature buffering performance. Carbohydrate Polymers. Published online, 2025p. 124033. doi:10.1016/j.carbpol.2025.124033

[230] Lin, F.; Liu, X.; Leng, G.; et al. Grid structure phase change composites with effective solar/electro-thermal conversion for multi-functional thermal application. Carbon. 2023, v. 201, p. 1001-1010. doi:10.1016/j.carbon.2022.09.077

[231] Kahwaji, S.; White, M. A. Edible Oils as Practical Phase Change Materials for Thermal Energy Storage. Applied sciences. 2019, v. 9, n. 8, p. 1627. doi:10.3390/app9081627

[232] Sabahannur, S.; Alimuddin, S. Identification of Fatty Acids in Virgin Coconut Oil (VCO), Cocoa Beans, Crude Palm Oil (CPO), and Palm Kernel Beans Using Gas Chromatography. IOP Conference Series: Earth and Environmental Science. 2022, v. 1083, n. 1, p. 12036. doi:10.1088/1755-1315/1083/1/012036

[233] Sonwai, S.; Rungprasertphol, P.; Nantipipat, N.; et al. Characterization of Coconut Oil Fractions Obtained from Solvent Fractionation Using Acetone. Journal of oleo science. 2017, v. 66, n. 9, p. 951-961. doi:10.5650/jos.ess16224

[234] Himran, S.; Suwono, A.; Mansoori, G. Characterization of Alkanes and Paraffin Waxes for Application as Phase Change Energy Storage Medium. Energy Sources. 1994, v. 16, n. 1, p. 117-128. doi:10.1080/00908319408909065

[235] Tahan Latibari, S.; Sadrameli, S. M. Carbon based material included-shaped stabilized phase change materials for sunlight-driven energy conversion and storage: An extensive review. Solar Energy. 2018, v. 170,

p. 1130-1161. doi:10.1016/j.solener.2018.05.007

[236] Suchorowiec, K.; Paprota, N.; Pielichowska, K. Aerogels for Phase-Change Materials in Functional and Multifunctional Composites: A Review. Materials. 2024, v. 17, n. 17, p. 4405. doi:10.3390/ma17174405

[237] Ren, J.; Jiang, X.; Han, X.; et al. Delignified sorghum straw/PEG/EP phase change composites: Combining biomass source, form-stabilities, and high performances. Materials Letters. 2023, v. 349, p. 134799. doi:10.1016/j.matlet.2023.134799

[238] Biesuz, M.; Valentini, F.; Bortolotti, M.; et al. Biogenic architectures for green, cheap, and efficient thermal energy storage and management. Renewable Energy. 2021, v. 178, p. 96-107. doi:10.1016/j.renene.2021.06.068

[239] Jeon, J.; Park, J. H.; Wi, S.; et al. Latent heat storage biocomposites of phase change material-biochar as feasible eco-friendly building materials. Environmental Research. 2019, v. 172, p. 637-648. doi:10.1016/j.envres.2019.01.058

[240] Jeon, J.; Park, J. H.; Wi, S.; et al. Characterization of biocomposite using coconut oil impregnated biochar as latent heat storage insulation. Chemosphere. 2019, v. 236, p. 124269. doi:j.chemosphere.2019.06.239

[241] Iguchi, M.; Hiraga, Y.; Kasuya, K.; et al. Viscosity and density of poly(ethylene glycol) and its solution with carbon dioxide at 353.2K and 373.2K at pressures up to 15MPa. The Journal of Supercritical Fluids. 2015, v. 97, p. 63-73. doi:10.1016/j.supflu.2014.10.013

[242] A.G., G. K.; Raj, G.; Bhatnagar, A.; et al. Coconut Oil: Chemistry, Production and Its Applications - A Review. Indian Coconut Journal. 2010, v. 73, n. 3, p. 15-27.

[243] Noureddini, H.; Teoh, B. C.; Davis Clements, L. Viscosities of vegetable oils and fatty acids. Journal of the American Oil Chemists' Society. 1992, v. 69, n. 12, p. 1189-1191. doi:10.1007/BF02637678

[244] Mert, H. H.; Eslek, A.; Mert, E. H.; et al. Preparation and characterization of shape-stable bio-based composite phase change materials for thermal energy storage: coconut oil / activated carbon from cherry stones doped

composites. Energy Sources, Part A: Recovery, Utilization, and Environmental Effects. 2022, v. 44, n. 2, p. 5381-5397. doi:10.1080/15567036.2022.2086946

[245] Németh, B.; Németh, Á. S.; Ujhidy, A.; et al. Fully bio-originated latent heat storing calcium alginate microcapsules with high coconut oil loading. Solar Energy. 2018, v. 170, p. 314-322. doi:10.1016/j.solener.2018.05.066

[246] Pang, Y.; Sun, J.; Zhang, W.; et al. Green, recyclable and high latent heat form-stable phase change composites supported by cellulose nanofibers for thermal energy management. International Journal of Biological Macromolecules. 2024, v. 264, p. 130633. doi:10.1016/j.ijbiomac.2024.130633

[247] Zhang, H. C.; Kang, B. hao; Sheng, X.; et al. Novel Bio-Based Pomelo Peel Flour/Polyethylene Glycol Composite Phase Change Material for Thermal Energy Storage. Polymers. 2019, v. 11, n. 12, p. 2043. doi:10.3390/polym11122043

[248] Timms, R. E. Phase behaviour of fats and their mixtures. Progress in Lipid Research. 1984, v. 23, n. 1, p. 1-38. doi:10.1016/0163-7827(84)90004-3

[249] Optris. PI 450i. Published 2025. Accessed: August 14, 2025. Available at <https://optris.com/us/products/infrared-cameras/precision-line/pi-450i/>.

[250] Jiang, X.; Liu, J.; Ren, J.; et al. Corn straw supported high-performance phase change composites: Strategy to turn agricultural residues into high efficient and stable thermal energy storage materials. Materials Today Sustainability. 2023, v. 24, p. 100571. doi:10.1016/j.mtsust.2023.100571

APPENDIX A

Table A.1: Stability, insoluble content, and insoluble fraction's water holding capacity (WHC) for washed (W) and unwashed (UW) biomass suspensions, at different concentrations. Citric acid concentration was 3%.

Washing/ Biomass (%)		Kinetic stability (%)			Insoluble content (%)	WHC (g H_2O/g solids)
		24 h	48 h	72 h		
UW	1	41 ± 2	37.6 ± 0.4	34 ± 4	30.5 ± 0.8	1.94 ± 0.06
UW	2.5	78 ± 1	69 ± 3	63 ± 2	34 ± 3	4.794 ± 0.009
UW	4	94 ± 0	92 ± 1	86 ± 0	37 ± 3	8.09 ± 0.09
W	1	60 ± 4	56 ± 7	46 ± 2	38.8 ± 0.7	2.0 ± 0.5
W	2.5	86 ± 7	78 ± 4	75 ± 4	44 ± 0	6 ± 1
W	4	98 ± 1	94 ± 1	93 ± 0	48.03 ± 0.02	10 ± 1

Table A.2: Stability, insoluble content, and insoluble fraction's water holding capacity (WHC) for orange biomass suspensions, at different citric acid concentrations. Biomass concentration was 4%.

Citric acid (%)	Kinetic stability (%)			Insoluble content (%)	WHC (g H_2O/g solids)
	24 h	48 h	72 h		
0	83.1 ± 0.3	80 ± 1	72 ± 2	74.4 ± 0.4	12.9 ± 0.6
1	96 ± 1	92.1 ± 0.7	88 ± 3	55 ± 1	10 ± 1
3	99 ± 1	97 ± 2	95 ± 2	48.03 ± 0.02	10 ± 1
5	100 ± 0	99.0 ± 0.4	98 ± 0	44 ± 2	11.8 ± 0.7

Table A.3: Stability, insoluble content, and insoluble fraction's water holding capacity (WHC) for suspensions from different biomass fractions. Biomass concentration was 4% and citric acid concentration was 5%.

Biomass fraction	Kinetic stability (%)			Insoluble content (%)	WHC (g H_2O/g solids)
	24 h	48 h	72 h		
Mixed	100 ± 0	99.0 ± 0.4	98 ± 0	44 ± 2	11.8 ± 0.7
Peels	99 ± 0	94 ± 1	93 ± 0	45 ± 1	11.0 ± 0.4
Bagasse	100 ± 0	100 ± 0	100 ± 0	39 ± 2	12.4 ± 0.7
Pulp	100 ± 0	99 ± 1	99 ± 1	46 ± 1	13.4 ± 0.7

APPENDIX B

Table B.1: Volumetric shrinkage of aerogels and cryogels obtained with different orange biomasses or LM pectin after solvent exchange, drying (supercritical or freeze-drying) and in total.

Drying method	Non-solvent	Biomass	Shrinkage (%)		
			after solvent exchange	after drying	total
Sc drying	Ethanol	Mixed	28 ± 3	43 ± 6	59 ± 4
Sc drying	Ethanol	Peels	27 ± 3	45 ± 3	60 ± 2
Sc drying	Ethanol	Bagasse	26 ± 4	42 ± 5	57 ± 4
Sc drying	Ethanol	Pulp	19 ± 5	45 ± 7	56 ± 4
Sc drying	Ethanol	LM pectin	32 ± 4	52 ± 4	68 ± 4
Sc drying	Acetone	Mixed	30 ± 3	18 ± 4	43 ± 3
Sc drying	Acetone	Peels	33 ± 3	29 ± 5	52 ± 4
Sc drying	Acetone	Bagasse	26 ± 4	23 ± 4	43 ± 4
Sc drying	Acetone	Pulp	24 ± 4	21 ± 5	39 ± 2
Sc drying	Acetone	LM pectin	36 ± 4	49 ± 5	66 ± 3
Freeze-drying	-	Mixed	-	27 ± 5	27 ± 5
Freeze-drying	-	Peels	-	25 ± 3	25 ± 3
Freeze-drying	-	Bagasse	-	19 ± 4	19 ± 4
Freeze-drying	-	Pulp	-	21 ± 4	21 ± 4
Freeze-drying	-	LM pectin	-	32 ± 5	32 ± 5

Table B.2: Apparent density (ρ_{ap}), specific surface aera (S_{BET}) and porosity (P) of aerogels and cryogels obtained with different biomasses or LM pectin.

Drying method	Non-solvent	Biomass	ρ_{ap} (g/cm³)	S_{BET} (m²/g)	P (%)
Sc drying	Ethanol	Mixed	0.091 ± 0.001	209 ± 28	94 ± 1
Sc drying	Ethanol	Peels	0.094 ± 0.004	191 ± 20	94 ± 4
Sc drying	Ethanol	Bagasse	0.086 ± 0.006	235 ± 20	94 ± 7
Sc drying	Ethanol	Pulp	0.079 ± 0.005	212 ± 18	95 ± 6
Sc drying	Ethanol	LM pectin	0.078 ± 0.005	150 ± 0	95 ± 6
Sc drying	Acetone	Mixed	0.068 ± 0.001	263 ± 9	95 ± 1
Sc drying	Acetone	Peels	0.076 ± 0.004	224 ± 25	95 ± 5
Sc drying	Acetone	Bagasse	0.069 ± 0.004	215 ± 34	95 ± 6
Sc drying	Acetone	Pulp	0.061 ± 0.001	205 ± 4	96 ± 2

Sc drying	Acetone	LM pectin	0.075 ± 0.003	130 ± 26	95 ± 4
Freeze-drying	-	Mixed	0.088 ± 0.004	8 ± 1	94 ± 5
Freeze-drying	-	Peels	0.086 ± 0.004	6 ± 3	94 ± 5
Freeze-drying	-	Bagasse	0.081 ± 0.002	6 ± 1	95 ± 3
Freeze-drying	-	Pulp	0.085 ± 0.004	9 ± 1	94 ± 4
Freeze-drying	-	LM pectin	0.093 ± 0.007	5 ± 1	94 ± 7

Table B.3: Volumetric shrinkage (ΔV), apparent density (ρ_{ap}), specific surface aera (S_{BET}) and porosity (P) of mixed aerogels shaped as beads and monoliths. Biomass concentration was 3%.

	Mixed 3% aerogels	
	Beads	**Monoliths**
ΔV after solvent exchange (%)	5.0 ± 0.9	30 ± 4
ΔV after sc drying (%)	49 ± 2	56 ± 5
ΔV total (%)	52 ± 2	69 ± 4
ρ_{ap} (g/cm³)	0.0779 ± 0.0003	0.087 ± 0.003
S_{BET} (m²/g)	308 ± 31	172 ± 4
P (%)	95 ± 1	94 ± 3